Advances in Understanding and Regulation of Sulfur Conversion Processes in Metal-Sulfur Batteries

Fangyi Shi[1,2#], Jingya Yu[1,3#], Chunhong Chen[1#], Shu Ping Lau[2], Wei Lv,[4] Zheng-Long Xu[1,3]*,

1. Department of Industrial and Systems Engineering, The Hong Kong Polytechnic University, Hung Hom, Hong Kong, P.R. China.

2. Department of Applied Physics, The Hong Kong Polytechnic University, Hung Hom, Hong Kong, P.R. China.

3. State Key Laboratory of Ultraprecision Machining Technology, The Hong Kong Polytechnic University, Hung Hom, Hong Kong, P.R. China.

4. *Shenzhen Geim Graphene Center, Engineering Laboratory for Functionalized Carbon Materials, Tsinghua Shenzhen International Graduate School, Tsinghua University, Shenzhen, P.R. China*

[#] S.F., Y.J., and C.C. contributed equally

*Corresponding author. Email: zhenglong.xu@polyu.edu.hk (Z.L.X.)

Abstract

Lithium-sulfur batteries (LSBs) have attracted intensive attention as a promising next-generation energy storage system, due to the high energy density and low cost of sulfur cathodes. Despite the substantial progress in improving LSB performance, their wide implementation still suffers great challenges, including the difficulties in achieving practically high energy density with long cycle life, and the concerns on the limited lithium resources. The former issue mainly arises from the insufficient mechanics understanding of the complex lithium-sulfur redox reactions, while, the latter triggers the exploration of a range of new metal-sulfur systems, such as sodium-sulfur, potassium-sulfur, magnesium-sulfur, calcium-sulfur, and aluminum-sulfur batteries. These lithium-free metal-sulfur batteries (MSBs) hold the potential to offer higher energy density or/and lower battery costs. The fundamental understanding and rational regulation of effective metal-sulfur conversion reactions are crucial for developing the advanced and emerging MSBs. Herein, this work aims to overview the state-of-the-art progress in circumventing these issues for MSBs, in terms of working mechanisms, key factors determining electrochemical behaviors and battery performance. Advanced *in-situ* characterization techniques used to disclose the sulfur conversion mechanisms are also elaborately discussed. Conclusions and perspectives for the future research direction in MSBs are proposed.

Keywords: lithium-sulfur battery, metal-sulfur battery, sulfur conversion chemistry, in-situ characterizations

1. Introduction

Rechargeable batteries hold the expectation of dealing with the energy crisis and environmental pollution caused by the combustion of fossil fuels.[1] Since its successful launch in the 1990s, lithium-ion batteries (LIBs) have dominated the portable power market and are now penetrating into the green transportation sector via propelling electric vehicles. However, the energy density for LIBs has encountered a bottleneck due to the limited capacity (below 300 mAh g^{-1}) of metal oxide cathodes.[1,2] Exploring new battery systems with higher energy densities and lower cost than current LIBs are crucial to realize further electrification and carbon neutrality of our modern society. Among the few options, metal-sulfur electrochemistry has been considered promising due to the 2-electron redox reaction per sulfur atom, leading to an exceptionally high theoretical capacity of 1672 mAh g^{-1} for sulfur cathodes. Together with the appealing properties of low cost (\$150 ton^{-1}), eco-friendliness, abundant supply of sulfur, metal-sulfur batteries (MSBs) are regarded as the next-generation energy storage devices.[3,4] Li-S batteries (LSBs) have been intensively investigated since Nazar's group reported a high-performance CMK-3/sulfur cathode in 2009.[5,6] Recently, propelled by the concerns on the Li supply due to its limited and uneven distribution in the Earth crust, researches on Li-free metal-sulfur (*i.e.*, Na-S, K-S, Mg-S, and Ca-S) batteries become prospering.[5,7] MSB systems share the similar cell configuration and working mechanisms. Their properties in terms of metal abundance, electrochemical properties, volume expansion, and energy density are summarized in Table 1.[7,8]

Unlike the intercalation chemistry for conventional LIB cathodes, metal-sulfur electrochemistry involves complicated phase transitions during cycling. Taking the LSB as an example, the discharging process involves the reduction of solid sulfur (S_8) to soluble polysulfides (Li_2S_n, $4 \leq n \leq 8$) and then to solid lithium sulfides (Li_2S_n, $1 \leq n \leq 2$).[9] During the following charging process,

lithium sulfides are oxidized to elemental sulfur inversely. The sulfur conversion processes are closely related to the starting materials, working conditions, and electrode structures. The soluble intermediates induce primary problems in LSBs, including the polysulfide shuttle effect, the corrosion of Li metal, the depletion of electrolyte due to the reaction of Li and S_x^{2-}, and the isolation of active materials from conductive hosts.[1] The precipitation of insulating lithium sulfides from soluble polysulfides is kinetically sluggish, which deteriorates polysulfide diffusion and incomplete sulfur utilization. Other categories of problems for LSB, such as the insulating nature of sulfur species, the large volume expansion of sulfur upon lithiation (*i.e.*, 80%), induce persistent challenges in conversion electrodes. Consequently, large polarization with poor rate capability and inferior cyclability are often prevalent in LSBs.

To address the above fundamental challenges, tremendous efforts have been devoted to engineering the cathode structure/chemistry and understanding the sulfur conversion mechanisms. At the early stage of LSB research, most studies focused on the development of composite cathodes for improved electrochemical performance,[10] such as porous carbon/sulfur, electrocatalyst/sulfur cathodes. In recent years, it is convergently realized that it is imperative to achieve better understanding of the reaction mechanisms and effective regulation of this system,[11] such as the redox process and the chemical/electrochemical reaction kinetics, to further pave the way towards commercial LSBs. Postmortem analyses of cycled LSB have been conducted to monitor the chemical/physical states of active materials. However, considering that the polysulfide intermediates are air-sensitive and transient, *ex-situ* characterizations often fail in presenting full picture of the electrochemical reaction occurring in LSBs. In contrast, various *in-situ* characterization methods, such as *in-situ* X-ray absorption near-edge structure (XANES) and X-ray diffraction (XRD) characterizations, allow real-time detection of the chemical structural

evolutions in working batteries, enabling the decipherment of the complicated reaction processes without sample contaminants.[11-22] Not only do they provide an in-depth understanding of the redox chemistry in MSBs, but *in-situ* characterizations also offer fundamental guidelines to the rational design of sulfur cathodes for improved electrochemical performance.[11]

Some review papers have appeared to summarize the sulfur cathode engineering strategies for LSBs by highlighting the improvement in battery performance. However, several fundamental features from the recent developments of MSBs have rarely been explored, namely, (i) the electrochemical and chemical working mechanisms in LSBs using different electrolytes, substrates, and catalysts, (ii) the sulfur conversion electrochemistry in Li-free MSB systems regarding the electrode/electrolyte compatibility, reaction kinetics for high valance cations, and the battery failing mechanisms, (iii) the state-of-the-art understandings in sulfur conversion mechanics through *in-situ* characterizations. Here, this paper primarily discusses these aspects (Figure 1). The reaction processes and strategies to regulate the sulfur conversion in LSBs will be elaborated by elucidating the correlation among starting materials, electrolytes, electrocatalysts, and reaction processes. Moreover, we discuss the most recent findings in Li-free MSBs, including Na-S, K-S, Mg-S, and Al-S cells with emphasis on surveying reaction processes and battery failure mechanisms. Subsequently, advanced *in-situ* characterization tools to reveal the working mechanisms of MSBs are highlighted. Finally, our perspectives are provided to the remaining issues for future research in MSBs.

2. Li-S batteries

2.1 Reaction mechanisms in a typical Li-S battery

A typical LSB consists of a Li metal anode, a sulfur-based cathode, and a separator soaked with electrolyte inserted between them. The discharge/charge process is the reversible conversion

between S_8 and Li_2S, involving complex phase transitions as shown in Figure 2a.[23,24] The Li-S conversion process in discharge can be categorized into four regions as listed below[9]:

Region I (solid-liquid two-phase conversion, α-sulfur is lithiated to Li_2S_8):

$$\alpha\text{-}\ S_8(s) + 2Li^+ \rightarrow Li_2S_8(l) \quad (1)$$

Region II (liquid-liquid single-phase conversion, Li_2S_8 is lithiated to short-chain polysulfides):

$$Li_2S_8(l) + 2Li^+ \rightarrow Li_2S_6(l) \quad (2)$$

$$Li_2S_6(l) + 2Li^+ \rightarrow Li_2S_4(l) \quad (3)$$

Region III (liquid-solid two-phase conversion, Li_2S_4 is reduced to Li_2S_2/Li_2S):

$$Li_2S_4(l) + 2Li^+ \rightarrow Li_2S_2(s) \quad (4)$$

$$Li_2S_4(l) + 2Li^+ \rightarrow Li_2S(s) \quad (5)$$

Region IV (solid-solid single-phase conversion, Li_2S_2 is lithiated to Li_2S):

$$Li_2S_2(s) + 2Li^+ \rightarrow Li_2S(s) \quad (6)$$

The diffusion of lithium polysulfides (LiPSs) is considered the most challenging issue, hindering the practical implementation of LSBs. In the following, we will give in-depth insights into the electrochemical/chemical reactions involving polysulfides in LSBs.

2.1.1 Redox reaction between sulfur and lithium polysulfides

In region I, the sulfur is converted to long-chain LiPSs (Li_2S_8) with an apparent discharge plateau at approximately 2.4V, which contributes 209 mAh g^{-1} (~12.5% of the theoretical capacity). During charging, the Li_2S_8 can be reversibly delithiated to sulfur. Interestingly, *in-situ* XRD studies show that the charging product was monoclinic β-phase instead of the original orthorhombic α-phase.[25] β-sulfur was considered stable normally above 96 °C but it can be stably existing in the electrochemical system at room temperature (RT).[26] Note that β-sulfur can also be obtained by the melt-diffusion method for sulfur/carbon cathodes.[27]

Another metastable sulfur generated through electrochemical redox of polysulfides is liquid sulfur, which was recently observed during polysulfide oxidation on Au substrate.[28] Liquid sulfur was also identified to form on the basal plane of two-dimensional (2D) materials (*i.e.*, graphite, MoS_2, and WS_2).[29] If the 2D material is thick (tens of nanometers), however, solid sulfur nucleates at the edge areas. The liquid sulfur formed on the basal plane would be quickly transferred to solid β-sulfur once in touch with the solid sulfur propagating from the edge areas (Figure 2b). In addition, the formation of liquid sulfur was reported substrate-dependent, where no sulfur droplets were observed on glassy carbon, graphene-nickel foams, and carbon-coated aluminum.[28,30] Compared to solid sulfur, liquid sulfur indicated superior reaction kinetics and area capacities due to its unique mobile and reshaping capability.[29] Liquid sulfur also creates an opportunity to let the conversion between sulfur and LiPSs from a solid/liquid reaction to a liquid/liquid reaction, which holds the promise to design flow batteries and fast-charging batteries. However, studies on liquid sulfur chemistry are still in infancy. Several critical questions remain to explore, namely, (i) the liquid sulfur is preserved much below the sulfur's melting point (115℃).[28] The origin to realize this thermodynamically instable phase is unclear; (ii) the liquid sulfur was virtually observed in flooded-electrolyte LSBs, the scenarios in high sulfur loading (>7 mg cm^{-2}) and lean-electrolyte (<4 μL mg^{-1}) conditions have not been explored; (iii) the liquid sulfur is metastable and ready to dissolve into electrolyte. Preserving the liquid sulfur for reversible liquid LSB is also challenging.

2.1.2 Redox reaction between long-chain and short-chain polysulfides

In Region II, long-chain Li_2S_8 is further reduced to short-chain Li_2S_x ($4<x\leq6$) showing a slop from 2.4 to 2.1 V.[31] At the end of this stage, the viscosity of electrolyte arrives at the vertex arising from the major product of S_4^{2-}.[32] This step associated with liquid-liquid single-phase

reaction is believed to exhibit fast reaction kinetics. The LiPS status is highly subject to electrolyte properties, such as the solvent species, the solubility of LiPSs, and salt concentration.[33] The electrolyte structure can also regulate the reaction pathway in Region II. For example, stable $S_3^{\bullet-}$ radical was generated through S_6^{2-} dissociation in a high-donor-number (DN) solvent electrolyte (*i.e.*, dimethyl sulfoxide, DMSO, DN_{DMSO}= 29.8), whereas, a low-DN solvent electrolyte (*i.e.*, dimethoxyethane/dioxolane, DME/DOL, DN_{DOL}= 18), mainly involves S_4^{2-} formation.[32]

Apart from the intrinsic LiPS chemistry, extrinsic behaviors for LiPSs (*e.g.*, diffusion, dissolution, and shuttling) can induce both favorable and unfavorable impacts on LSBs. The electronic insulating LiPSs are soluble in ether-based electrolytes. During discharging, they are susceptible to lose contact with the cathode and gradually diffuse to the anode side driven by the concentration gradient or/and electric field, resulting in corrosion of Li metal and irreversible loss of active materials. During charging, the short-chain LiPSs deposited on Li metal would be re-oxidized and diffuse back to the cathode, leading to low Coulombic efficiency and severe self-discharge. Therefore, the LiPS shuttling forth and back between electrodes, the so-called shuttling effect, results in amplified electrolyte depletion, capacity degradation, and battery failure.[34] Alternatively, LiPSs also play favorable roles in improving the reaction kinetic in LSBs. Upon discharging, LiPSs are able to react with insulating sulfur via chemical disproportionation, (*e.g.*, $S_8 + Li_2S_4 \rightarrow Li_2S_6$), thus dragging the insulating sulfur into electrolyte for further conversion reaction. A similar effect also occurs in the charging process, where liquid LiPSs catalyze the oxidation of Li_2S to overcome its dramatically high activation energy barrier.[34] In short, soluble LiPSs is a double-edged sword that is both harmful and beneficial to the Li-S electrochemistry. How to rationally manipulate the LiPS behaviors to reinforce the advantageous

property while suppressing the negative effect is a challenging and rewarding direction for the future LSB study.

2.1.3 Redox reaction between short-chain LiPSs and Li_2S

The further reduction from soluble Li_2S_4 to solid Li_2S/Li_2S_2 (Region III) is kinetically sluggish, and the solid-solid conversion kinetic between Li_2S and Li_2S_2 in Region IV is slower. A potential dip is usually observed at the beginning of Region III, due to the centripetal polarization from highly viscous Li_2S_4[35] and the overpotential to drive solid phase nucleation.[20] Regions III and IV contribute 1254 mAh g^{-1} (*i.e.*, 75% of the theoretical capacity), and thus their reaction kinetics, depth, and reversibility play critical roles in the battery performance.

The electrochemical deposition of Li_2S_2/Li_2S from soluble polysulfides involves the solid nucleation and growth behaviors. Chiang *et al.*[36] demonstrated that the nucleation of lithium sulfides on conductive substrates occurred along the three-phase boundary between solid lithium sulfide precipitates, the conductive substrate, and the polysulfide solutions. The deposition behaviors stick to the host surface chemistry,[37] separators,[38] and electrolyte structures.[39] For example, three-dimensional (3D) Li_2S precipitation was achieved by decorating carbon hosts with black phosphorus quantum dot (BPQD) catalysts.[40] High-DN solvent-based electrolytes can meliorate the LiPS solubility to promote 3D Li_2S deposition.[41] In addition, current densities also influenced the deposition morphologies of Li_2S_2/Li_2S.[42] It was reported that the precipitation of Li_2S_2/Li_2S at high current density (360 μA cm^{-2}) followed a surface deposition route but a solution-mediated growth model at low current density (9 μA cm^{-2}, Figure 2c). As a result, Li_2S would form thin and continuous films with large nucleation density at high current density, in contrast, large and discrete Li_2S particles were observed at low deposition current.[42,43] Given the

insulating nature of Li_2S/Li_2S_2, in-solution growth model is more favorable with larger precipitate volumes and higher sulfur utilization than the surface-deposition counterpart.

During the charging process, Li_2S_2/Li_2S would be dissolved and converted to LiPSs. Similar to its precipitation mechanism, dissolution of Li_2S_2/Li_2S only occurs at the three-phase boundary among Li_2S/Li_2S_2, host, and electrolyte with electronic and ionic conductivities.[44] At the beginning of the charging curve (Figure 2a), a potential hill can be clearly observed, representing an extra driving force to activate the Li_2S_2/Li_2S oxidation.[10,44] The potential hill is related to several key parameters, namely, (i) the phase and crystallinity of Li_2S/Li_2S_2, (ii) the electronic/ionic conductivity of the substrate, and (iii) the presence of mediators, like LiPSs. Compared to highly crystalline Li_2S/Li_2S_2, oxidation of the amorphous phase was reported easier without residuals after full charging.[45] Because of the improved conductivity for few-layer graphene wrapped Li_2S, the Li_2S@graphene nanocapsules exhibited notable area capacities of 8.1 mAh cm^{-2} at a high loading of 10 mg cm^{-2}.[46] When micronized Li_2S is directly used as the cathode, it required an activation voltage over 3.5V, the activation process is displayed in Figure 2d.[47] After the first cycle, the overpotential for charging in the latter cycles became much smaller. It is attributed to the presence of LiPSs to mediate the Li_2S dissolution.[44] Moreover, Li_2S-metal/carbon composites,[47,48] redox mediators in electrolytes,[49,50] electrocatalyst[51,52] have also been demonstrated efficient in alleviating the Li_2S_2/Li_2S activation barriers for improved cyclic capacities.

2.1.4 Chemical reaction among polysulfides

Apart from electrochemical reactions, chemical reactions among LiPSs also occur in LSBs and contribute capacities. In DMSO and DME/DOL electrolytes, for example, the (electro)chemical reactions can be depicted as follows[53]:

$S_8 + 2e^- \rightarrow S_8^{2-}$ electrochemical (7)

$S_8^{4-} \rightarrow 2S_4^{2-}$ disproportionation (8)

$S_8^{2-} \rightarrow S_6^{2-} + 1/4S_8$ (in DMSO) disproportionation (9)

$S_6^{2-} \leftrightarrow S_3^{\bullet-}$ (in DMSO) disproportionation (10)

$2S_4^{2-} \rightarrow 6/7\ S_8^{2-} + 8/7\ S_1^{2-}$ disproportionation (11)

Taking the electrochemical reaction into consideration as well, we can find the reaction process in LSBs is very complex. In addition, different solvents would induce different reaction pathways (both chemical and electrochemical reactions). For example, the disproportionations in Equations 9 and 10 are prone to happen in electron-pair donor solvents with high dielectric constant (*i.e.*, DMSO). Some disproportionation reaction is disadvantageous to battery cycling. The solid products generated in the disproportionation reactions of LiPSs (Equations 9 and 11) would increase the interfacial resistance by passivating electrode surfaces.[54] The disproportionation between LiPSs may also induce LiPSs accumulation and diffusion.[55] Therefore, understanding and regulating the chemical reactions are of significance to draw a whole picture of sulfur conversion chemistry and guide the Li_2S or S_8 activation through selected disproportionation routes.[56]

2.2 Li-S conversion chemistry in other sulfur-containing materials

It is clearly observed from the above contents that the formation and dissolution of LiPSs are inevitable and disruptive in LSBs. Apart from elaborating LiPS-retain strategies,[57] avoiding and depressing the existence of LiPS in the sulfur conversion process can also improve the LSB cyclability. Some sulfur-containing compounds, including small sulfur molecules, organosulfur polymers, and metal sulfides, can meet this requirement.

2.2.1 Small sulfur allotropes

Small sulfur allotropes S_{2-4} confined in microporous carbon (pore size ~0.5nm, Figure 3a) is a successful example to avoid LiPSs diffusion in bulk electrolyte through a solid-solid conversion.[58,59] The narrow pores can successfully prevent the direct contact between sulfur molecules and electrolyte by desolvating the solvated-Li before solid Li diffusion in carbon host (Figure 3b).[58] Therefore, the electrode can be cycled in both ether-based and carbonate-based electrolytes (Figure 3c). The smaller sulfur molecules showed excellent cyclic stability with capacities above 600 mAh g^{-1} after 500 cycles at 400 mA g^{-1}.

Despite the extended cycle life in LSBs, this approach faces several fundamental challenges. First, the charge-transfer kinetics depend on the electronic conductive carbon, resulting in S_{2-4}/microporous carbon with higher resistance than the 'open-type' S_8/porous carbon due to the large energy barriers for Li desolvation, solid Li-ion diffusion, and solid-solid Li-S conversion processes. Second, due to the limited space, the sulfur content is restricted to less than 50%,[57,58] which value is far from sufficient to meet practically high energy LSBs demanding sulfur loadings of above 70wt% and 7 mg cm^{-2}. Third, the conditions to realize solid-solid reactions are ambiguous. It is argued that solid electrolyte interface (SEI) layers formed on the surface of sulfur/mesoporous carbon cathode would also trigger the solid-solid reaction,[60] disrupting the complusary micropores. Forth, the reduction mechanism of S_{2-4} in microporous carbon is under debate. Some papers proposed that S_{2-4} is lithiated to long-chain LiPS, short-chain LiPS, and finally Li_2S, similar to the lithiation of S_8, through operando XAS characterizations (Figure 3d).[61] Others argued that the redox process between S_{2-4} and Li only involves sulfur and Li_2S without any intermediates, the same as the alucone C–S cathodes in carbonate-based electrolytes (Figure 3e).[62] Therefore, both the electrochemical performance and fundamental understanding of reaction mechanisms for small sulfur allotropes need investigations in future studies.

2.2.2 Organosulfur polymers

Organosulfur polymers consisting of organic groups and sulfur chains have also been widely investigated as promising alternatives to S_8 to solve the problems of LiPSs.[63] In organosulfur compounds, sulfur atoms are covalently bonded with organic frameworks. This structure can inherently entrap sulfur species, especially LiPSs, and avoid agglomeration or re-displacement of sulfur during cycling, thus the sulfur utilization is improved, and the shuttle effect is suppressed by molecular immobilization.[63] The electrochemical process of organosulfur compounds can be classified into three types as shown in Figure 4a.

The first class of organosulfur undergoes the solid-liquid-solid conversion path, resembling the electrochemical process of S_8.[63] An representative example is the poly(sulfur-random-1,3-diisopropenylbenzene (S-DIB) as synthesized by heating polymeric sulfur and DIB together.[64] The S-DIB displayed a S_8-like discharge/charge potential profile with two typical reaction plateaus. Due to the chemical bonding of the copolymers, pristine S-DIB exhibited a reasonable cycle life of 100 cycles at 0.1 C. Following, S-DIB@CNT cathode was prepared with enhanced electrical and ionic conductivities,[65] which presented a high initial capacity of 1300 mAh g^{-1} and cyclic capacities of 880 mAh g^{-1} at 1 C. Inspired by the S-DIB structure, organosulfur polymers containing conjunction units of benzene rings, thiophene, and thiazine have also been exploited for improved battery performance.[66] To alleviate shuttle effect, Zhou et al.[67] prepared a linear copolymer of thiokol rubber-like poly(methylenetetrasulfide) or poly(ethylenetetrasulfide) (PMTS or PETS). The $–CH_2–$ or $–CH_2CH_2–$ unit exists soluble LiPSs ((e.g., Li–S_2– CH2–S–Li or Li–S–CH2CH2–S–Li)) during conversion process and display a large binding energy with the surface of chitosan derived porous carbon, resulting in diminishing shuttling effect. For this kind of organosulfur compounds, the future study should pay attention to two key parameters, namely,

(i) the length of sulfur chain and the organic unit, which determines the physicochemical stability and the sulfur content, (ii) the bandgap of polymers, which governs their conductivity and rate capability in LSBs.

The second class of organosulfur polymers only undergoes solid-solid reaction without the LiPSs formation. [68, 69] Sulfurized polyacrylonitrile (SPAN) is one of the most attractive examples with remarkable electrochemical stability cycling in carbonate-based electrolytes.[70] The SPAN can be simply produced by heating mixtures of sulfur and acrylonitrile, which is polymerized and sulfurized into a conjugated structure as shown in Figure 4b. During lithiation/delithiation, it was proposed that the SPAN underwent a solid-phase conversion where the C-S bonds were reversibly broken and reformed.[71] It is noted that there are two models to explain the sulfur storage in SPAN, namely, sulfur chains act as bridges to connect the conjugated PAN skeleton in model A, while the sulfur is siding chains on the conjugated PAN in model B.[72] Although SPAN can avoid the shuttle effect, this kind of material also has problems, such as the low sulfur loading (~40%), poor conductivity, and sluggish redox kinetics. In order to improve the conductivity and reaction kinetics, Wang *et al.*[73] reported a freestanding fibrous SPAN/ CNTs cathode. After the activation, the cathode could remain a reversible capacity of 1400 mAh g^{-1} over 200 cycles at 200mA g^{-1} and 1180 mAh g^{-1} over 800 cycles at 800mA g^{-1}. Chen *et al.*[72] reported a Se-doped SPAN (Se_xSPAN) cycling in carbonate-based and ether-based electrolytes. Interestingly, different from the solid-solid phase transition of pure SPAN in ether electrolytes,[73] a solid-liquid-solid transition path was detected for Se_xSPAN with high rate capabilities. This study suggests that the sulfur conversion processes and electrochemical performance of SPAN are tunable by heteroatom doping. In addition to SPAN, a series of sulfur-rich organosulfur materials with well-designed structure and short sulfur-chain(the sulfur atoms are no more than 4

in sulfur chains) have also been reported, which also exhibit no soluble LiPSs during cycling. Shadike et al.[68] reported a novel organodisulfide compound, 2,3,4,6,8,9,10,12-Octathia biscyclopenta[b,c]-5,11-anthraquinone-1,7-dithione (TPQD). There are two types of electrochemically active groups in this well-designed organodisulfides, one is carbonyl group; another is disulfides group. Through introducing 1-4-benzoquinone (BQ)(high specific capacity but high solubility in organic electrolytes) into rigid backbone structure of TPQD(insoluble in the electrolyte), the cathode achieved shuttle effect free during cycling and display high specific capacity, great rate capability and stable cycling performance. Zhang et al.[69] synthesized disulfide polymers (DSP) and trisulfide polymers (TSP) as cathode materials. During the cycling, the electrolyte keeps colorless in the TSP optical cell, which demonstrate no soluble LiPSs formation.

As for the third type of organosulfur, they are usually small molecules in the liquid phase, undergoing a liquid-solid transformation in LSBs.[63] Bhargav *et al.*[74] synthesized phenyl polysulfides $C_6H_5S_xC_6H_5$ ($4 \leq x \leq 6$) as a liquid cathode, as shown in Figure 4c. During lithiation, the phenyl polysulfides were reduced to solid Li_2S and phenyl-SLi. Due to the liquid-solid conversion, the cell conducted great performance with lean electrolyte, for example, an area capacity of 7.6 mAh cm^{-2} was retained after 500 cycles at 1 C under an E/S ratio of 3 ul mg^{-1}.

2.2.3 Inorganic sulfur compounds

When some sulfur-containing inorganic compounds exhibit working voltages close to 2 V vs. Li/Li^+ and sulfur content of >40wt%, they were regarded as sulfur-equivalent cathodes in LSBs.[75] Ye *et al.*[75] reported an amorphous MoS_3 as a LSB cathode. MoS_3 was proposed to have a chain-like structure consisting of Mo bridged by sulfide and disulfide ligands. *Operando* XAS spectrum was carried out to learn the reaction mechanisms of the MoS_3 cathode. It shows that

both the sulfur and Mo were reduced during lithiation but they did not form Li_2S or polysulfides. The Li ions were supposed to store at the bridge sites between two adjacent sulfur atoms. No disintegration of sulfur or MoS_3 took place during cycling. As a result, the MoS_3 cathode delivered a high capacity of ~383 mAh g^{-1} after 1000 cycles at 0.45 A g^{-1}. Selenium (Se), an element in the same groups as oxygen and sulfur has also been compounded with S to form Se_xS_y as sulfur-equivalent cathodes in LSBs. It was found that the Se in CMK-3/Se_xS_y could induce the formation of a thin cathode electrolyte interface (CEI) layer on cathodes in carbonate electrolyte.[76] As shown in Figure 4d, electrolyte molecules would be blocked by the CEI to attack polysulfides or polyselenides encapsulated within the carbon host. The thickness of the CEI layer signified a positive relationship with the Se content. Thus, optimal CMK-3/Se_5S_3 with desirably thick CEI achieved remarkable capacity retention of 609 mAh g^{-1} after 300 cycles at 1 A g^{-1}.[77]

Overall, in the past decade, tremendous progress has been achieved in understanding the fundamental mechanisms of sulfur conversion chemistry in LSBs. Inherently, the Li-S conversion behaviors are determined by the stage of reaction, the nature of starting materials, and the intermediate chemical species. It is also observed that the complicated reaction processes involve both favorable (*i.e.*, disproportionation reaction to dissolve insulating sulfur or Li_2S) and unfavorable (*i.e.*, sluggish conversion of polysulfides) steps. To improve the electrochemical performance, effective strategies have been developed to regulate the sulfur conversion processes to be interpreted in the following section.

2.3 Regulating the sulfur conversion chemistry

2.3.1 Current collector engineering

The current collector functions as the bridge between electric circuits and electrode materials.[78] It also possesses a great impact on the electrochemical behaviors of LSBs. In general, the sulfur cathode is fabricated by casting the mixture of active materials, binders, and conductive carbon black on Al foil.[79] Other 2D films or foils such as Ni, Pt, Cu, and carbon cloth (CC) have also been investigated as potential current collectors. It shows that Cu and Ni are unstable as being corroded by polysulfides or components in the electrolytes.[80] LSBs with CC and graphene film current collectors exhibit better electrochemical performance than Al counterpart,[81] attributable to their larger surface area and better anti-corrosion capability.[82]

3D current collectors have also been studied as promising alternatives to the 2D counterparts in view of their interconnected conductive networks, large surface area, and abundant ion diffusion channels, all of which are important for high sulfur loading and fast reaction kinetics.[83] For example, 3D carbon nanotubes (CNT) films have been prepared as current collectors in LSBs. Compared with 2D Al foil and graphene current collectors, LSBs with 3D CNT current collector displayed much superior electrochemical performance (Figure 5a) with a high cycling ability (95 cycles with 0.029% decay rate) under high sulfur loadings.[82] Other carbon materials have also been built into 3D current collectors, like graphene foam (GF)[84] and 3D melamine formaldehyde-based carbon foam (MFC)[85]. However, the nonpolar carbon cannot entrap LiPSs to suppress the shuttle effect in LSBs.

To regulate the entrapment and catalytic capability of current collectors for high-performance LSBs, surface modifications have been conducted for light and 3D carbon current collectors.[86] For example, we have prepared MoS_2/carbon nanofiber (CNF) films by electrospinning.[37] Then, catholyte containing polysulfides and electrolyte was dropped on MoS_2/CNF as cathodes. Owing to the 1T MoS_2 catalyst and the 3D conductive carbon network, the MoS_2/CNF/Li_2S_6 delivered

remarkable capacity retention of 9.3 mAh cm^{-2} after 300 cycles with an exceptionally high sulfur loading of 12.9 mg cm^{-2} and lean electrolyte of 4.6 μl mg^{-1}. Mo_2C decorated N-doped CNF current collector has also been proved to effectively mitigate the shuttle effect by taking advantage of the strong LiPSs affinity from MoC_2.[87] Pyrrole polymer with strong chemical bonding with LiPS was introduced into GF current collectors. The pyrrole GF/S cathode displayed a great cycle ability (over 100 cycles with 81% capacity retention) and high specific capacity (1220 mAh g^{-1}).[88] In addition to polysulfide entrapment, functional current collectors have also been designed to regulate the LiPSs conversion kinetic and the Li_2S deposition behaviors. For example, the Co, N-CNTs-CNS (carbon nanosheet)/CFC (carbon fiber cloth) current collector induced a 3D deposition of Li_2S.[89] Compared to the routine 2D growth of Li_2S, the 3D structure of Li_2S enables higher LiPS utilization and thus effectively suppresses their diffusion to bulk electrolytes.

Apart from the discharging (or lithiation) process, the current collectors also play a non-negligible role in the charging process in LSBs. Using *in-situ* optical microscopy, Zhou *et al.*[30] observed distinct sulfur growth behaviors on Al, C, and Ni current collectors. They found that solid sulfur emerged on the carbon surface while liquid sulfur droplets grew on Ni substrates (Figure 5b). The different sulfur growth behaviors were attributed to different binding energies of S_8 with Ni, C, or Al substrate through DFT calculations. The moderate interaction between Ni and S_8 (-1.4eV vs -0.93eV for S_8 on C, -5.44eV for S_8 on Al) was the precondition for sulfur droplet formation. As aforementioned, liquid sulfur enables high mobility and fast phase transition, thus accelerating the reaction kinetics in LSBs. Consequently, a lightweight, 3D Ni-coated melamine current collector was synthesized for high-rate and long-life LSBs. Similarly, two-dimensional materials (*i.e.*, MoS_2 and graphene)[29] or deposited Au layer[90] current collectors

have also been reported to generate the liquid sulfur product with high area capacities in on-chip micro-LSBs.

Overall, the nature of current collectors is important in influencing the electrochemical behaviors in both discharging and charging processes. Self-supporting and 3D current collectors are desirable as high-loading sulfur hosts. Functional materials on 3D networks are also recommended to accelerate the Li-S redox kinetics. Research on the impact of the current collector in the charging process is still at an initial stage. More efforts are expected to unveil the origins of current collectors regulating a whole charging/discharging cycle in LSBs.

2.3.2 *Electrocatalyst design*

One of the fundamental challenges for sulfur utilization is the insulating nature of sulfur species. Therefore tremendous efforts have been paid to design carbon nanomaterials as highly conductive hosts for sulfur particles. Although the improvement in electrochemical performance has been witnessed by compositing sulfur and conductive carbon, the long-term and high-rate capacities of such sulfur/carbon cathodes are often jeopardized due to the eventual dissolution of polysulfides as caused by the weak interaction between polar polysulfides and nonpolar carbon. In this respect, studies of electrocatalysts, enabling chemical trapping and catalytic conversion of polysulfides, have recently been carried out and demonstrated the effectiveness in regulating sulfur conversion chemistry for high-performance LSBs. According to their functions and the report timeline, electrocatalysts can be divided into four categories, namely, chemical adsorber, adsorption-diffusion-conversion catalyst, bi-directional catalyst, and selective catalyst.

At the early stage of catalyst study for LSBs, it was believed that polar materials, such as N-doped carbon, metal oxides, and dichalcogenides can form polar-polar interactions or Lewis acid-based bonding with LiPSs, thus preventing their diffusion.[91] One of the typical examples is

mesoporous silica, which was added in CMK-3/S composite as the sulfur reservoir to trap and store the soluble polysulfides during cycling, thus indicating better cyclic stability than pure CMK-3/S.[92] Similarly, TiO_2, NiO and CoO [93-95] have also been investigated to block the LiPSs diffusion. However, it was quickly found that improvement in battery performance using these materials was limited because the entrapped LiPSs cannot be effectively converted to Li_2S due to the poor electronic conductivities of these catalysts (Figure 5c).[96]

To improve the sulfur usage rate and suppress LiPSs diffusion, conductive catalysts were then reported to supply a consecutive LiPS adsorption-diffusion-conversion pathway.[97] Taking black phosphorus (BP) as an example, it possesses a good bulk conductivity, a fast Li-ion diffusion constant, and high binding energies with polysulfides. Few layered BP sheets were therefore adopted in separator[98] or current collector[99] to suppress the diffusion of LiPSs. Through DFT calculations, we discovered that BP presented edge-selective catalytic property, where the zig-zag terminated BP indicated stronger binding energies with polysulfides at the edge than at terrace sites.[40] This finding suggests that we can largely increase the catalytic property by downsizing BP flakes into BPQDs. The electrochemical performance revealed that BPQDs had the robust catalytic capability, and the porous carbon/S/BPQD cathodes presented rapid reaction kinetics and no shuttling of polysulfides. Another representative electrocatalyst worth mentioning is the TiO_2/TiN heterostructure enabling smooth trapping-diffusion-conversion of polysulfides towards stable LSBs.[100] The heterostructure combined the merits of highly adsorptive TiO_2 (for trapping) and conductive TiN (for conversion), thus providing a complete strategy to synchronously realize LiPS adsorption and conversion. Other polar materials (*i.e.*, metal oxides, metal sulfides, metal nitrides)[101] and single-atom catalysts (*i.e.*, Co-N-C, Fe-N-C)[102] have also been developed to enhance the reduction of LiPSs into Li_2S.

The catalytic oxidation of Li_2S during charing is equally important to obtain highly reversible LSBs. Zhou *et al.*[52] illustrated VS_2-, TiS_2- and CoS_2-modified cathodes promoted the dissolution and conversion of Li_2S to LiPSs (Figure 5d). Owning to the high binding energy between the isolated Li-ion and sulfur in sulfides, the metal sulfides would lower the oxidation of the Li_2S energy barrier to improve the Li_2S deposition kinetics. Inspired by the outstanding catalytic capability of Pt and Ni in fuel cells, noble metals were also investigated to reduce the energy barrier for the oxidation process from lithium sulfides to soluble LiPSs.[103] However, most of the synthesized catalysts function in one direction (reduction or oxidation) because of their intrinsic electron donor or acceptor nature, which is unsatisfactory to accelerate the discharge/charge reactions in LSB simultaneously. To mitigate this challenge, a TiO_2-Ni_3N_2 heterostructure[104] was prepared as a bidirectional catalyst. Typically, TiO_2 traps while Ni_3N_2 catalytically reduces LiPSs during discharging, and both TiO_2 and Ni_3N_2 catalyze the Li_2S dissolution during charging. The sulfur cathode containing TiO_2-Ni_3N_2 delivered a low capacity decay rate of 0.038% per cycle over 900 cycles, accordingly.

When we recall the sulfur conversion processes in Section 2.1, it shows that the transformation of polysulfides from high order to low order is generally fast, but the kinetics of further reducing Li_2S_4 to solid Li_2S_2/Li_2S is slow. The kinetic mismatch would lead to saturation of polysulfides on the surface of catalysts and stall further LiPS adsorption. Therefore, precisely regulating the sulfur conversion to ensure compatible LiPS formation and consumption speeds becomes another challenging issue for electrocatalyst design. Hua *et al.*[105] reported an In_2O_3 catalyst that would selectively decelerate the conversion from S to LiPSs while accelerating the reduction of Li_2S_4 to Li_2S. This catalysis could alleviate the accumulation of LiPSs around the cathode to suppress the shuttle effect, leading to enhanced electrochemical performance. The dynamically

changing catalytic mechanism was unveiled by *in-situ* Raman analysis. It showed that In_2O_3 was reversibly converted to $LiInS_2$ to accelerate LiPS disposition to insoluble Li_2S during discharging, while $LiInS_2$ was converted back to In_2O_3 for activating Li_2S oxidation during the following charging process. Similarly, Li *et al.*[106] reported a stepwise polysulfide conversion catalyst, defect-rich Co_3O_4/TiO_2 (denoted as p-Co_3O_4/n-TiO_2-HPs). The Co_3O_4 physiochemically immobilized pristine sulfur and controlled the reduction of S_8 to Li_2S_4, while TiO_2 dots facilitated the diffusion and reduction of Li_2S_4 to solid Li_2S attributed to the p-Co_3O_4/n-TiO_2 built-in electric field. As a result, the precisely regulated LSB delivered exceptionally high rate capability at 10 C with a low capacity decay rate of 0.07% per cycle over 500 cycles.

In summary, different kinds of material display specific functions to catalyze the redox reactions of LSBs. Heterostructures signify the most promising strategy, which can combine specific functions of different catalysts into one structure, thus precisely regulating the sulfur conversion dynamics and kinetics for complex Li-S systems. Despite the encouraging progress, the investigations on electrochemical catalysts still lie in the very beginning stage with a large unknown room to explore. Several directions are suggested, namely, (i) understanding and *in-situ* evaluation of the structural evolution of catalysts during cycling, (ii) reducing the content of electrochemically inert catalyst in LSBs, and (iii) understanding catalytic mechanisms under extreme conditions, like high-sulfur loading, lean electrolyte, and extreme working temperatures.

2.3.3 Electrolyte engineering

The electrolyte chemistry indicates considerable abilities to regulate the sulfur conversion behaviors, thus critically affecting the energy density and cycling performance of LSBs. 1M LiTFSI in equal volume DME and DOL is the most common electrolyte formula in LSBs. The

DME/DOL solvent presents limited LiPSs dissolvability, rendering ready saturation of short-chain polysulfides, especially in lean electrolyte conditions.[107,108] To mitigate this issue, Cheng *et al.*[109] designed a novel ε-caprolactam/acetamide-based eutectic-solvent electrolyte, which had the ability to completely dissolve Li_2S_8 and Li_2S (Figure 6a). The phase transformation from 'solid-liquid-solid' in DME/DOL was turned to 'solid-liquid' in this new electrolyte. Therefore, the kernel problems of voltages polarization and Li_2S activation can be settled. Dominko *et al.*[61] studied the sulfur reduction processes in ether-based electrolytes (TEGDME: DOL with high LiPSs solubility), fluorinated ether-based electrolytes (TTFE: DOL with low LiPSs solubility), and carbonate-based electrolytes (EC: DMC, with S_{2-4}/microporous carbon cathode, no LiPSs formation) by XAS characterizations. In all three cases, the sulfur reduction went through the same processes, sulfur→ long-chain LiPSs→ short-chain LiPSs→ Li_2S/Li_2S_2, with a difference in the type of polysulfides formed at corresponding steps of discharge. When the sulfur was converted to LiPSs, the potential of the discharge plateau in the ether-based electrolyte was higher than that in the fluorinated ether-based electrolyte, indicating a positive relationship between the LiPS solubility in electrolyte and overpotentials for discharging. The discharging product in the carbonate-based electrolyte was a mixture of Li_2S and Li_2S_2 (mole ratio of 2:1), which is different from the end-product of Li_2S in coexistence with polysulfides in ether-based electrolytes.

The solvents with different DN can affect the Li-S redox pathways, intermediate species, and Li_2S deposition morphologies.[32] As shown in Figure 6b, in the high-DN solvent electrolyte (*i.e.*, DMSO, DN= 29.8), Li-S reactions undergo multiple electrochemical and chemical reactions involving S_8^{2-}, S_6^{2-}, S_4^{2-}, and $S_3^{\bullet-}$ where $S_3^{\bullet-}$ is the most stable intermediate to converse to solid lithium sulfides. However, in the low-DN-solvent electrolyte (*i.e.*, DOL: DME), S_4^{2-} was the

main intermediates before Li_2S_2/Li_2S deposition. It is clear that the presence of $S_3^{\bullet-}$ is solvent-dependent. The reaction pathway involving $S_3^{\bullet-}$ radical was favorable to promote sulfur utilization by exacerbating dissociations to allow full conversion of sulfur and lithium sulfides.[110] High-DN-solvent DMSO appeals to the $S_3^{\bullet-}$ formation, but it presents poor anodic stability against metallic Li. Note that the high-DN solvent always presents high dielectric constant (ε).[32] Tetramethylurea (TMU) with better compatibility with Li metal and comparably high ε (ε= 23.6) was investigated to form active $S_3^{\bullet-}$ radicals.[107] Large amounts of $S_3^{\bullet-}$ in DOL/TMU co-solvent were confirmed by Raman characterization. The presence of $S_3^{\bullet-}$ radicals enabled the efficient conversion of Li_2S in TMU during charging and the deposition of thick and porous Li_2S during discharging, which appreciable performance was not observed in DOL/DME electrolyte. The pouch cells using TMU electrolyte delivered a remarkable capacity of 1524 mAh g^{-1} and a high energy density of 324 Wh kg^{-1}.

Although high DN solvents can facilitate the rapid and complete conversion of sulfur and Li_2S by increasing polysulfide dissolution, other electrolyte properties such as ionic conductivity, viscosity, and electrode wettability also govern the Li_2S deposition behaviors. Pan *et al.*[111] quested Li_2S deposition in three representative solvents, including tetramethylene sulfone (TMS) with low-DN, DOL: DME with mid-DN, and DMSO with high-DN. SEM images showed the deposited Li_2S on carbon nanofiber surface were thin film in TMS, micro-sized "flower-like" sheets in DOL: DME, and small nanoparticles in DMSO. Although DMSO indicated 3D growth of Li_2S, the relatively smaller Li^+ diffusion coefficient restricted the growth of small nucleation seeds into 3D Li_2S, causing inferior sulfur utilization and cyclic capacities to these in DOL: DME-based electrolyte. Li *et al.*[112] studied the effects of DN (high DN induce Li_2S 3D deposition), dielectric constant (high ε leads to high Li_2S solubility) and viscosity (high η leads

to low polysulfide mobility and poor wettability) on the electrochemical deposition behaviors of Li_2S (Figure 6c). Among ether-based solvents, DME (G1) with low DN and Li_2S solubility displayed fast 2D lattice growth of Li_2S film and passivated the electrode surface for impeding the further reduction reaction. The low Li_2S solubility and high viscosity of TEGDME (G4) electrolyte induced insufficient sulfur utilization as well. In the high DN electrolytes group, sulfur cathode displayed the largest discharge capacity of 1100 mAh g^{-1} in DMA solvent due to the high Li_2S solubility, suitable DN and high ionic mobility. The battery with highest-DN DMSO electrolyte displayed the smallest discharging capacity of 220 mAh g^{-1} because of the ultralow Li_2S solubility.

The polysulfide dissociation behaviors can be tuned by the lithium salt species and concentration in electrolytes. Chu *et al*.[113] investigated how the salt anions with different DN could tailor the Li_2S deposition behaviors. Lithium bromide (LiBr), lithium triflate (LiTf), and lithium bistriflimide (LiTFSI) with DN= 33.7, 16.9, 5.4 respectively, were dissolved in DOL/DME as electrolytes. The battery with LiBr and LiTf-based electrolytes exhibited superior reversible capacities to that for LiTFSI electrolytes (1535, 1214 vs. 400 mAh g^{-1}) due to the high efficiency of Li_2S deposition and decomposition. 3D Li_2S micron particles were deposited on CC in LiTf and LiBr electrolytes while 2D passivating film was detected in LiTFSI electrolyte. The 3D deposition was related to the precipitated Li_2S possessing strong absorption to S^{2-}. The free S^{2-} anion preferred to deposit on the surface of precipitated Li_2S seeds, resulting in a 3D growth of Li_2S under the action of high DN anions to promote free S^{2-} formation. Suo *et al*.[114] reported a solvent-in-salt electrolyte with high LiTFSI concentration in DOL: DME. In the 7M highly concentrated electrolyte, few free solvent molecules significantly limited the dissolution and diffusion of LiPSs. LSB in solvent-in-salt elecrolytes delivered an initial capacity of 1041mAh g^{-}

[1] and 74% capacity retention after 100 cycles. However, high salt concentration causes problems of high cost, low ionic conductivity, and high viscosity.

Adding electrolyte additives into diluent electrolytes is another promising way to regulate LiPSs dissociation in LSBs. $ZrO(NO_3)_2$ with strong negative charge nature was employed as an additive to regulate LiPS shuttling by putting a strong repulsion force to LiPSs.[115] Yang *et al.*[17] introduced bis(4-nitrophenyl) carbonate (BNC) additive to suppress LiPSs diffusion by reacting with soluble Li_2S_8 to form lithium 4-nitrophenolate (LiNPH) and insoluble lithium sulfides (Figure 7a). Cobalt hexadecachlorophthalocyanine (CoPcCl) has been added into electrolytes to lower the energy barrier for Li_2S decomposition as well as improve the LiPSs conversion kinetics.[116] A nickel chloride dimethoxyethane adduct (NiDME) additive was also prepared to interact with Li_2S_n to form $NiCl_2$.[39] $NiCl_2$ could suppress LiPSs diffusion and accelerate its conversion, and the $NiCl_2$ was returned to NiDME when $NiCl_2$•Li_2S_n is oxidized to sulfur during charging (Figure 7b).

Solid-state electrolytes (SSEs) and hybrid electrolytes (*e.g.*, gel polymer electrolytes-GPE and solid-liquid hybrid electrolytes) have also been investigated to manipulate the sulfur conversion behaviors. For example, the GPEs electrolyte with titanium–oxo clusters (TOC) fillers can suppress the Li_2S_6 dissolution for the dense polymer matrix.[117] Fang *et al.*[118] designed a polyvinylidene fluoride (PVDF) wrapped sulfur cathode to work in a poly (ethylene oxide) (PEO)- GPE. This solid-state LSB exhibited a single-step solid-solid reaction without intermediary product generation. In order to improve the utilization of active materials and thermal stability of LSBs, SSEs have also been developed for LSBs.[119,120] Chiochan *et al.*[119] reported a metal-organic framework (MOF)-based solid electrolyte which used Universitetet i Oslo (UIO) structure with a lithium sulfonate (-SO3Li) group (UIOSLi). The UIOSLi SSE can

provide a great Li^+ transport pathway and prevent LiPSs diffusion simultaneously. Compared with the Celgard separator, UIOSLi SSE showed excellent shuttling inhibition capability even after 7 days (Figure 7c), which resulted in good cycling stability of UIOSLi SSE-based LSB with Li_2S_6 catholyte at 0.2 C after 250 cycled (capacity decay rate of 0.06% per cycle). The $Li_7P_{2.9}S_{10.85}Mo_{0.01}$ ceramic electrolyte can also prevent the formation of LiPSs via solid-solid reaction with one discharge plateau.[121] It is noted that for both SSEs and GPEs, the slow Li-ion migration kinetics and the high electrode/electrolyte interfacial impedance are the key challenges impeding high-power LSBs.

In summary, the sulfur conversion chemistry is highly dependent on different electrolyte chemistries, such as the physicochemical property of solvent, the salt concentration and anion species, electrolyte additives, and the electrolyte phases. In the past years, what was greatly ignored for electrolyte engineering is the lack of understanding of LSB electrochemistry in lean electrolyte conditions. The sulfur conversion mechanisms, reaction kinetics, reactant distribution, and electrode compatibility are largely different from those evaluated in flooded electrolytes. GPE and SSE studies are just at their beginning stage, which demands more research in the future.

2.3.4 Separators engineering

The separator is a critical component in the battery system. It is between the cathode and anode to ensure the battery can be away from electrical short circuits while providing a pathway for ion transport. In recent years, modified separators have attracted extensive attention as functional components on the cathode side with the ability to suppress the shuttle effect, reduce the interfacial resistance, boost the reaction kinetics, and improve the utilization of active materials.

Among the strategies to mitigate the shuttle effect (trapping effect, shield effect and sieve effect), the trapping effect is the most common method. Functional separators can trap soluble LiPSs through physical, chemical and catalytic absorption effects. [122] These strategies can be combined to architect effective separators, achieving shuttle-free as well as fast sulfur conversion kinetics. For instance, Hong et al.[123] reported using Ce-based metal-organic frameworks (MOFs) with CNT to adjust the separator. CNTs having great electrical conductivity can as a secondary charge collector to decrease interface resistance and their porous network can physically block the shuttle effect; Ce-MOFs as the catalyst and absorber can chemically absorb soluble LiPSs and promote the conversion of LiPSs. Li et al.[124] prepared a Janus separator to regulate the reaction on the cathode side and suppress the lithium dendrites. On the cathode side, single-atom Ru on the surface of reduced graphene oxide(rGO@ Ru SAs) with CNT not only immobilize the soluble LiPSs through chemical and physical barrier, but also favor higher conversion kinetics among sulfur species. In the anode side, boron nitride nanosheets with oxygen-group-grafted cellulose nanofibers (BNNs@ CNFs) homogenize Li-ion flux to avoid the dendrite formation.

Apart from mitigating the shuttle effect, a conductive network on separators can provide additional reaction locations to improve sulfur utilization and decrease interface resistance. Many conductive materials modified separators have been reported, like CNT, [123] MXenes[125], and GO[124]. The trapped active materials on the conductive network will be reused.

In summary, to regulate sulfur conversion, the separator should be designed to combine multi-function, efficiently suppressing the shuttle effect and providing excellent conductive networks to ensure high sulfur utilization.

3. Li-free metal sulfur batteries

Following the great advances in LSBs, the sulfur cathode has been coupled with other alkali or alkaline earth metal anodes, such as Na, K, Mg, Ca, and Al, for Li-free MSBs. These metals are either available in the ocean or much richer than Li in the Earth's crust. In addition to addressing the concerns on unsustainability issues of Li metal anode, some of these metals also have high reduction potentials or/and dendrite free stripping/plating properties, thus can contribute to high energy and safe MSBs. Briefly, the newly emerged "metal-sulfur" systems with similar conversion reactions as LSBs demonstrate great promise in either approaching high energy density or lowering the battery cost for large-scale applications. Li-free metal sulfur batteries suffer more sluggish reaction kinetics compared with the LSBs due to different metal anode. One of the reasons lead to poor reaction kinetics is large ionic radii (Shannon's ionic radius: Li^+: 0.76; Na^+: 1.02; K^+: 1.38; Ca^{2+}:1). Though Mg^{2+} and Al^{3+} have smaller ionic radii (Mg^+:0.72; Al^{3+}: 0.535), the multivalent-ion charges also bring slow kinetics.[126] In this section, we survey the state-of-the-art process in mechanics understandings and battery failure mechanisms for Li-free MSBs.

3.1 Na-S batteries

Sodium has similar physical and chemical properties to lithium and is an economically attractive substitute to lithium.[127] Indeed, Na-S battery is nothing new, which has been successfully commercialized for stationary energy storage applications at high operating temperatures (300-350℃) to melt electrodes and activate the solid beta-alumina electrolyte.[128,129] Unfortunately, the high operation temperature blocks its widespread application, especially in electric vehicles. In this context, room-temperature sodium-sulfur batteries (RT-SSBs) have come into the community's view in recent years to adopt the advantages of sulfur cathodes at low temperature and safer working conditions.[130,131] By taking advantage of the knowledge gained in LSBs, RT-

SSB has demonstrated discernible progress in fundamental understanding and improvement in battery performance.

A typical RT-SSB resembled the configuration of LSBs consisting of a sulfur/carbon cathode, a Na metal anode, and a separator filled with organic electrolyte (Figure 8a).[129] During sodiation, the Na metal is oxidized to Na ions, which travel through the electrolyte/separator to reach the sulfur cathode. By accepting Na ions, sulfur will be reduced into sodium polysulfides (Na_2S_n, $4 \leq n \leq 8$) and followed by Na_2S. RT-SSBs offer a high theoretical capacity of 1672 mAh g^{-1} and an energy density of 1230 Wh kg^{-1} with Na_2S as the final product. During the following charging process, Na_2S will be oxidized back to sulfur. Na ions are reduced to Na metal, synchronously. The overall redox reactions can be described as:

$$S + 2Na^+ + 2e^- \leftrightarrow Na_2S \quad (12)$$

A series of sodium polysulfides are generated between the two solid-state end-products, similar to LSB. The chemical composition and structures of reaction products at different discharging stages are illustrated in Figure 8b,[132] which can be divided into four consecutive stages. At approximately 2.2 V, elemental sulfur is reduced into soluble Na_2S_8 (Stage I):

$$S_8 + 2Na^+ + 2e^- \rightarrow Na_2S_8 \quad (13)$$

In the sloping region between 2.2-1.65 V, a liquid-liquid reaction between Na_2S_8 and Na_2S_4 occurs (Region II):

$$Na_2S_8 + 2Na^+ + 2e^- \rightarrow 2Na_2S_4 \quad (14)$$

Following, the soluble Na_2S_4 is further reduced to insoluble Na_2S_3, Na_2S_2, or Na_2S at approximate 1.65 V (Region III):

$$Na_2S_4 + 2/3Na^+ + 2/3e^- \rightarrow 4/3Na_2S_3 \quad (15)$$

$$Na_2S_4 + 2Na^+ + 2e^- \rightarrow 2Na_2S_2 \quad (16)$$

$$Na_2S_4 + 6Na^+ + 6e^- \rightarrow 4Na_2S \quad (17)$$

Residual Na_2S_2 is finally reduced to Na_2S in the sloping range of 1.65 to 1.20 V (Region IV):

$$Na_2S_2 + 2Na^+ + 2e^- \rightarrow 2Na_2S \quad (18)$$

RT-SSBs inherit the intrinsic challenges of sulfur cathodes, such as the insulative nature of sulfur and sodium sulfides, volume expansion, and polysulfide shuttle effects.[133] RT-SSB also suffers problems of the low reactivity of sulfur/Na_2S_x and the slow Na ion diffusion in electrolytes.[134] In this context, smart cathode structures, catalysts, and electrolytes have been investigated. In order to improve the conductivity and sulfur utilization in RT-SSBs, similar to LSBs, various porous carbon materials have been prepared for sulfur/carbon cathodes. For example, Wang *et al.*[135] reported interconnected mesoporous carbon hollow nanospheres (iMCHS) as an effective matrix to hold sulfur particles (Figure 8c). The mesoporous carbon shell provided conductive paths to individual sulfur particles, thereby ensuring high sulfur utilization. As a result, the iMCHS/S cathode delivered a high capacity of 292 mAh g^{-1} after 200 cycles. Further, functionalized and heteroatom-doped porous carbon materials were prepared to chemically adsorb polysulfides.[136,137] Xiao *et al.*[136] synthesized S, N-doped porous carbon with 3D tubular holes for sulfur storage. The uniform dispersion and incorporation of sulfur by covalent bonds in the carbon host were enabled by a vapor-infiltration method at high temperatures. Interestingly, the covalently bonded sulfur inhibited the formation of soluble polysulfide during cycling in the 1M $NaClO_4$ PC electrolyte. Together with the strong polarity of the S, N-doped carbon to restrict sulfur diffusion, the cathode showed excellent long-term cycling stability of 1000 cycles and rate capabilities of 543 mAh g^{-1} at 5 A g^{-1}. Ultra-microporous carbon/sulfur[138] and SPAN[139] proven successful in LSBs have also been used in RT-SSBs to eliminate the problematic polysulfides by transforming the Na-S reaction from “solid-liquid-solid” to “solid-solid” phase transformations.

As shown in Figure 8d, metastable small sulfur molecules (S_{2-4}) were confined in microporous carbon.[138] In the confined space, NaS_2 can only be converted to small S_{2-4} molecules instead of the large S_8 ring during charing, further excluding the possible formation of souble polysulfides. The "solid-solid" conversion SSB lead to a high specific capacity of 1610 mAh g^{-1} after 200 cycles.

Although porous carbon can physically constraint polysulfides for enhanced reversibility in RT-SSBs, carbon alone is apparently insufficient to accelerate the Na-S conversion.[140] The use of catalysts has become main stream to improve electrochemical performance by engineering active sites to accelerate the diffusion-conversion process of polysulfides.[141,142] For metal catalysts in RT-SSB, Zhang *et al*.[130] loaded transition-metal (M = Fe, Cu, and Ni) nanoclusters on hollow carbon nanospheres (HC)/sulfur composites. The M-S chemical bonds assisted the immobilization of sulfur and enhanced the activity and conductivity of the cathode. The battery thus remained at a high capacity of 394 mAh g^{-1} after 1000 cycles at 0.1A g^{-1}. Ni is another representative metallic catalyst in RT-SSBs. Guo *et al*.[143] reported a 3D network (Ni-NCFs) host composed of nitrogen-doped carbon fibers (NCFs) and Ni hollow spheres. Each nickel hollow sphere could fully accommodate the volume expansion of sulfur during cycling and the nickel atoms displayed great catalytic effects (Figure 8e). The cross-linked carbon fibers surrounding the nickel hollow sphere allowed the electrons to transport unimpeded, thus enhancing the conductivity of the electrodes. The results showed the conductive Ni-NCFs host could accelerate electrochemical reaction kinetics by catalyzing the transformation of liquid polysulfide to solid Na_2S. Yan *et al*.[144] prepared a FeS_2 nanograins/ hierarchical carbon matrix (FeS_2@NCM) as host. The hierarchical carbon confined polysulfides and FeS_2 nanograins absorbed and catalyzed

polysulfides. Compared to pure HCM, the FeS_2@NCM exhibited a better reaction kinetic (Figure 8f). The cell delivered a reversible capacity of 395 mAh g^{-1} after 850 cycles at 1 A g^{-1}.

3.2 K-S batteries

As another member of alkali MSB, the K-S battery (KSB) technology is just demonstrated possible compared to the Li-S and Na-S systems. Similar to LSBs, the reaction process of KSB also involves complicated chemical and electrochemical reactions (Figure 9a).[145] Besides the specified problems for Li/Na-S batteries that also exist for KSB, potassiation of sulfur cathodes has a much larger volume change (300% for S →K_2S vs. 80% for S →Li_2S).[146] Moreover, it still opens to debate about the detailed reaction processes in KSBs owing to the difficulties in analyzing the potassium polysulfides such as K_2S_8, K_2S_5, and K_2S_3.[147] The final discharging products can be K_2S_3 (Figure 9b),[148] K_2S_2,[145] or K_2S[147,149] (Figure 9c), depending on the electrode material and electrolyte structure. The reaction pathway for most KSB is that sulfur is reduced to long-chain polysulfides, short-chain polysulfides, finally to K_2S_3 (Figure 9c). The discharge, charge, and overall reaction are shown as below:

$$\text{Discharge: } 3S + 2K^+ + 2e^- \rightarrow K_2S_3 \quad (19)$$

$$\text{Charge: } K_2S_3 \rightarrow 3S + 2K^+ + 2e^- \quad (20)$$

$$\text{Overall: } 3S + 2K \leftrightarrow K_2S_3 \quad (21)$$

The final product to be K_2S_3 rather than K_2S may be caused by the low reactivity between sulfur and large K ion in the liquid electrolyte.

A survey of the recent process in KSB research indicates that the knowledge gained on the path of developing LSB and RT-SSB provides paramount guidance towards dealing with the shuttle effect and slow reaction kinetics in KSBs.[147-151] For example, the ultramicroporous carbon/S_{2-4} cathode succeeded in long-term LSBs,[58,59] and RT-SSBs[138] were also studied in KSBs.[151] XPS

and theoretical calculations analyses revealed that K_2S was the final potassiation product through the "solid-solid" reaction of $2K + S \rightarrow K_2S$, leading to a theoretical capacity of 1672 mAh g^{-1}. The reaction product is different from the K_2S_3 for CMK-3/S [148] and the K_2S_2 for K_2S_2/C.[145] Such a disparity was interpreted by theoretical calculations which proposed a disproportionation reaction of K_2S_2 to form thermodynamically stable K_2S as the final potassiation product. The microporous carbon/small sulfur cathode showed a reversible capacity of 869.9 mAh g^{-1} after 150 cycles. Modified separator, high concentrated electrolyte, and electrocatalyst have also been developed to regulate K-S conversions.[147,152] For example, to promote the reduction kinetics from K_2S_3 to K_2S, Lai *et al*. [153] reported imidazole-solvated copper catalysts to weaken the S-S bond of K_2S_3 and promote the formation of K_2S, thus achieving a high sulfur capacity of 922 mAh g^{-1}. In order to suppress the polysulfide diffusion in KSBs, Ge *et al*.[154] prepared N-doped Co nanoclusters as catalysts and coupled them with N-doped porous carbon. Both the N-doped carbon and Co nanoclusters can entrap polysulfides. Polysulfide can be smoothly converted on the surface of the Co nanocluster catalyst, thus fundamentally suppressing the shuttle effect in KSBs.

3.3 Mg-S batteries

Mg-S batteries have the highest volumetric energy density and lowest volume expansion among the MSBs (as shown in Table 1). In addition, they display a safety superiority due to the nonvulnerable Mg dendrite formation during Mg plating/stripping in Mg anodes. The safe Mg-S battery would be able to deliver a high theoretical capacity of 1675 mAh g^{-1} and energy density of 1330 Wh kg^{-1} by forming a Mg_2S final product. The high abundance of both sulfur and Mg also appeals Mg-S battery to be a sustainable energy storage system. The key challenge

impeding the development of Mg-S battery is now the lack of compatible electrolytes for the high-valent Mg metal and effective transport of Mg^{2+} between anodes and cathodes.[155]

The first Mg-S battery was reported in 2011 using a non-nucleophilic electrolyte derived from hexamethyldisilazide magnesium chloride (HMDSMgCl) and $AlCl_3$,[156] which broke the long-term difficulty in finding a non-nucleophilic electrolyte that was chemically compatible with both sulfur cathode and Mg metal anode. Although this pioneering work only cycled two times with a capacity degradation from 1200 to 395 mAh g^{-1}, it constituted the first step towards developing reversible Mg-S batteries. Later, the receipt to synthesize chloride electrolyte was simplified by a one-step reaction between magnesium-bis(hexamethyldisilazide) [$(HMDS)_2Mg$] and $AlCl_3$ in different ethers. The simplified synthesis route made it possible to further study and curb the Mg-S reaction pathways.[157] When a S/CMK400PEG cathode was discharged in diglyme/PP14TFSI/$(HMDS)_2Mg$ electrolyte, it was found that the S_8 was reduced to soluble Mg polysulfide (MgS_4), insoluble MgS_2, and finally to the MgS, indicating an overall electrochemical reaction of S + Mg → MgS.[158] Similar to LSBs, the reduction process associated with soluble polysulfides is much faster than the solid conversion from polysulfides to MgS (Figure 9d).[159] Bieker *et al.*[160] studied the chemical stability and solubility of chemically prepared Mg_2S_8 and Li_2S_8 in various electrolytes by UV/vis spectroscopy. They found that the magnesium polysulfide had very similar disproportionation and dissociated equilibria as observed for LiPSs. This finding implicates the possibility to cycle Mg-S batteries in the high-ε electrolyte to amplify the formation of beneficial $S_3^{\bullet-}$.[161]

The unfavorable electrolyte has thus far been considered the 'Achille's heel' on the path to developing stable Mg-S batteries. To mitigate this challenge, $Mg[TFSI]_2$-diglyme was cycled in Mg-S cells but failed quickly due to the severe passivation layer of MgS and S-O on Mg metal.

$MgCl_2$ was added to the above electrolyte to facilitate Mg plating by removing the detrimental passivation layers on Mg, thus giving rise to a 69% capacity retention after 110 cycles.[162] Nevertheless, chloride-containing electrolytes would severely corrode the Mg metal. The community further explored non-corrosive electrolytes for stable Mg-S batteries. *Zhao et al*.[163] investigated a magnesium fluoroalkoxy borate electrolyte (MgBOR(hfip)/DME) for Mg-S batteries. The Cl-free Mg electrolyte allowed 100 times Mg stripping/plating with high Coulombic efficiencies of >98%. The compatibility of the MgBOR(hfip) electrolyte and sulfur cathodes were also demonstrated excellent with a reversible capacity of 200 mAh g^{-1} after 100 cycles. Furthermore, LiTFSI additive was introduced into the $(HMDS)_2Mg$-based electrolyte to enhance the reversibility of Mg-S chemistry.[164] Two possible mechanisms were suggested for the enhanced reversibility: (i) Li^+ may participate in the cathode reaction to for hybrid Mg/Li polysulfides, or (ii) the hard Lewis acid Li^+ coordinates to low order Mg-polysulfides, thus enhancing the solubility and lowering the reoxidation energy barrier of polysulfides, finally making them electrochemically active. The LiTFSI-mediated electrolyte increased the reversible capacity from 200 mAh g^{-1} to 1000 mAh g^{-1} for more than 30 cycles.

The performance improvement in Mg-S batteries has also been demonstrated by using highly conductive carbon materials as sulfur hosts. For instance, sulfur particles were incorporated with carbon black, carbon nanotubes, graphene to improve the sulfur utilization in Mg-S batteries.[165-171] Li *et al*.[168] reported a N, Co co-doped carbon framework as effective S support where the Co catalyst, polar N-dopant and the porous carbon structure work synergistically to improve the capacity reversibility, rate and cycling performance. Furthermore, microporous carbon/small sulfur electrodes were also explored to decrease the shuttle effect in Mg-S batteries.[169]

3.4 Ca-S batteries

In comparison to the Mg-S battery research, another alkaline-earth metal Ca-S battery has just been demonstrated regarding the proof-of-concept. The volume capacity and reduction potential of Ca metal are close to those of metallic Li (2073 mAh cm^{-3} Vs. 2044 mAh cm^{-3} and -2.9V vs. SHE Vs. -3.04V vs. SHE).[172,173] Fortunately, Ca exhibits a much higher elemental abundance of 41500 ppm than the 20 ppm for Li in the Earth's crust (Table 1). These merits suggest the divalent Ca possesses a high potential couple with sulfur cathodes as high-energy and safe Ca-S batteries. However, the lack of compatible electrolytes for reversible Ca metal anode and sulfur cathode restricts the Ca-S technology. So far, only three papers showed reversible Ca-S batteries. Yu *et al*.[174] introduced $LiCF_3SO_3$ mediator into $Ca(CF_3SO_3)$/TEGDME electrolyte to realize the first reversible Ca-S battery in 2019. The Li-ion in the electrolyte can react with the redox products of calcium polysulfides and facilitate ion diffusion in bulk electrolyte and the SEI layer. This pioneering Ca-S cell showed a high discharge capacity of 800 mAh g^{-1}. However, these cells consumed $LiCF_3SO_3$ to form irreversible Li_2S, leading to the loss of capacity and limited lifetime of the batteries. Following, Li *et al*.[175] reported a high-voltage Ca-S cell (2.1 V) with the novel electrolyte of calcium tetrakis(hexafluoroisopropyloxy) borate $Ca[B(hfip)_4]_2$/DME. In the ether-based electrolyte, the reduction pathway of sulfur is very similar to that in LSBs, *e.g.*, sulfur was reduced to soluble polysulfides and then to solid CaS (Figure 10a).[172] Insights into the electrochemical mechanism governing the Ca-S chemistry were also intensively examined by X-ray photoelectron spectroscopy and X-ray absorption spectroscopy.[172] These investigations demonstrate the possibility of exploring high-energy and sustainable Ca-S batteries.

3.5 Al-S batteries

Al-S battery holds the potential to be the cheapest MSBs because Al is the most abundant metal element in the Earth's crust. Each Al atom provides 3 electron transfer, thus achieving a high

specific gravimetric capacity of 2980 mAh g^{-1} and volumetric capacity of 8050 mAh cm^{-3}, due to its relatively high density of 2.7 g cm^{-3}. Al-S battery can attain a high theoretical energy density of 1300 Wh kg^{-1} at an operating voltage of 1.23 V. Batteries assembled with high capacity and low-cost Al and sulfur have attracted increasing research attention.

The study of Al-S batteries can be traced back to the 1980s when the first nonaqueous Al-S battery was propped by Marrassi *et al.*[176] in 1977 and the aqueous Al-S battery was initiated by Licht *et al*.[177] in 1993. Although the concept was proposed almost 30 years ago, the development of reversibly high energy Al-S batteries is still at its infancy. The main challenge lies in the lack of compatible electrolytes and feasible cathodes.[178,179] Different from other MSBs operated in ether or carbonate-based electrolytes, most Al-S batteries operate in ionic liquid electrolytes or deep eutectic solvent-based electrolytes. The mixture of anhydrous aluminum chloride ($AlCl_3$) and 1-ethyl-3-methylimidazolium chloride (EMIC) ionic liquid is by far the most widely used electrolyte in Al-S batteries.[180-185] The Al-S reaction process in [EMIC]/$AlCl_3$ was described as (Figure 10b): [186]

$$\text{Anode: } 2Al + 14AlCl_4^- \leftrightarrow 8Al_2Cl_7^- + 6e^- \quad (22)$$

$$\text{Cathode: } 8Al_2Cl_7^- + 6e^- + 3S \leftrightarrow Al_2S_3 + 14AlCl_4 \quad (23)$$

$$\text{Overall: } 2Al + 3S \leftrightarrow Al_2S_3 \quad (24)$$

In the ionic liquid electrolyte system, a microporous carbon/S cathode was cycled as a rechargeable Al-S battery.[178] By confining sulfur in micropores, the sulfur and Al undergo solid-state conversion. The microporous C/S cathode delivered a high capacity of 1000 mAh g^{-1}, even after 20 cycles (Figure 10c). The successful implementation of the Al-S cell is attributed to the improved oxidation kinetics of AlS_x by encapsulating sulfur from electrolyte attack and shortening the ion diffusion path with nanostructures. It is noted that there is not yet a standard

electrolyte developed for Al-S systems, thus detailed battery reaction mechanisms are elusive and preliminary.

In order to extend the cycle life of Al-S batteries, a carbonized metal-organic framework (MOF) with Cu was prepared to hold sulfur particles.[187] The Cu in the carbon matrix can improve the conductivity of the matrix so that it decreased the sulfur conversion barrier. In addition, XRD and Auger spectrum analyses revealed S–Cu ionic clusters in the carbonized MOF/S composite, which facilitated the redox reaction and sulfur reversibility during cycling. As a result, the Al-S battery achieved a reversible capacity of 460 mAh g^{-1} at the 500th cycle. To modify the electrolyte structure, Yu *et al.*[188] introduced $LiCF_3SO_3$ into the [EMIM]$AlCl_4$ ionic liquid (denoted as Li^+-Al[EMI]Cl_4, see Figure 10d). The presence of Li^+-ion mediator indicated more soluble short chain Al polysulfides, which lowered the electrochemical kinetic barrier for reduction or oxidation of Al polysulfides. XPS results and DFT calculations further suggested that the Li^+ ions promoted the reactivation of sulfide species by suppressing the formation of Al=S bonds upon full discharging. Operating in the Li^+-mediated electrolyte, the Al-S battery achieved 50 cycles with a residual capacity of 600 mAh g^{-1}. To mitigate the high dissociation energy from $Al_2Cl_7^-$ to Al^{3+} in [EMIM]$AlCl_4$ ionic liquid electrolyte, Br atom was incorporated to form $Al_2Cl_6Br^-$ for lower dissociation energies, which is another efficient method to improve the kinetic process in the Al-S system.[189] Another main obstacle for the Al-S system is the low reduction potential of sulfur (~1V vs. SHE) in [EMIM]$AlCl_4$. Li *et al.*[179] reported to replace EMIC with urea to cooperate with $AlCl_3$ for high voltage Al-S batteries. The reaction pathway changed from the redox of sulfur ↔ Al_2S_3 in EMIC/$AlCl_3$ electrolyte to $AlSCl_7$ ↔ sulfur in $AlCl_3$/urea electrolyte. The latter contributed a ~1.8V discharging potential, which is much

higher than the ~0.5V for the former reaction path (Figure 10e). Benefiting from the high electrochemical potential, the Al-S battery can run 200 cycles at around 1.8V.

According to above examinations of the Li-free MSBs, it reveals that studies on the emerging battery systems are evidently at the early stage. Compared to LSBs, the high abundance of elemental resources and potentially high energy density for Li-free metal anodes (Table. 1) motivate the exploration of these new MSB technologies. However, insights show that the emerging MSBs suffer from similar critical issues encountered in LSBs, such as insulation of active materials and polysulfide shutting effects, coupled with challenges associated with the lack of suitable electrolyte for stable metal anode striping/plating, sluggish reaction kinetics and poor cycling efficiencies. In particular, MSBs using the alkali-metal anodes (i.e., Na, K) face severe safety issues arising from the high chemical activity and dendrite-plating behaviors of Na and K. Although alkaline-earth MSBs (Mg-S, Ca-S, Li-S) pose better safety due to the dense and dendrite-free plating of metal anodes, these systems encountered challenges of sluggish ion conductivity, the lack of compatible electrolyte, and poor cyclic stability. A general problem for Li-free MSBs is the huge volume expansion of sulfur particles during lithiation (*i.e.*, 309% in K-S battery and 180% for Na-S battery), stemming from larger ionic radius of Na^+, K^+ than Li^+. The large volume changes could cause electrode degradation and rapid battery failure. Robust hosts with flexible and abundant space are thus highly wanted to accommodate this issue. Last but no least, understandings for the conversion mechanisms in Li-free MSBs are far from sufficient and solid. Some contradictory descriptions for the K-S reaction are even reported. Therefore, intensive characterizations together with theoretical calculations are recommended to further unveil their working processes before achieving profound improvements in electrochemical performance.

We summarized the performance of the state-of-the-art lithium-free metal sulfur batteries. In terms of the cathodes, constricting the carbon matrix and introducing catalysts are the most common strategies to prepare sulfur cathodes. Due to the different properties of the metal anode, different electrolyte systems are applied to different MSBs. Exploring suitable electrolytes is crucial for the development of lithium-free metal sulfur batteries. Except for Na-S batteries, other Li-free battery systems that can operate stability for more than 1000 cycles have not been reported. In addition, some batteries only work for a few dozen cycles and display fast capacity decaying. Sulfur utilization and cycle stability should be further improved to satisfy the energy requirement.

4. In situ characterizations to understand sulfur conversion mechanisms

The multi-step metal-sulfur reactions occurring during cycling lead to complex reaction mechanisms. An in-depth and systematic understanding of the reaction processes in MSBs will be beneficial to offer radical strategies to address the fundamental problems hindering their practical applications.[8] Manifold in-situ/operando characterization methods have been undertaken to quest unveiling the underlying mechanisms in MSBs, such as transmission electron microscopy (TEM),[13,93,190-192] ultraviolet-visible (UV-vis) absorption spectroscopy,[32,193-196] XANES,[197-200] and XRD[20,179,200-203]. Each characterization has its specific strength in disclosing the structural or/and compositional evolutions.

In-situ XRD is an effective method to probe the phase evolutions during charging and discharging, especially for the crystalline S_8 and metal sulfides.[20,179,201] As mentioned in Section 2.1, *in-situ* XRD study demonstrated the irreversibility of α-sulfur phase after the 1st cycle in LSBs.[25] Soluble LiPSs have long been considered undetectable by XRD, due to their lack of long-range order and rapid molecular reorientation in the bulk electrolyte. This has been taken

for granted until Conder *et al*.[9] found that long-chain LiPSs were visible by adsorbing at the silica surface of a glass-fiber separator. During lithiation, two broad peaks at 25.56° and 28.32° were formed along with the rapid disappearance of crystalline α-sulfur peaks. The new peaks were assigned to long-chain LiPSs, whose intensity decreased over time towards the end of discharging processes, referring the reduction of LiPSs into lithium sulfides (Figure 11a). However, the LiPSs peaks did not completely disappear during the whole discharging/charging process, indicating long-chain LiPSs absorbed on glass-fiber separators preserved, for this reason, a lot of irreversible charge capacities were observed during cycling. They also directly monitored LiPSs in electrolytes without silica absorbers, which showed negligible XRD peaks, indicating the importance of adsorption to form organized LiPS layers. *In-situ* XRD has also been utilized to probe the phase evolutions in RT-SSBs.[18, 27] By monitoring the reaction process of a NiS_2/N-doped CNT/S cathode, it showed that the XRD peak of crystalline sulfur disappeared after the first cycle, and reversible (dis)appearance of polysulfide (Na_2S_x) and Na_2S occurred in the following cycles, illustrating a polysulfides and sodium sulfides conversion mechanism (Figure 11b).[203] The reversible redox process between $AlSCl_7$ and S, S and Al_2S_3 in Al-S batteries has also been verified by *in-situ* XRD measurements (Figure 11c).[179]

Apart from monitoring the intrinsic reaction processes, *in-situ* XRD studies can provide circumstantial evidences to the favorable catalytic effect in MSBs.[204-207] According to the clear appearance and disappearance of sulfur and Li_2S peaks during cycling in an *in-situ* XRD testing, Girt *et al*.[206] demonstrated that the heterostructure MoN-VN catalyst could regulate the LiPSs diffusion and complete sulfur conversion during cycling, which was in sharp contrast to the MoN/S cathode retaining the α-S_8 peaks during the whole discharging process. This result was in accordance with the high capacity of 708 mAh g^{-1} at 2C for MoN-VN-based LSBs. He *et al*.[208]

compared the XRD patterns of carbon/S and MoB/S cathodes under synchrotron *in-situ* XRD measurement. Residual α-S_8 peaks were detectable but the peaks for lithiation product Li_2S were indiscernible at the end of discharge for C/S, whereas, the α-S_8 peaks in MoB/S cathodes disappeared completely at the initial discharge associated with the increasing peak intensity of Li_2S (Figure 11d). Such distinctive results illustrated that MoB catalyst can restrict LiPSs diffusion and facilitate the Li_2S deposition/dissolution. Similarly, *in-situ* XRD characterizations illustrated the reversible redox between S and Na_2S in Mo_2N–W_2N catalyst-mediated RT-SSB.[209] *In-situ* XRD has also been of service to identify the selective catalytic mechanisms in RT-SSBs. Distinctive XRD peak changes from Na_2S_4 to Na_2S illustrates that in RT-SSBs with the Fe single-atom catalyst, short-chain polysulfides are ready to be catalyzed into Na_2S. Whereas, the generation of long-chain polysulfides is catalytically promoted in single-atom Pt modified RT-SST.[22]

Besides keeping track of sulfur phase change, *in-situ* XRD is also a powerful tool to probe the phase evolution of electrocatalysts in MSBs.[210,211] Wang *et al.*[210] demonstrated the function of niobium tungsten oxide (NWO) in a working LSB. In the discharging process, the NWO peaks shifted to lower angles arising from the formation of Li_xNWO. The Li_xNWO was demonstrated to plays a unique role in promoting the LiPS conversion efficiency by acting as a Li-transfer bridge between LiPSs and Li_2S, thus jumping across the sluggish solid-solid conversion from Li_2S_2 to Li_2S. In addition, the Li_xNWO exhibited stronger chemical interactions with LiPSs. Likewise, Liu *et al.*[211] observed the reversible lithiation and delithiation of TiS_2 catalyst in TiS_2/S cathodes. This work claimed that the lithiated TiS_2 was the conductive catalyst and strong LiPS adsorber, rather than TiS_2, revealing the dynamic nature of electrocatalysts during discharging/charging in LSBs. For Mg-S battery, a reversible chlorination of Ag metal catalyst to

precent Ag_2S formation for shielding the sulfur active material was demonstrated by an *in-situ* XRD study.[21]

In-situ TEM is a powerful tool to understand the electrochemical reaction dynamics of MSBs at high spatial and temporal resolutions by revealing the morphological evolution, phase change and chemical composition transformations.[13,93,190-192] _ENREF_172 By observing the lithiation process of sulfur particles sealed in CNTs under *in-situ* TEM, Kim *et al*.[14] reported that sulfur was directly reduced to Li_2S without the formation of any intermediates and the Li-S reaction front was flat, suggesting the interface of Li_2S/S possibly to be electrically conductive (Figure 12a). Our group studied the volume expansion of sulfur particles in meso- and microporous CNFs during lithiation by using *in-situ* TEM.[13] It was found that the lithiation product, Li_2S, was constrained within the microporous CNF with only ≈35% volume expansion and the carbon host remained intact without fracture. In contrast, the mesoporous CNF/S electrode exhibited a larger volume expansion of over 61%, and overflowing of Li_2S, a testament to its poor cyclic stability in real batteries. Unlike the direct Li_2S formation in LSB studies, under the same measurement condition, sodiation of sulfur involved a series intermediates, including Na_2S_x ($x \geq 6$), Na_2S_5, Na_2S_4, Na_2S_2, before approaching Na_2S (Figure 12b).[192] More interestingly, large proportion of sulfur would not be converted to Na_2S in RT *in-situ* TEM study. When increasing the operating temperature to 200-300 ℃, the discharge product would be Na_2S_2 and Na_2S without sulfur residuals, which was attributable to the improved electron/ion transport kinetics at high temperatures.

Although these open-cell setups using metal/metal oxide as counter electrode/electrolyte could provide useful information on the metal-sulfur reactions, they are infeasible to study the formation and conversion of soluble polysulfides in real batteries. To mitigate this issue, our

group constitutes the first step towards realizing the real-time observation of the nucleation and growth of solid lithium sulfides from soluble polysulfides by employing a graphene liquid cell (GLC)-based liquid *in-situ* TEM technique (Figure 12c).[93] By analyzing the lithiation of sulfur in a series of hollow spheres, including nonpolar carbon, polar/nonpolar TiO_2-TiN/C sphere, nonpolar/polar C/TiO_2-TiN sphere, it was found that the sulfur host with inner polar materials indicated the most favorable formation of lithium sulfides without the risk of polysulfide diffusion. For the C (outer wall)/TiO_2-TiN (inner wall)/S structure, it is presented that the formation of lithium sulfides followed diffusion-controlled-to-reaction-limited growth kinetics and a crystalline-to-amorphous phase transition. The correlations established among the nucleation and growth dynamics of lithium sulfides, the immobilization of polysulfides and the chemical nature of host materials not only provided a whole picture of the unique liquid/solid transition in LSBs but also offered fundamental guidelines to design high-performance sulfur cathodes. In order to understand the polysulfide electrochemistry, Wang *et al.*[212] constructed a hollow CNT/S-ionic liquid electrolyte cell that allowed real-time imaging of polysulfides evolutions in LSB using an environmental TEM (Figure 12d). They found that the long-chain LiPS would be coordinated immediately by Py_{14}^+ cation in ionic liquid electrolyte, which was mitigated by adding low polarized solvents in the electrolyte thus rendering a rapid polysulfide-to-Li_2S transition.

In-situ UV is a useful tool to qualitatively/quantitatively determine soluble polysulfides in MSB.[213] The peaks referring to Li_2S_8, Li_2S_6, Li_2S_4, and Li_2S_2 can be clearly distinguished by UV-vis (Figure 13a), which makes *in-situ* UV feasible to give insights into the sulfur chemistry in a bulk electrolyte.[32,193,194] Xu *et al.*[194] analyzed the LiPSs transformation in sulfydryl-functionalized graphene nanosheets with sulfur copolymer (S-GSH) cathode. With proceeding

the discharge process, S-GSH was mainly converted to Li_2S_2 and Li_2S_4, then with further lithiation, the Li_2S_4 and Li_2S_2 intermediates were transferred to Li_2S_3 and Li_2S, respectively. During charging, the peaks referring to long-chain polysulfides were trivial. It was thus concluded that the sulfur conversion for S-GSH in LSBs mainly based on S-S bond breakage/formation associated with the formation of short-chain LiPSs. The absence of highly soluble long-chain LiPSs has a prominent effect on immobilizing sulfur and ensuring superior cyclic reversibility to conventional S/rGO counterpart. As mentioned in Section 2.3, $S_3^{\bullet-}$ radical is essential to accelerate the Li_2S precipitation, especially in lean electrolyte condition. By using *in-situ* UV, Zou *et al.*[32] explored the relationship among polysulfide species, reaction pathways and the DN of solvent in LSBs. They demonstrated that the light $S_3^{\bullet-}$ radical was the main reaction intermediate in high-DN solvent (*i.e.*, DMSO), while in low-DN solvent (DOL: DME), the S_4^{2-} was a major intermediate. Through monitoring of the signal changes of polysulfides in electrolytes, Zou *et al.*[214] proposed that large-size alkali metal cations (*i.e.*, Rb^+, K^+) could be more effectively in stabilizing short-chain polysulfides than Na^+ and K^+. For Mg-S battery, the polysulfide structures and concentration evolution in glyme-based electrolyte were surveyed by *in-situ* UV-vis.[215] A reaction pathway was proposed with S_8, S_6^{2-} and S_4^{2-} being present in the electrolyte as shown in Figure 13b.

According to the change in UV-vis reflection intensity, the concentration of sulfur species can also be quantitatively analyzed, which is of importance to precisely confirm the polysulfide regulation effect.[195] For example, Zhou *et al.*[195] monitored the concentration of LiPSs on the surface of anode side to check whether the ultra-high ion-conducting gel polymer (SHGP) electrolyte can suppress the shuttle effect. With the discharge process proceeding, the LiPS reflection intensity changes of LSBs assembled with poly(ethylene oxide) (PEO) and SHGP

electrolytes are shown in Figure 13c. The concentration of soluble Li_2S_8 and Li_2S_6 maintained smaller values for SHGP-assembled LSB, which indicates the effective block of LiPS diffusion. For RT-SSB, soluble long-chain polysulfides would cause shuttle effect and self-discharge while insoluble short-chain polysulfides would slow down the reaction kinetics and passivate conductive hosts. *In-situ* UV-vis analyses of an ultra-microporous carbon/small sulfur cathodes showed no polysulfides during cycling, a testament to its excellent reversiblity.[19]

In summary, *in-situ* characterization techniques have been developed to provide deep insights into the phase transformation, metal polysulfide migration, preservation of active materials with catalysts in MSBs. Apart from the representative *in-situ* XRD, TEM and UV-Vis tools mentioned above, other advanced *ex-situ/in-situ* techniques like Raman, FTIR, and NMR[143,216] have also been widely applied to explore the fundamental issues underpinning the MSB shuttle effect, for example, metal sulfide formation dynamics, the interaction of polysulfide intermediates with electrolyte and catalysts. The summary of representative *in situ/operando* characterization for MSB study is listed in Table 2. It is believed that a combination of various techniques offering characterized information would lead to more integrated and insightful understandings of metal-sulfur mechanics for advanced MSBs.

5. Summary and perspective

In recent years, tremendous interests have been aroused to investigate MSBs as promising alternatives to conventional LIBs, due to the exceptionally high theoretical energy densities and the low cost of sulfur materials. This review is dedicated to summarizing the most recent advances in understanding sulfur conversion mechanisms and effective regulation strategies to achieve long-life and high energy MSBs. We have initially summarized the current progress in LSBs and emphasized the Li-S reaction mechanisms and the roles of the current collectors,

electrolytes and electrocatalysts on regulating the LiPSs diffusion, reaction kinetics, and Li_2S deposition behaviors. It is unambiguous that the research community has built systemic understandings of Li-S electrochemistry with significantly improved battery performance. As a follow-up battery technology developed from Li-S, Li-free MSBs made with Na, K, Mg, Ca and Al-metal anodes have also been summarized and explored in terms of the electrochemical reaction processes, electrode materials and challenges. It shows that strategies developed in LSBs have also been adopted to explore the electrochemical reactions in Li-free MSBs. The polysulfide immobilizing methods and the catalyst design to accelerate sulfur conversion kinetics, for example, have been demonstrated useful in both LSB and Li-free MSBs. *In situ* characterization tools have been demonstrated imperative and constructive in gaining insights into the complex sulfur conversion mechanisms in MSB. Although discernible progress has been achieved so far, various fundamental challenges need to be addressed to promote the further development of MSBs. Based on the progress summarized in this review, we propose several suggestions for the future studies of MSB (Figure 14).

(1) *Understanding the reaction mechanisms in MSBs*. With the assistance of *in-situ/ex-situ* characterizations, we have gained comprehensive insights into Li-S reactions. However, the charge-discharge mechanisms of Li-free MSBs are still quite ambiguous. For example, there are contradictory descriptions on the first discharge step for Mg-S batteries, *i.e.*, some papers report the reduction of S_8 to MgS_4[217] whereas others report MgS_8 as the reduction product.[218] For the well-established LSB system, the studies of sulfur conversion chemistry in lean-electrolyte and high-loading conditions are very limited. The Li-S reaction processes observed under idealized conditions (*i.e.*, electrolyte/sulfur, E/S ratio >10 μL mg^{-1}) shall be significantly different from those in practical conditions (*i.e.*, E/S<4 μL mg^{-1}). Without comprehensively understanding the

conversion mechanisms of metal-sulfur systems, it would be puzzling and difficult to achieve rational regulation of advanced electrode materials for high-performance MSBs.

(2) *Suitable electrolytes for Li-free MSBs*. There are few established electrolytes for the emerging Li-free MSBs. For example, the poor reversibility of Ca metal plating/stripping processes in ether electrolytes also considerably contributed to the short cycle life of a Ca-S battery.[175] Thus, further research should pay more attention to the exploitation of new electrolyte systems for Li-free MSBs. When developing an electrolyte, some principles or lessons shall be followed, namely, (i) the electrolytes should present the compatibility with sulfur species in the cathode side and the ability for reversible metal plating/stripping in the anode side. (ii) Their ability to obstruct polysulfide migration is also required to achieve desirable reversibility and thus long battery cycling life. (iii) The importance of solvents should not be underrated, given their direct influence on the stable polysulfide species (*i.e.*, S_4^{2-} in DME/DOL, $S_3^{\bullet-}$ in DMSO) and the metal sulfide deposition morphologies.[161]

(3) ~~*Electrode structure and*~~ *Catalyst design*. The catalyst materials, especially those with selective and bidirectional catalytic properties, have been demonstrated successfully in regulating sulfur conversion kinetics in advanced LSBs. Catalysts can not only be used as host, but also can be additives introducing into host and separators. To achieve great electrochemical properties, optimizing materials of separators and host design is important. Some studies have also proved the effectiveness of catalysts in improving the performance of Li-free MSB. For instance, in a K-S battery system, the operating voltage is limited to 2.4 V with K_2S_3 formation for CMK-3/S cathode,[148] whereas the charge voltage can arrive at 2.8 V with the final K_2S product for imidazole-solvated copper catalyst mediated cathode;[153] the reported functional separator based on “single-atom array mimic” on the ultrathin metal-organic framework (MOF)

nanosheets can absorb the LiPSs(by Co single-atom array mimic) and guide the Li-ion uniformly deposition.[219] However, the functional mechanisms and structural design for catalysts in Li-free MSBs are still elusive, which requires more investigations in future studies. It is our belief that advances in a more fundamental understanding of the operating principles of various metal-sulfur chemistries by intensive studies in the future will definitely accelerate the implementation of MSBs in practical applications.

(4) Achieve practical cell scale of LSBs and Li-free sulfur batteries

Many great efforts have been devoted to improving the electrochemical performance of LSBs. There are many excellent performances that have been reported, such as the stable operation of more than 2000 cycles,[209,210] working at an ultra-high rate of 40C,[211,212] or performing a high specific capacity than 1200 mAh g^{-1} at 1C.[213,214] However, there is still a large gap between the lab cell level and the practical cell scale. To solve this gap, three important parameters should be emphasized in the further development of LSBs, that is low E/S ratio, low lithium anode with the negative to positive electrode ratio (N/P ratio) and high sulfur loading, which is important to build a high energy density LSBs.[215] To achieve these parameters, optimizing the design of electrolytes, hosts, and separators is very important. Cathode hosts should provide excellent conductive networks, abundant reaction sites for sulfur species conversion and immobilization, and effective electrolyte infiltration. Constructing heterostructures, such as combining electrocatalysts and conductive substrates, is one direction to satisfy these requirements. In terms of electrolytes, the development of highly solvating electrolytes and sparingly solvating electrolyte provide the opportunity to enable the Li-S to operate under lean electrolytes. However, lacking suitable methods to protect the Lithium anode led to the LSBs cannot cycle stably in these electrolytes systems. In terms of separators, developing multifunctional separators to

benefit both cathode and anode sides should be more focused in the future. Furthermore, these parameters and design strategies also should be considered to develop practical Li-free sulfur batteries.

Conflicts of interest

There are no conflicts to declare.

Acknowledgements

This work described in this paper was fully supported by grants from the Research Grants Council of the Hong Kong Special Administrative Region, China (Project No. PolyU25216121, PolyU15303219), the National Natural Science Foundation of China for Young Scholar (Project No. 52102310), the Research Committee of the Hong Kong Polytechnic University under project codes of A-PB1M, 1-BBXK and G-UAMV.

Notes and references

1. Z. W. Seh, Y. Sun, Q. Zhang and Y. Cui, *Chem. Soc. Rev.*, 2016, **45**, 5605-5634.
2. S. F. Ng, M. Y. L. Lau and W. J. Ong, *Adv. Mater.*, 2021, **33**, e2008654.
3. M. Salama, Rosy, R. Attias, R. Yemini, Y. Gofer, D. Aurbach and M. Noked, *ACS Energy Lett.*, 2019, **4**, 436-446.
4. S. H. Chung and A. Manthiram, *Adv. Mater.*, 2019, **31**, e1901125.
5. S. Dorfler, S. Walus, J. Locke, A. Fotouhi, D. J. Auger, N. Shateri, T. Abendroth, P. Hartel, H. Althues and S. Kaskel, *Energy Technol.*, 2021, **9**, 2000694.
6. X. Ji, K. T. Lee and L. F. Nazar, *Nat. Mater.*, 2009, **8**, 500-506.
7. F. Shi, C. Chen and Z.-L. Xu, *Adv. Energy Mater.*, 2021, **3**, 275-301.
8. H. Ye and Y. Li, *InfoMat*, 2022, e12291.
9. J. Conder, R. Bouchet, S. Trabesinger, C. Marino, L. Gubler and C. Villevieille, *Nat. Energy*, 2017, **2**, 17069.
10. Y. Son, J.-S. Lee, Y. Son, J.-H. Jang and J. Cho, *Adv. Energy Mater.*, 2015, **5**, 1500110.
11. L. Zhang, T. Qian, X. Zhu, Z. Hu, M. Wang, L. Zhang, T. Jiang, J. H. Tian and C. Yan, *Chem. Soc. Rev.*, 2019, **48**, 5432-5453.
12. Z. Wang, Y. Tang, L. Zhang, M. Li, Z. Shan and J. Huang, *Small*, 2020, **16**, e2001899.
13. Z.-L. Xu, J.-Q. Huang, W. G. Chong, X. Qin, X. Wang, L. Zhou and J.-K. Kim, *Adv. Energy Mater.*, 2017, **7**, 1602078.
14. H. Kim, J. T. Lee, A. Magasinski, K. Zhao, Y. Liu and G. Yushin, *Adv. Energy Mater.*, 2015, **5**, 1501306.
15. H. Liu, W.-H. Lai, Y. Liang, X. Liang, Z.-C. Yan, H.-L. Yang, Y.-J. Lei, P. Wei, S. Zhou, Q.-F. Gu, S.-L. Chou, H. K. Liu, S. X. Dou and Y.-X. Wang, *J. Mater. Chem. A*, 2021, **9**, 566-574.
16. W. Chen, T. Qian, J. Xiong, N. Xu, X. Liu, J. Liu, J. Zhou, X. Shen, T. Yang, Y. Chen and C. Yan, *Adv. Mater.*, 2017, **29**, 1605160.
17. T. Yang, T. Qian, J. Liu, N. Xu, Y. Li, N. Grundish, C. Yan and J. B. Goodenough, *ACS Nano*, 2019, **13**, 9067-9073.

18. X. Liu, T. Qian, J. Liu, J. Tian, L. Zhang and C. Yan, *Small*, 2018, **14**, e1801536.
19. Q. Guo, S. Li, X. Liu, H. Lu, X. Chang, H. Zhang, X. Zhu, Q. Xia, C. Yan and H. Xia, *Adv. Sci.* , 2020, **7**, 1903246.
20. S. Waluś, C. Barchasz, R. Bouchet, J.-C. Leprêtre, J.-F. Colin, J.-F. Martin, E. Elkaïm, C. Baehtz and F. Alloin, *Adv. Energy Mater.*, 2015, **5**, 1500165.
21. Y. Xu, Y. Zhao, S. Zhao, J. Zhang, J. Li, J. Guo and Y. Zhang, *Energy Storage Mater.*, 2021, **42**, 513-516.
22. W. H. Lai, H. Wang, L. Zheng, Q. Jiang, Z. C. Yan, L. Wang, H. Yoshikawa, D. Matsumura, Q. Sun, Y. X. Wang, Q. Gu, J. Z. Wang, H. K. Liu, S. L. Chou and S. X. Dou, *Angew. Chem. Int. Ed.*, 2020, **59**, 22171-22178.
23. H. Yuan, H.-J. Peng, J.-Q. Huang and Q. Zhang, *Adv. Mater. Interfaces*, 2019, **6**, 1802046.
24. F. Qi, Z. Sun, X. Fan, Z. Wang, Y. Shi, G. Hu and F. Li, *Adv. Energy Mater.*, 2021, **11**, 2100387.
25. S. C. Jung and Y.-K. Han, *J. Power Sources*, 2016, **325**, 495-500.
26. C. Villevieille and P. Novák, *J. Mater. Chem. A*, 2013, **1**, 13089.
27. B. He, W.-C. Li, Y. Zhang, X.-F. Yu, B. Zhang, F. Li and A.-H. Lu, *J. Mater. Chem. A*, 2018, **6**, 24194-24200.
28. N. Liu, G. Zhou, A. Yang, X. Yu, F. Shi, J. Sun, J. Zhang, B. Liu, C. L. Wu, X. Tao, Y. Sun, Y. Cui and S. Chu, *Proc. Natl. Acad. Sci. U.S.A.* , 2019, **116**, 765-770.
29. A. Yang, G. Zhou, X. Kong, R. A. Vila, A. Pei, Y. Wu, X. Yu, X. Zheng, C. L. Wu, B. Liu, H. Chen, Y. Xu, D. Chen, Y. Li, S. Fakra, H. Y. Hwang, J. Qin, S. Chu and Y. Cui, *Nat. Nanotechnol.*, 2020, **15**, 231-237.
30. A. Y. Guangmin Zhou, Guoping Gao, Xiaoyun Yu, Jinwei Xu, Chenwei Liu, Yusheng Ye, Allen Pei, Yecun Wu, Yucan Peng, Yanxi Li, Zheng Liang, Kai Liu, Lin-Wang Wang, Yi Cui, *Sci. Adv.*, 2020, **6**, eaay5098.
31. S. S. Zhang and D. T. Tran, *J. Power Sources*, 2012, **211**, 169-172.
32. Q. Zou and Y. C. Lu, *J. Phys. Chem. Lett.*, 2016, **7**, 1518-1525.
33. Y. Liu, Y. Elias, J. Meng, D. Aurbach, R. Zou, D. Xia and Q. Pang, *Joule*, 2021, **5**, 2323-2364.
34. X. Yu and A. Manthiram, *Phys. Chem. Chem. Phys.*, 2015, **17**, 2127-2136.
35. J. Yan, X. Liu and B. Li, *Adv. Sci.*, 2016, **3**, 1600101.
36. F. Y. Fan, W. C. Carter and Y. M. Chiang, *Adv. Mater.*, 2015, **27**, 5203-5209.
37. Z.-L. Xu, N. Onofrio and J. Wang, *J. Mater. Chem. A*, 2020, **8**, 17646-17656.
38. G. Zeng, Y. Liu, D. Chen, C. Zhen, Y. Han and W. He, *Adv. Energy Mater.*, 2021, **11**, 2102058.
39. C. Luo, X. Liang, Y. Sun, W. Lv, Y. Sun, Z. Lu, W. Hua, H. Yang, R. Wang, C. Yan, J. Li, Y. Wan and Q.-H. Yang, *Energy Storage Mater.*, 2020, **33**, 290-297.
40. Z. L. Xu, S. Lin, N. Onofrio, L. Zhou, F. Shi, W. Lu, K. Kang, Q. Zhang and S. P. Lau, *Nat. Commun.*, 2018, **9**, 4164.
41. Q. Lin, L. Huang, W. Liu, Z. Li, R. Fang, D. W. Wang, Q. H. Yang and W. Lv, *Phys. Chem. Chem. Phys.*, 2021, **23**, 21385-21398.
42. L. Kong, J.-X. Chen, H.-J. Peng, J.-Q. Huang, W. Zhu, Q. Jin, B.-Q. Li, X.-T. Zhang and Q. Zhang, *Energy Environ. Sci.* , 2019, **12**, 2976-2982.
43. T. Zhang, M. Marinescu, S. Walus, P. Kovacik and G. J. Offer, *J. Electrochem. Soc.*, 2017, **165**, A6001-A6004.
44. Y. Yang, G. Zheng, S. Misra, J. Nelson, M. F. Toney and Y. Cui, *J. Am. Chem. Soc.*, 2012, **134**, 15387-15394.
45. H. Noh, J. Song, J.-K. Park and H.-T. Kim, *J. Power Sources*, 2015, **293**, 329-335.
46. G. Tan, R. Xu, Z. Xing, Y. Yuan, J. Lu, J. Wen, C. Liu, L. Ma, C. Zhan, Q. Liu, T. Wu, Z. Jian, R. Shahbazian-Yassar, Y. Ren, D. J. Miller, L. A. Curtiss, X. Ji and K. Amine, *Nat. Energy*, 2017, **2**, 17090.

47. M. R. Kaiser, Z. Han, J. Liang, S.-X. Dou and J. Wang, *Energy Storage Mater.*, 2019, **19**, 1-15.
48. Y. Feng, Y. Zhang, G. Du, J. Zhang, M. Liu and X. Qu, *New J. Chem.*, 2018, **42**, 13775-13783.
49. L. C. Gerber, P. D. Frischmann, F. Y. Fan, S. E. Doris, X. Qu, A. M. Scheuermann, K. Persson, Y. M. Chiang and B. A. Helms, *Nano Lett.*, 2016, **16**, 549-554.
50. C. Y. Chen, H. J. Peng, T. Z. Hou, P. Y. Zhai, B. Q. Li, C. Tang, W. Zhu, J. Q. Huang and Q. Zhang, *Adv. Mater.*, 2017, **29**, 1606802.
51. D.-Q. Cai, J.-L. Yang, T. Liu, S.-X. Zhao and G. Cao, *Nano Energy*, 2021, **89**, 106452.
52. G. Zhou, H. Tian, Y. Jin, X. Tao, B. Liu, R. Zhang, Z. W. Seh, D. Zhuo, Y. Liu, J. Sun, J. Zhao, C. Zu, D. S. Wu, Q. Zhang and Y. Cui, *Proc. Natl. Acad. Sci. U.S.A.*, 2017, **114**, 840-845.
53. Y.-C. Lu, Q. He and H. A. Gasteiger, *J. Phys. Chem. C*, 2014, **118**, 5733-5741.
54. M. Li, Y. Zhang, Z. Bai, W. W. Liu, T. Liu, J. Gim, G. Jiang, Y. Yuan, D. Luo, K. Feng, R. S. Yassar, X. Wang, Z. Chen and J. Lu, *Adv. Mater.*, 2018, **30**, e1804271.
55. J. Guo, Y. Huang, S. Zhao, Z. Li, Z. Wang, G. Shao and J. Liu, *ACS Nano*, 2021, **15**, 16322-16334.
56. H. Wang, Y. Shao, H. Pan, X. Feng, Y. Chen, Y.-S. Liu, E. D. Walter, M. H. Engelhard, K. S. Han, T. Deng, G. Ren, D. Lu, X. Lu, W. Xu, C. Wang, J. Feng, K. T. Mueller, J. Guo, K. R. Zavadil and J.-G. Zhang, *Nano Energy*, 2020, **76**, 105041.
57. G. Li, S. Wang, Y. Zhang, M. Li, Z. Chen and J. Lu, *Adv. Mater.*, 2018, **30**, e1705590.
58. Z. Li, L. Yuan, Z. Yi, Y. Sun, Y. Liu, Y. Jiang, Y. Shen, Y. Xin, Z. Zhang and Y. Huang, *Adv. Energy Mater.*, 2014, **4**, 1301473.
59. S. Xin, L. Gu, N. H. Zhao, Y. X. Yin, L. J. Zhou, Y. G. Guo and L. J. Wan, *J. Am. Chem. Soc.*, 2012, **134**, 18510-18513.
60. E. Markevich, G. Salitra, A. Rosenman, Y. Talyosef, F. Chesneau and D. Aurbach, *J. Mater. Chem. A*, 2015, **3**, 19873-19883.
61. R. Dominko, A. Vizintin, G. Aquilanti, L. Stievano, M. J. Helen, A. R. Munnangi, M. Fichtner and I. Arcon, *J. Electrochem. Soc.*, 2017, **165**, A5014-A5019.
62. X. Li, M. Banis, A. Lushington, X. Yang, Q. Sun, Y. Zhao, C. Liu, Q. Li, B. Wang, W. Xiao, C. Wang, M. Li, J. Liang, R. Li, Y. Hu, L. Goncharova, H. Zhang, T. K. Sham and X. Sun, *Nat. Commun.*, 2018, **9**, 4509.
63. X. Zhang, K. Chen, Z. Sun, G. Hu, R. Xiao, H.-M. Cheng and F. Li, *Energy Environ. Sci.* , 2020, **13**, 1076-1095.
64. W. J. Chung, J. J. Griebel, E. T. Kim, H. Yoon, A. G. Simmonds, H. J. Ji, P. T. Dirlam, R. S. Glass, J. J. Wie, N. A. Nguyen, B. W. Guralnick, J. Park, A. Somogyi, P. Theato, M. E. Mackay, Y. E. Sung, K. Char and J. Pyun, *Nat. Chem.*, 2013, **5**, 518-524.
65. G. Hu, Z. Sun, C. Shi, R. Fang, J. Chen, P. Hou, C. Liu, H. M. Cheng and F. Li, *Adv. Mater.*, 2017, **29**, 1603835.
66. H. Kim, J. Lee, H. Ahn, O. Kim and M. J. Park, *Nat. Commun.*, 2015, **6**, 7278.
67. H. Zhou, F. Yu, M. Wei, Y. Su, Y. Ma, D. Wang and Q. Shen, *Chem Commun.*, 2019, **55**, 3729-3732.
68. Z. Shadike, H. S. Lee, C. Tian, K. Sun, L. Song, E. Hu, I. Waluyo, A. Hunt, S. Ghose, Y. Hu, J. Zhou, J. Wang, P. Northrup, S. M. Bak and X. Q. Yang, *Adv. Energy Mater.*, 2019, **9**, 1900705.
69. X. Zhang, G. Hu, K. Chen, L. Shen, R. Xiao, P. Tang, C. Yan, H.-M. Cheng, Z. Sun and F. Li, *Energy Storage Mater.*, 2022, **45**, 1144-1152.
70. Z. Pan, D. J. L. Brett, G. He and I. P. Parkin, *Adv. Energy Mater.*, 2022, 2103483.
71. S. Zhang, *Energies*, 2014, **7**, 4588-4600.
72. X. Chen, L. Peng, L. Wang, J. Yang, Z. Hao, J. Xiang, K. Yuan, Y. Huang, B. Shan, L. Yuan and J. Xie, *Nat. Commun.*, 2019, **10**, 1021.
73. X. Wang, Y. Qian, L. Wang, H. Yang, H. Li, Y. Zhao and T. Liu, *Adv. Funct. Mater.*, 2019, **29**, 1902929.

74. A. Bhargav, M. E. Bell, J. Karty, Y. Cui and Y. Fu, *ACS Appl. Mater. Interfaces*, 2018, **10**, 21084-21090.
75. H. Ye, L. Ma, Y. Zhou, L. Wang, N. Han, F. Zhao, J. Deng, T. Wu, Y. Li and J. Lu, *Proc. Natl. Acad. Sci. U.S.A.* , 2017, **114**, 13091-13096.
76. B. He, D. Liu, Z. Cheng, Z. Miao, Z. Rao, H. Zhang, L. Yuan, Z. Li and Y. Huang, *Adv. Energy Mater.*, 2021, **12**, 2102832.
77. H. Du, S. Feng, W. Luo, L. Zhou and L. Mai, *J. Mater. Sci. Technol.* , 2020, **55**, 1-15.
78. P. Zhu, D. Gastol, J. Marshall, R. Sommerville, V. Goodship and E. Kendrick, *J. Power Sources*, 2021, **485**, 229321.
79. W. Yang, R. Huang, Z. Ni, H. Cheng, S. Zhou, Y. Wang, X. Li, Y. Zhang and Y. Zhang, *Ionics*, 2022, DOI: 10.1007/s11581-022-04461-2.
80. I. Raguzin, S. Choudhury, F. Simon, M. Stamm and L. Ionov, *Adv. Mater. Interfaces*, 2017, **4**, 1600811.
81. A. Benítez, F. Luna-Lama, A. Caballero, E. Rodríguez-Castellón and J. Morales, *J. Energy Chem.*, 2021, **62**, 295-306.
82. H.-J. Peng, W.-T. Xu, L. Zhu, D.-W. Wang, J.-Q. Huang, X.-B. Cheng, Z. Yuan, F. Wei and Q. Zhang, *Adv. Funct. Mater.*, 2016, **26**, 6351-6358.
83. Y. Hu, W. Chen, T. Lei, Y. Jiao, J. Huang, A. Hu, C. Gong, C. Yan, X. Wang and J. Xiong, *Adv. Energy Mater.*, 2020, **10**, 2000082.
84. Y. Wang, J. Huang, X. Chen, L. Wang and Z. Ye, *Carbon*, 2018, **137**, 368-378.
85. Q. Zhao, Q. Zhu, J. Miao, Z. Guan, H. Liu, R. Chen, Y. An, F. Wu and B. Xu, *ACS Appl. Mater. Interfaces*, 2018, **10**, 10882-10889.
86. L. Kong, H.-J. Peng, J.-Q. Huang and Q. Zhang, *Nano Res.*, 2017, **10**, 4027-4054.
87. C. Shang, L. Cao, M. Yang, Z. Wang, M. Li, G. Zhou, X. Wang and Z. Lu, *Energy Storage Mater.*, 2019, **18**, 375-381.
88. K. Zhang, K. Xie, K. Yuan, W. Lu, S. Hu, W. Wei, M. Bai and C. Shen, *J. Mater. Chem. A*, 2017, **5**, 7309-7315.
89. D. Fang, Y. Wang, C. Qian, X. Liu, X. Wang, S. Chen and S. Zhang, *Adv. Funct. Mater.*, 2019, **29**, 1900875.
90. G. Zhou, A. Yang, Y. Wang, G. Gao, A. Pei, X. Yu, Y. Zhu, L. Zong, B. Liu, J. Xu, N. Liu, J. Zhang, Y. Li, L. W. Wang, H. Y. Hwang, M. L. Brongersma, S. Chu and Y. Cui, *Nat. Commun.*, 2020, **11**, 606.
91. X. Tang, Z. Xu, Z. Sun, J. Zhou, X. Wu, H. Lin, J. Rong, S. Zhuo and F. Li, *Energy Technol.*, 2019, **7**, 1900574.
92. X. Ji, S. Evers, R. Black and L. F. Nazar, *Nat. Commun.*, 2011, **2**, 325.
93. Z.-L. Xu, S. J. Kim, D. Chang, K.-Y. Park, K. S. Dae, K. P. Dao, J. M. Yuk and K. Kang, *Energy Environ. Sci.* , 2019, **12**, 3144-3155.
94. L. Hu, C. Dai, H. Liu, Y. Li, B. Shen, Y. Chen, S.-J. Bao and M. Xu, *Adv. Energy Mater.*, 2018, **8**, 1800709.
95. N. Wang, B. Chen, K. Qin, E. Liu, C. Shi, C. He and N. Zhao, *Nano Energy*, 2019, **60**, 332-339.
96. Mingliang Yua, Si Zhoub, Zhiyu Wanga, Yuwei Wanga, Nan Zhanga, Song Wanga, Jijun Zhaob and J. Qiu, *Energy Storage Mater.*, 2019, **20**, 98–107.
97. H. Wang, W. Zhang, J. Xu and Z. Guo, *Adv. Funct. Mater.*, 2018, **28**, 1707520.
98. J. Sun, Y. Sun, M. Pasta, G. Zhou, Y. Li, W. Liu, F. Xiong and Y. Cui, *Adv. Mater.*, 2016, **28**, 9797-9803.
99. L. Li, L. Chen, S. Mukherjee, J. Gao, H. Sun, Z. Liu, X. Ma, T. Gupta, C. V. Singh, W. Ren, H. M. Cheng and N. Koratkar, *Adv. Mater.*, 2017, **29**, 1602734.
100. T. Zhou, W. Lv, J. Li, G. Zhou, Y. Zhao, S. Fan, B. Liu, B. Li, F. Kang and Q.-H. Yang, *Energy Environ. Sci.* , 2017, **10**, 1694-1703.

101. F. Wang, J. Li, J. Zhao, Y. Yang, C. Su, Y. L. Zhong, Q.-H. Yang and J. Lu, *ACS Mater. Lett.*, 2020, **2**, 1450-1463.
102. Z. Du, X. Chen, W. Hu, C. Chuang, S. Xie, A. Hu, W. Yan, X. Kong, X. Wu, H. Ji and L. J. Wan, *J. Am. Chem. Soc.*, 2019, **141**, 3977-3985.
103. Y. Liu, W. Kou, X. Li, C. Huang, R. Shui and G. He, *Small*, 2019, **15**, e1902431.
104. R. Wang, C. Luo, T. Wang, G. Zhou, Y. Deng, Y. He, Q. Zhang, F. Kang, W. Lv and Q. H. Yang, *Adv. Mater.*, 2020, **32**, e2000315.
105. W. Hua, H. Li, C. Pei, J. Xia, Y. Sun, C. Zhang, W. Lv, Y. Tao, Y. Jiao, B. Zhang, S. Z. Qiao, Y. Wan and Q. H. Yang, *Adv. Mater.*, 2021, **33**, 2101006.
106. H. Li, C. Chen, Y. Yan, T. Yan, C. Cheng, D. Sun and L. Zhang, *Adv. Mater.*, 2021, **33**, e2105067.
107. G. Zhang, H. J. Peng, C. Z. Zhao, X. Chen, L. D. Zhao, P. Li, J. Q. Huang and Q. Zhang, *Angew. Chem. Int. Ed.*, 2018, **57**, 16732-16736.
108. M. Zhao, B. Q. Li, H. J. Peng, H. Yuan, J. Y. Wei and J. Q. Huang, *Angew. Chem. Int. Ed.*, 2020, **59**, 12636-12652.
109. Q. Cheng, W. Xu, S. Qin, S. Das, T. Jin, A. Li, A. C. Li, B. Qie, P. Yao, H. Zhai, C. Shi, X. Yong and Y. Yang, *Angew. Chem. Int. Ed.*, 2019, **58**, 5557-5561.
110. M. Cuisinier, C. Hart, M. Balasubramanian, A. Garsuch and L. F. Nazar, *Adv. Energy Mater.*, 2015, **5**, 1401801.
111. H. Pan, J. Chen, R. Cao, V. Murugesan, N. N. Rajput, K. S. Han, K. Persson, L. Estevez, M. H. Engelhard, J.-G. Zhang, K. T. Mueller, Y. Cui, Y. Shao and J. Liu, *Nat. Energy*, 2017, **2**, 813-820.
112. Z. Li, Y. Zhou, Y. Wang and Y.-C. Lu, *Adv. Energy Mater.*, 2019, **9**, 1802207.
113. H. Chu, H. Noh, Y. J. Kim, S. Yuk, J. H. Lee, J. Lee, H. Kwack, Y. Kim, D. K. Yang and H. T. Kim, *Nat. Commun.*, 2019, **10**, 188.
114. L. Suo, Y. S. Hu, H. Li, M. Armand and L. Chen, *Nat. Commun.*, 2013, **4**, 1481.
115. J. Li, L. Zhang, F. Qin, B. Hong, Q. Xiang, K. Zhang, J. Fang and Y. Lai, *J. Power Sources*, 2019, **442**, 227232.
116. Z. Shi, L. Wang, H. Xu, J. Wei, H. Yue, H. Dong, Y. Yin and S. Yang, *Chem. Commun.*, 2019, **55**, 12056-12059.
117. F. Pei, S. Dai, B. Guo, H. Xie, C. Zhao, J. Cui, X. Fang, C. Chen and N. Zheng, *Energy Environ. Sci.* , 2021, **14**, 975-985.
118. R. Fang, H. Xu, B. Xu, X. Li, Y. Li and J. B. Goodenough, *Adv. Funct. Mater.*, 2020, **31**, 2001812.
119. P. Chiochan, X. Yu, M. Sawangphruk and A. Manthiram, *Adv. Energy Mater.*, 2020, **10**, 2001285.
120. R. Fang, B. Xu, N. S. Grundish, Y. Xia, Y. Li, C. Lu, Y. Liu, N. Wu and J. B. Goodenough, *Angew. Chem. Int. Ed.*, 2021, **60**, 17701-17706.
121. R.-c. Xu, X.-h. Xia, X.-l. Wang, Y. Xia and J.-p. Tu, *J. Mater. Chem. A*, 2017, **5**, 2829-2834.
122. Z. Wei, Y. Ren, J. Sokolowski, X. Zhu and G. Wu, *InfoMat*, 2020, **2**, 483-508.
123. X. J. Hong, C. L. Song, Y. Yang, H. C. Tan, G. H. Li, Y. P. Cai and H. Wang, *ACS Nano*, 2019, **13**, 1923-1931.
124. Y. Li, T. Gao, D. Ni, Y. Zhou, M. Yousaf, Z. Guo, J. Zhou, P. Zhou, Q. Wang and S. Guo, *Adv. Mater.*, 2022, **34**, e2107638.
125. N. Li, W. Cao, Y. Liu, H. Ye and K. Han, *Colloids Surf. A: Physicochem. Eng. Asp.*, 2019, **573**, 128-136.
126. H. Yang, H. Li, J. Li, Z. Sun, K. He, H. M. Cheng and F. Li, *Angew. Chem. Int. Ed.*, 2019, **58**, 11978-11996.
127. X. Xu, D. Zhou, X. Qin, K. Lin, F. Kang, B. Li, D. Shanmukaraj, T. Rojo, M. Armand and G. Wang, *Nat. Commun.*, 2018, **9**, 3870.
128. K. B. Hueso, M. Armand and T. Rojo, *Energy Environ. Sci.* , 2013, **6**, 734–749.

129. Y. X. Wang, B. Zhang, W. Lai, Y. Xu, S. L. Chou, H. K. Liu and S. X. Dou, *Adv. Energy Mater.*, 2017, **7**, 1602829.
130. B. W. Zhang, T. Sheng, Y. X. Wang, S. Chou, K. Davey, S. X. Dou and S. Z. Qiao, *Angew. Chem. Int. Ed.*, 2019, **58**, 1484-1488.
131. D. Liu, Z. Li, X. Li, Z. Cheng, L. Yuan and Y. Huang, *Chemphyschem*, 2019, **20**, 3164-3176.
132. X. Yu and A. Manthiram, *ChemElectroChem*, 2014, **1**, 1275-1280.
133. Y. Wang, Y. Zhang, H. Cheng, Z. Ni, Y. Wang, G. Xia, X. Li and X. Zeng, *Molecules*, 2021, **26**, 1535.
134. A. Y. S. Eng, V. Kumar, Y. Zhang, J. Luo, W. Wang, Y. Sun, W. Li and Z. W. Seh, *Adv. Energy Mater.*, 2021, **11**, 2003493.
135. Y. X. Wang, J. Yang, W. Lai, S. L. Chou, Q. F. Gu, H. K. Liu, D. Zhao and S. X. Dou, *J. Am. Chem. Soc.*, 2016, **138**, 16576-16579.
136. F. Xiao, X. Yang, H. Wang, J. Xu, Y. Liu, D. Y. W. Yu and A. L. Rogach, *Adv. Energy Mater.*, 2020, **10**, 2000931.
137. Z. Yang, R. Xiao, X. Zhang, X. Wang, D. Zhang, Z. Sun and F. Li, *Energy Environ. Sci.* , 2021, **0**, 1-18.
138. S. Xin, Y. X. Yin, Y. G. Guo and L. J. Wan, *Adv. Mater.*, 2014, **26**, 1261-1265.
139. H. Kim, M. K. Sadan, C. Kim, J. Jo, M. Seong, K.-K. Cho, K.-W. Kim, J.-H. Ahn and H.-J. Ahn, *Chem. Eng. J.*, 2021, **426**, 130787.
140. S. Li, Y. Han, P. Ge and Y. Yang, *Chempluschem*, 2021, **86**, 1461-1471.
141. H. Liu, W. Pei, W. H. Lai, Z. Yan, H. Yang, Y. Lei, Y. X. Wang, Q. Gu, S. Zhou, S. Chou, H. K. Liu and S. X. Dou, *ACS Nano*, 2020, **14**, 7259-7268.
142. X. L. Huang, S. X. Dou and Z. M. Wang, *Mater. Horiz.*, 2021, **8**, 2870-2885.
143. B. Guo, W. Du, T. Yang, J. Deng, D. Liu, Y. Qi, J. Jiang, S. J. Bao and M. Xu, *Adv. Sci.*, 2020, **7**, 1902617.
144. Z. Yan, Y. Liang, J. Xiao, W. Lai, W. Wang, Q. Xia, Y. Wang, Q. Gu, H. Lu, S. L. Chou, Y. Liu, H. Liu and S. X. Dou, *Adv. Mater.*, 2020, **32**, e1906700.
145. S. Gu, N. Xiao, F. Wu, Y. Bai, C. Wu and Y. Wu, *ACS Energy Lett.*, 2018, **3**, 2858-2864.
146. J. Ding, H. Zhang, W. Fan, C. Zhong, W. Hu and D. Mitlin, 2020, **32**, 1908007.
147. X. Yu and A. Manthiram, *Energy Storage Mater.*, 2018, **15**, 368-373.
148. Q. Zhao, Y. Hu, K. Zhang and J. Chen, *Inorg. Chem.*, 2014, **53**, 9000-9005.
149. J.-Y. Hwang, H. M. Kim and Y.-K. Sun, *J. Mater. Chem. A*, 2018, **6**, 14587-14593.
150. X. Lu, M. E. Bowden, V. L. Sprenkle and J. Liu, *Adv. Mater.*, 2015, **27**, 5915-5922.
151. P. Xiong, X. Han, X. Zhao, P. Bai, Y. Liu, J. Sun and Y. Xu, *Journal*, 2019, **13**, 2536-2543.
152. L. Wang, J. Bao, Q. Liu and C.-F. Sun, *Energy Storage Mater.*, 2019, **18**, 470-475.
153. N.-C. Lai, G. Cong and Y.-C. Lu, *J. Mater. Chem. A*, 2019, **7**, 20584-20589.
154. X. Ge, H. Di, P. Wang, X. Miao, P. Zhang, H. Wang, J. Ma and L. Yin, *ACS Nano*, 2020, **14**, 16022-16035.
155. Y. Lu, C. Wang, Q. Liu, X. Li, X. Zhao and Z. Guo, *Small Methods*, 2021, **5**, e2001303.
156. H. S. Kim, T. S. Arthur, G. D. Allred, J. Zajicek, J. G. Newman, A. E. Rodnyansky, A. G. Oliver, W. C. Boggess and J. Muldoon, *Nature Communications*, 2011, **2**, 427.
157. Z. Zhao-Karger, X. Zhao, D. Wang, T. Diemant, R. J. Behm and M. Fichtner, 2015, **5**, 1401155.
158. J. Zhu, J. Zou, H. Cheng, Y. Gu and Z. Lu, *Green Energy & Environment*, 2019, **4**, 345-359.
159. T. Gao, X. Ji, S. Hou, X. Fan, X. Li, C. Yang, F. Han, F. Wang, J. Jiang, K. Xu and C. Wang, *Adv. Mater.*, 2018, **30**, 1704313.
160. G. Bieker, J. Wellmann, M. Kolek, K. Jalkanen, M. Winter and P. Bieker, *Phys. Chem. Chem. Phys.*, 2017, **19**, 11152-11162.
161. Q. Zou, Y. Sun, Z. Liang, W. Wang and Y. C. Lu, *Adv. Energy Mater.*, 2021, **11**, 2101552.
162. T. Gao, S. Hou, F. Wang, Z. Ma, X. Li, K. Xu and C. Wang, 2017, **56**, 13526-13530.

163. Z. Zhao-Karger, M. E. Gil Bardaji, O. Fuhr and M. Fichtner, *J. Mater. Chem. A*, 2017, **5**, 10815-10820.
164. T. Gao, M. Noked, A. J. Pearse, E. Gillette, X. Fan, Y. Zhu, C. Luo, L. Suo, M. A. Schroeder, K. Xu, S. B. Lee, G. W. Rubloff and C. Wang, *J. Am. Chem. Soc.*, 2015, **137**, 12388-12393.
165. W. Li, S. Cheng, J. Wang, Y. Qiu, Z. Zheng, H. Lin, S. Nanda, Q. Ma, Y. Xu, F. Ye, M. Liu, L. Zhou and Y. Zhang, 2016, **55**, 6406-6410.
166. A. Du, Z. Zhang, H. Qu, Z. Cui, L. Qiao, L. Wang, J. Chai, T. Lu, S. Dong, T. Dong, H. Xu, X. Zhou and G. Cui, *Energy Environ. Sci.* , 2017, **10**, 2616-2625.
167. J. Häcker, C. Danner, B. Sievert, I. Biswas, Z. Zhao-Karger, N. Wagner and K. A. Friedrich, *Electrochimica Acta*, 2020, **338**, 135787.
168. X. Zhou, J. Tian, J. Hu and C. Li, 2018, **30**, 1704166.
169. W. Wang, H. Yuan, Y. NuLi, J. Zhou, J. Yang and J. Wang, *J. Phys. Chem. C*, 2018, **122**, 26764-26776.
170. X. Zhou, J. Tian, J. Hu and C. Li, *Adv. Mater.*, 2018, **30**, 1704166.
171. Z. Zhao-Karger, R. Liu, W. Dai, Z. Li, T. Diemant, B. P. Vinayan, C. Bonatto Minella, X. Yu, A. Manthiram, R. J. Behm, M. Ruben and M. Fichtner, *ACS Energy Lett.*, 2018, **3**, 2005-2013.
172. A. Scafuri, R. Berthelot, K. Pirnat, A. Vizintin, J. Bitenc, G. Aquilanti, D. Foix, R. Dedryvère, I. Arčon, R. Dominko and L. Stievano, *Chem. Mater.*, 2020, **32**, 8266-8275.
173. Z. L. Xu, J. Park, J. Wang, H. Moon, G. Yoon, J. Lim, Y. J. Ko, S. P. Cho, S. Y. Lee and K. Kang, *Nat. Commun.*, 2021, **12**, 3369.
174. X. Yu, M. J. Boyer, G. S. Hwang and A. Manthiram, *Adv. Energy Mater.*, 2019, **9**, 1803794.
175. Z. Li, B. P. Vinayan, T. Diemant, R. J. Behm, M. Fichtner and Z. Zhao-Karger, *Small*, 2020, **16**, e2001806.
176. Gleb Mamantov and R. Marassi, *US Pat.*, 4 063 005, 1997.
177. Dharmasena Peramunage, R. Dillon, and t. Licht, *J. Power Sources*, 1993, **45**, 311-323.
178. T. Gao, X. Li, X. Wang, J. Hu, F. Han, X. Fan, L. Suo, A. J. Pearse, S. B. Lee, G. W. Rubloff, K. J. Gaskell, M. Noked and C. Wang, *Angew. Chem. Int. Ed.*, 2016, **55**, 9898-9901.
179. H. Li, R. Meng, Y. Guo, B. Chen, Y. Jiao, C. Ye, Y. Long, A. Tadich, Q. H. Yang, M. Jaroniec and S. Z. Qiao, *Nat. Commun.*, 2021, **12**, 5714.
180. X. Yu and A. Manthiram, *Adv. Energy Mater.*, 2017, **7**, 1700561.
181. W. Wang, Z. Cao, G. A. Elia, Y. Wu, W. Wahyudi, E. Abou-Hamad, A.-H. Emwas, L. Cavallo, L.-J. Li and J. Ming, *ACS Energy Lett.*, 2018, **3**, 2899-2907.
182. K. Zhang, T. H. Lee, J. H. Cha, R. S. Varma, J. W. Choi, H. W. Jang and M. Shokouhimehr, *Sci. Rep.*, 2019, **9**, 13573.
183. J. Lampkin, H. Li, L. Furness, R. Raccichini and N. Garcia-Araez, *ChemSusChem*, 2020, **13**, 3514-3523.
184. X. Xiao, J. Tu, Z. Huang and S. Jiao, *Phys. Chem. Chem. Phys.*, 2021, **23**, 10326-10334.
185. X. Zheng, R. Tang, Y. Zhang, L. Ma, X. Wang, Y. Dong, G. Kong and L. Wei, *Sustain. Energy Fuels*, 2020, **4**, 1630-1641.
186. Sungjemmenla, C. B. Soni and V. Kumar, *Nanoscale Adv.*, 2021, **3**, 1569-1581.
187. Y. Guo, H. Jin, Z. Qi, Z. Hu, H. Ji and L.-J. Wan, *Adv. Funct. Mater.*, 2019, **29**, 1807676.
188. X. Yu, M. J. Boyer, G. S. Hwang and A. Manthiram, *Chem*, 2018, **4**, 586-598.
189. H. Yang, L. Yin, J. Liang, Z. Sun, Y. Wang, H. Li, K. He, L. Ma, Z. Peng, S. Qiu, C. Sun, H. M. Cheng and F. Li, *Angew. Chem. Int. Ed.*, 2018, **57**, 1898-1902.
190. W. Tang, Z. Chen, B. Tian, H. W. Lee, X. Zhao, X. Fan, Y. Fan, K. Leng, C. Peng, M. H. Kim, M. Li, M. Lin, J. Su, J. Chen, H. Y. Jeong, X. Yin, Q. Zhang, W. Zhou, K. P. Loh and G. W. Zheng, *J. Am. Chem. Soc.*, 2017, **139**, 10133-10141.
191. Y. Hwa, H. K. Seo, J. M. Yuk and E. J. Cairns, *Nano Lett.*, 2017, **17**, 7086-7094.

192. Y. Li, Y. Tang, X. Li, W. Tu, L. Zhang and J. Huang, *Small*, 2021, **17**, e2100846.
193. X. Ding, S. Yang, S. Zhou, Y. Zhan, Y. Lai, X. Zhou, X. Xu, H. Nie, S. Huang and Z. Yang, *Adv. Funct. Mater.*, 2020, **30**, 2003354.
194. N. Xu, T. Qian, X. Liu, J. Liu, Y. Chen and C. Yan, *Nano Lett.*, 2017, **17**, 538-543.
195. J. Zhou, H. Ji, J. Liu, T. Qian and C. Yan, *Energy Storage Mater.*, 2019, **22**, 256-264.
196. J. Liu, T. Qian, M. Wang, X. Liu, N. Xu, Y. You and C. Yan, *Nano Lett.*, 2017, **17**, 5064-5070.
197. V. Celorrio, A. S. Leach, H. Huang, S. Hayama, A. Freeman, D. W. Inwood, D. J. Fermin and A. E. Russell, *ACS Catal.*, 2021, **11**, 6431-6439.
198. N. V. Srinath, A. Longo, H. Poelman, R. K. Ramachandran, J.-Y. Feng, J. Dendooven, M.-F. Reyniers and V. V. Galvita, *ACS Catal.*, 2021, **11**, 11320-11335.
199. Y. Xu, Y. Ye, S. Zhao, J. Feng, J. Li, H. Chen, A. Yang, F. Shi, L. Jia, Y. Wu, X. Yu, P. A. Glans-Suzuki, Y. Cui, J. Guo and Y. Zhang, *Nano Lett.*, 2019, **19**, 2928-2934.
200. C. Wu, Y. Lei, L. Simonelli, D. Tonti, A. Black, X. Lu, W. H. Lai, X. Cai, Y. X. Wang, Q. Gu, S. L. Chou, H. K. Liu, G. Wang and S. X. Dou, *Adv. Mater.*, 2022, **34**, e2108363.
201. E. Zhao, K. Nie, X. Yu, Y. S. Hu, F. Wang, J. Xiao, H. Li and X. Huang, *Adv. Funct. Mater.*, 2018, **28**, 1707543.
202. C. Ye, Y. Jiao, D. Chao, T. Ling, J. Shan, B. Zhang, Q. Gu, K. Davey, H. Wang and S. Z. Qiao, *Adv. Mater.*, 2020, **32**, e1907557.
203. Z. Yan, J. Xiao, W. Lai, L. Wang, F. Gebert, Y. Wang, Q. Gu, H. Liu, S. L. Chou, H. Liu and S. X. Dou, *Nat. Commun.*, 2019, **10**, 4793.
204. C. Ma, Y. Zhang, Y. Feng, N. Wang, L. Zhou, C. Liang, L. Chen, Y. Lai, X. Ji, C. Yan and W. Wei, *Adv. Mater.*, 2021, **33**, e2100171.
205. H. Ci, J. Cai, H. Ma, Z. Shi, G. Cui, M. Wang, J. Jin, N. Wei, C. Lu, W. Zhao, J. Sun and Z. Liu, *ACS Nano*, 2020, **14**, 11929-11938.
206. Chao Ye, Yan Jiao, Huanyu Jin, Ashley D. Slattery, Kenneth Davey, Haihui Wang and S.-Z. Qiao, *Angew. Chem. Int. Ed.*, 2018, **57**, 16703 –16707.
207. J. Qian, F. Wang, Y. Li, S. Wang, Y. Zhao, W. Li, Y. Xing, L. Deng, Q. Sun, L. Li, F. Wu and R. Chen, *Adv. Funct. Mater.*, 2020, **30**, 2000742.
208. J. He, A. Bhargav and A. Manthiram, *Adv. Mater.*, 2020, **32**, e2004741.
209. S. Zhang, Y. Yao, X. Jiao, M. Ma, H. Huang, X. Zhou, L. Wang, J. Bai and Y. Yu, *Adv. Mater.*, 2021, **33**, e2103846.
210. L. Wang, Z.-Y. Wang, J.-F. Wu, G.-R. Li, S. Liu and X.-P. Gao, *Nano Energy*, 2020, **77**, 105173.
211. X.-C. Liu, Y. Yang, J. Wu, M. Liu, S. P. Zhou, B. D. A. Levin, X.-D. Zhou, H. Cong, D. A. Muller, P. M. Ajayan, H. D. Abruña and F.-S. Ke, *ACS Energy Lett.*, 2018, **3**, 1325-1330.
212. Z. Wang, Y. Tang, X. Fu, J. Wang, Z. Peng, L. Zhang and J. Huang, *ACS Appl. Mater. Interfaces*, 2020, **12**, 55971-55981.
213. J. H. Tian, T. Jiang, M. Wang, Z. Hu, X. Zhu, L. Zhang, T. Qian and C. Yan, *Small Methods*, 2019, **4**, 1900467.
214. Q. Zou, Z. Liang, G. Y. Du, C. Y. Liu, E. Y. Li and Y. C. Lu, *J. Am. Chem. Soc.*, 2018, **140**, 10740-10748.
215. J. Häcker, D. H. Nguyen, T. Rommel, Z. Zhao-Karger, N. Wagner and K. A. Friedrich, *ACS Energy Lett.*, 2021, **7**, 1-9.
216. D. Zhang, X. Zhang, B. Wang, S. He, S. Liu, M. Tang and H. Yu, *J. Mater. Chem. A*, 2021, **9**, 8966-8974.
217. Z. Zhao-Karger, X. Zhao, D. Wang, T. Diemant, R. J. Behm and M. Fichtner, *Adv. Energy Mater.*, 2015, **5**, 401155.
218. P. Wang, K. Küster, U. Starke, C. Liang, R. Niewa and M. R. Buchmeiser, *J. Power Sources*, 2021, **515**, 230604.

219. Y. Li, S. Lin, D. Wang, T. Gao, J. Song, P. Zhou, Z. Xu, Z. Yang, N. Xiao and S. Guo, *Adv. Mater.*, 2020, **32**, e1906722.
220. S. Ma, P. Zuo, H. Zhang, Z. Yu, C. Cui, M. He and G. Yin, *Chem Commun.*, 2019, **55**, 5267-5270.
221. Z. Zhang, Z. Cui, L. Qiao, J. Guan, H. Xu, X. Wang, P. Hu, H. Du, S. Li, X. Zhou, S. Dong, Z. Liu, G. Cui and L. Chen, *Adv. Energy Mater.*, 2017, **7**, 1602055.
222. D. Muthuraj, A. Ghosh, A. Kumar and S. Mitra, *ChemElectroChem*, 2018, **6**, 684-689.
223. A. Robba, A. Vizintin, J. Bitenc, G. Mali, I. Arčon, M. Kavčič, M. Žitnik, K. Bučar, G. Aquilanti, C. Martineau-Corcos, A. Randon-Vitanova and R. Dominko, *Chem. Mater.*, 2017, **29**, 9555-9564.
224. C. Zech, P. Hönicke, Y. Kayser, S. Risse, O. Grätz, M. Stamm and B. Beckhoff, *J. Mater. Chem. A*, 2021, **9**, 10231-10239.
225. Q. Pang, D. Kundu, M. Cuisinier and L. F. Nazar, *Nat. Commun.*, 2014, **5**, 4759.
226. X. Yang, X. Gao, Q. Sun, S. P. Jand, Y. Yu, Y. Zhao, X. Li, K. Adair, L. Y. Kuo, J. Rohrer, J. Liang, X. Lin, M. N. Banis, Y. Hu, H. Zhang, X. Li, R. Li, H. Zhang, P. Kaghazchi, T. K. Sham and X. Sun, *Adv. Mater.*, 2019, **31**, e1901220.
227. C. Zha, D. Wu, X. Gu and H. Chen, *J. Energy Chem.*, 2021, **59**, 599-607.
228. A. Benayad, J. E. Morales-Ugarte, C. C. Santini and R. Bouchet, *J. Phys. Chem. A*, 2021, **125**, 1069-1081.
229. M. I. Nandasiri, Luis E. Camacho-Forero, Ashleigh M. Schwarz, Vaithiyalingam Shutthanandan, Suntharampillai Thevuthasan, Perla B. Balbuena, Karl T. Mueller, and Vijayakumar Murugesan, *Chem. Mater.*, 2017, **29**, 4728–4737.
230. Y. Zhang, S. Yang, S. Zhou, L. Zhang, B. Gu, Y. Dong, S. Kong, D. Cai, G. Fang, H. Nie and Z. Yang, *Chem. Commun.*, 2021, **57**, 3255-3258.
231. B. W. Zhang, T. Sheng, Y. D. Liu, Y. X. Wang, L. Zhang, W. H. Lai, L. Wang, J. Yang, Q. F. Gu, S. L. Chou, H. K. Liu and S. X. Dou, *Nat. Commun.*, 2018, **9**, 4082.
232. Q. Yang, T. Yang, W. Gao, Y. Qi, B. Guo, W. Zhong, J. Jiang and M. Xu, *Inorg. Chem. Front*, 2020, **7**, 4396-4403.
233. A. Kumar, A. Ghosh, M. Forsyth, D. R. MacFarlane and S. Mitra, *ACS Energy Lett.*, 2020, **5**, 2112-2121.
234. R. K. Bhardwaj, S. Jayanthi, P. S. Adarakatti, A. K. Sood and A. J. Bhattacharyya, *ACS Appl. Mater. Interfaces*, 2020, **12**, 28120-28128.
235. R. K. Bhardwaj, R. Gomes and A. J. Bhattacharyya, *J. Phys. Chem. Lett.*, 2022, **13**, 1159-1164.
236. J. Wang, S. Cheng, W. Li, L. Jia, Q. Xiao, Y. Hou, Z. Zheng, H. Li, S. Zhang, L. Zhou, M. Liu, H. Lin and Y. Zhang, *Nano Energy*, 2017, **40**, 390-398.
237. C. Dillard, A. Singh and V. Kalra, *J. Phys. Chem. C*, 2018, **122**, 18195-18203.
238. N. Saqib, G. M. Ohlhausen and J. M. Porter, *J. Power Sources*, 2017, **364**, 266-271.
239. X.-C. Hu, Y. Shi, S.-Y. Lang, X. Zhang, L. Gu, Y.-G. Guo, R. Wen and L.-J. Wan, *Nano Energy*, 2018, **49**, 453-459.
240. S. Y. Lang, Y. Shi, Y. G. Guo, D. Wang, R. Wen and L. J. Wan, *Angew. Chem. Int. Ed.*, 2016, **55**, 15835-15839.
241. S. Y. Lang, Y. Shi, Y. G. Guo, R. Wen and L. J. Wan, *Angew. Chem. Int. Ed.*, 2017, **56**, 14433-14437.

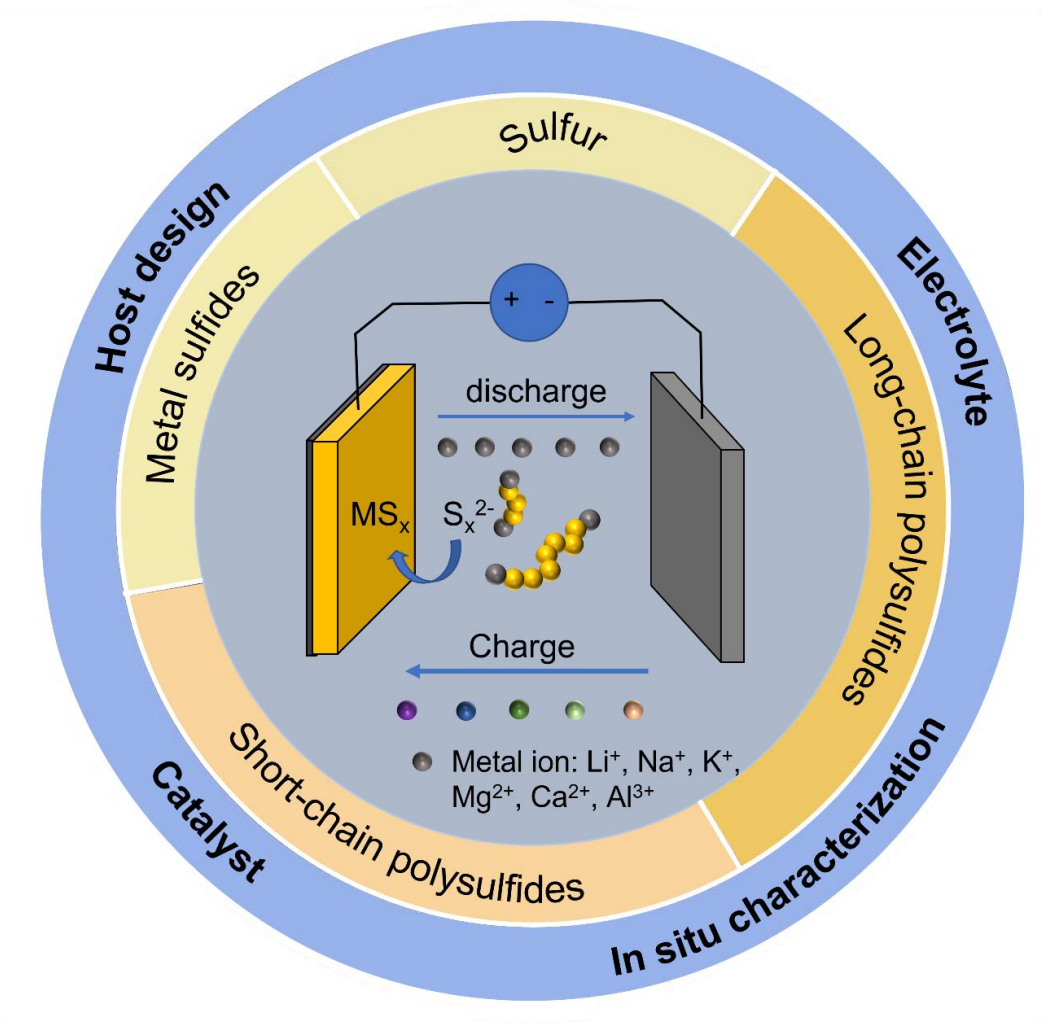

Figure 1 Schematic illustration of representative strategies to regulate sulfur conversion in metal-sulfur batteries.

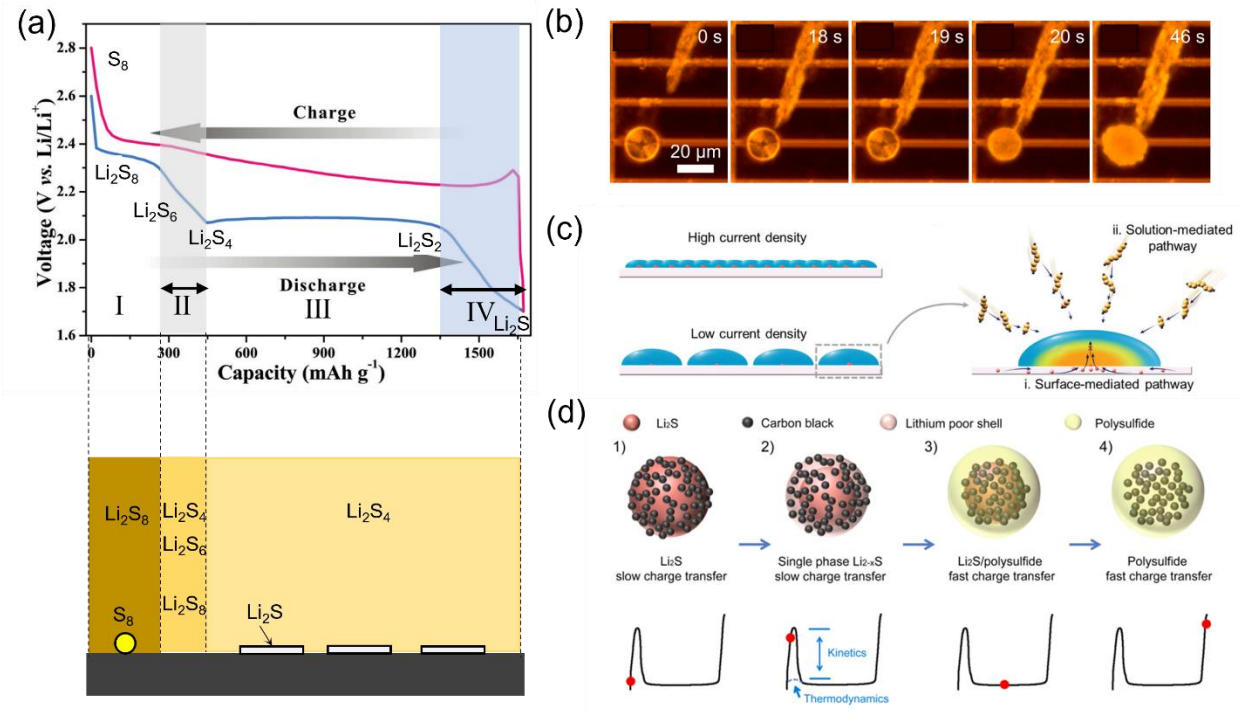

Figure 2 (a) Schematic illustration of the reaction process and related reaction products of the Li-S batteries. Reproduced with permission: Copyright 2019, Royal Society of Chemistry.[11] (b) Photo of liquid sulfur converted to solid sulfur. Reproduced with permission: Copyright 2019, National Academy of Sciences.[28] (c) The different Li_2S growth mechanisms under high current density and low current density. Reproduced with permission: Copyright 2019, Royal Society of Chemistry.[42] (d) Schematic diagram of the activation process of Li_2S. Reproduced with permission: Copyright 2012, American Chemistry Society.[44]

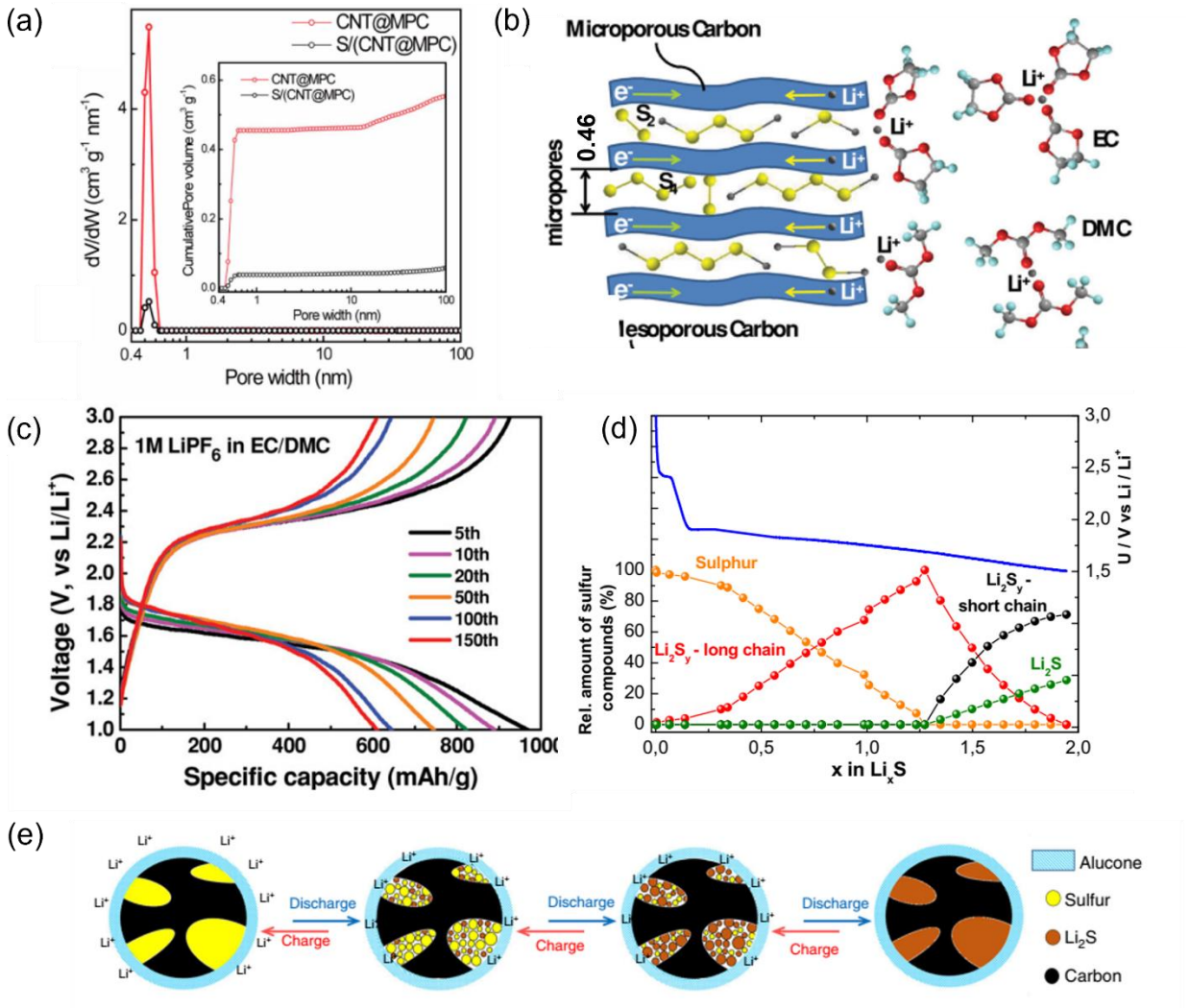

Figure 3 (a) Sulfur confined by CNT with 0.5 nm-sized pore. Reproduced with permission: Copyright 2012, American Chemistry Society.[59] (b) Exclusion of carbonate electrolyte molecules from 0.46 nm micropores. (c) Potential curves of S_{2-4} in carbonate-based electrolyte. Reproduced with permission: Copyright 2014, Wiley-VCH.[58] (d) The change of relative amount S, long-chain Li_2S_y, short-chain Li_2S_y, and Li_2S during the discharge process using the ultra-microporous carbon/S as the cathode in carbonate solvent-based electrolytes. Reproduced with permission: Copyright 2018, Electrochemical Society.[61] (e) The proposed redox reaction process of alucone C–S cathodes in carbonate solvent-based electrolytes. Reproduced with permission: Copyright 2018, Nature Reseach.[62]

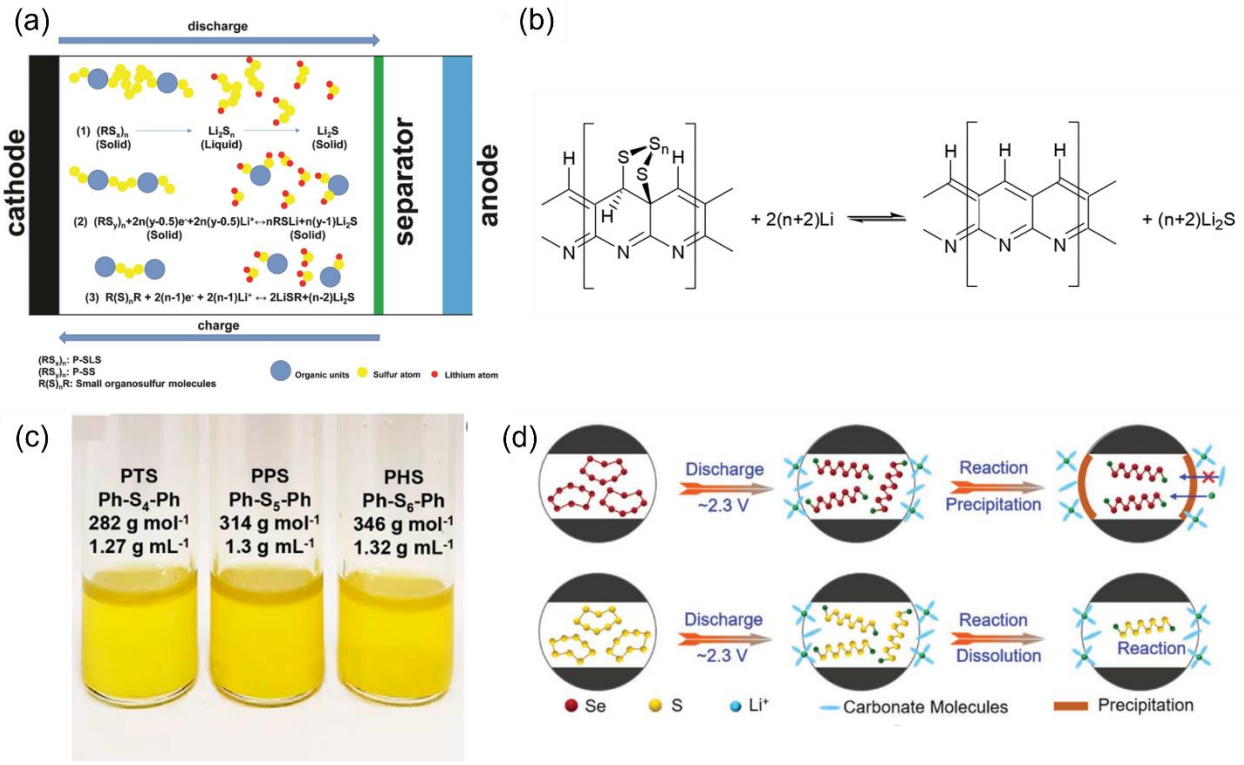

Figure 4 (a) The different electrochemical processes of different organosulfur compounds.[63] Reproduced with permission: Copyright 2020, Royal Society of Chemistry. (b) The general reaction equation of the overall Li/SPAN reaction. Reproduced with permission: Copyright 2014, Multidisciplinary Digital Publishing Institute.[71] (c) The photos of a series of liquid phenyl polysulfides. Reproduced with permission: Copyright 2018, American Chemistry Society.[74] (d) Schematic illustration of the CEI formed on CMK-3/Se and CMK-3/S cathodes in the carbonate-based electrolyte. Reproduced with permission: Copyright 2021, Wiley-VCH.[76]

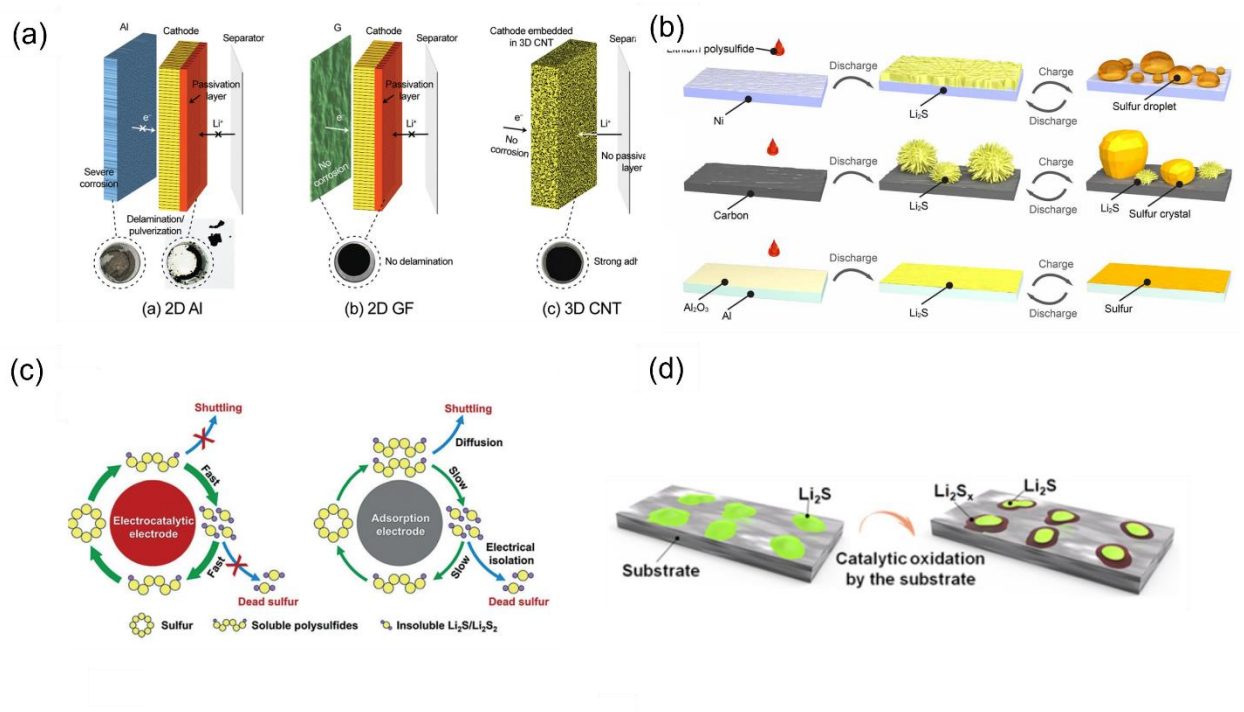

Figure 5 (a) Comparison of 2D Al current collectors, 2D graphene foam current collectors, 3D CNT current collectors. Reproduced with permission: Copyright 2016, Wiley-VCH.[82] (b) Schematic illustration of the sulfur species evolution on Ni, C, and Al substrates during charging and discharging processes. Reproduced with permission: Copyright 2020, The American Association for the Advancement of Science.[30] (c) The comparison of electrocatalytic electrodes and absorption electrodes. Reproduced with permission: Copyright 2018, Elsevier.[96] (d) Schematic showing the promotion of Li_2S dissolution to LiPSs on metal sulfides. Reproduced with permission: Copyright 2017, National Academy of Sciences.[52]

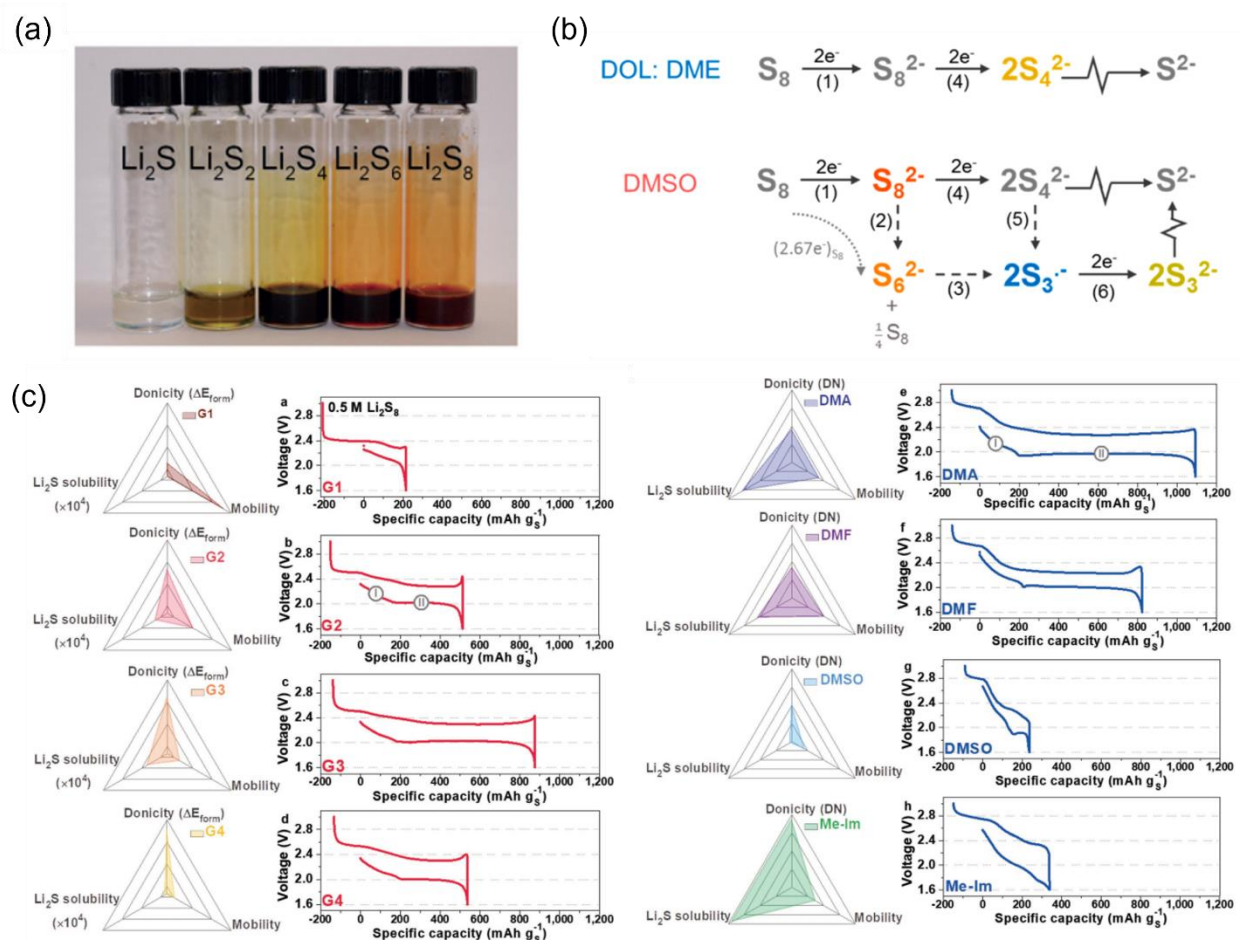

Figure 6 (a) Li_2S, Li_2S_2, Li_2S_4, Li_2S_6, Li_2S_8 dissolved in ε-caprolactam/acetamide based eutectic solvent electrolyte. Reproduced with permission: Copyright 2019, Wiley-VCH.[109] (b) Sulfur reaction pathways in DOL: DME and DMSO. Reproduced with permission: Copyright 2016, American Chemical Society.[32] (c) The relationship of solvent properties (*i.e.*, donicity, Li_2S solubility, mobility) and battery performance. Reproduced with permission: Copyright 2019, Wiley-VCH.[112]

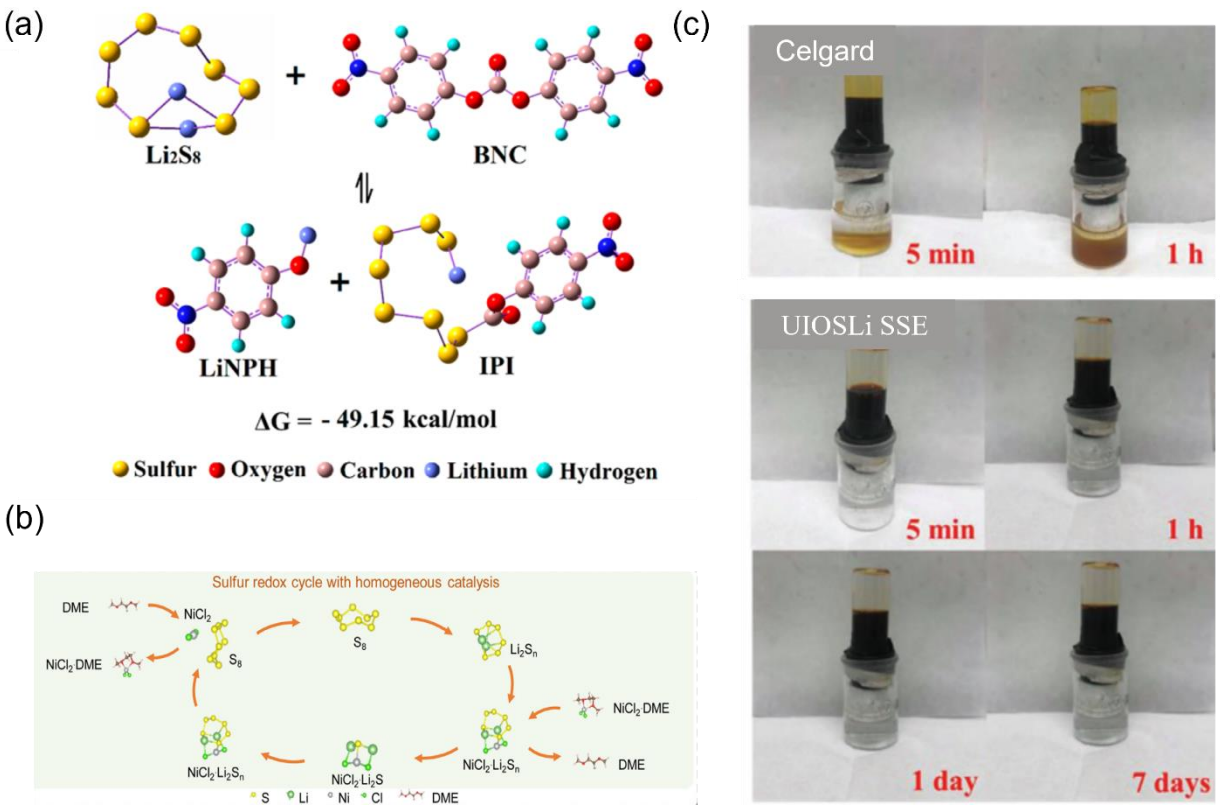

Figure 7 (a) Schematic illustration of the reaction of bis(4-nitrophenyl) carbonate (BNC) with soluble Li_2S_8 to produce lithium 4-nitrophenolate (LiNPH) and insoluble sulfur species. Reproduced with permission: Copyright 2019, American Chemical Society.[17] (b) Schematic demonstration of NiDME additive working in a LSB. Reproduced with permission: Copyright 2020, Elsevier.[39] (c) The suppress shuttle effect ability comparison between Celgard (up) and UIOSLi SSE (down). Reproduced with permission: Copyright 2020, Wiley-VCH [119]

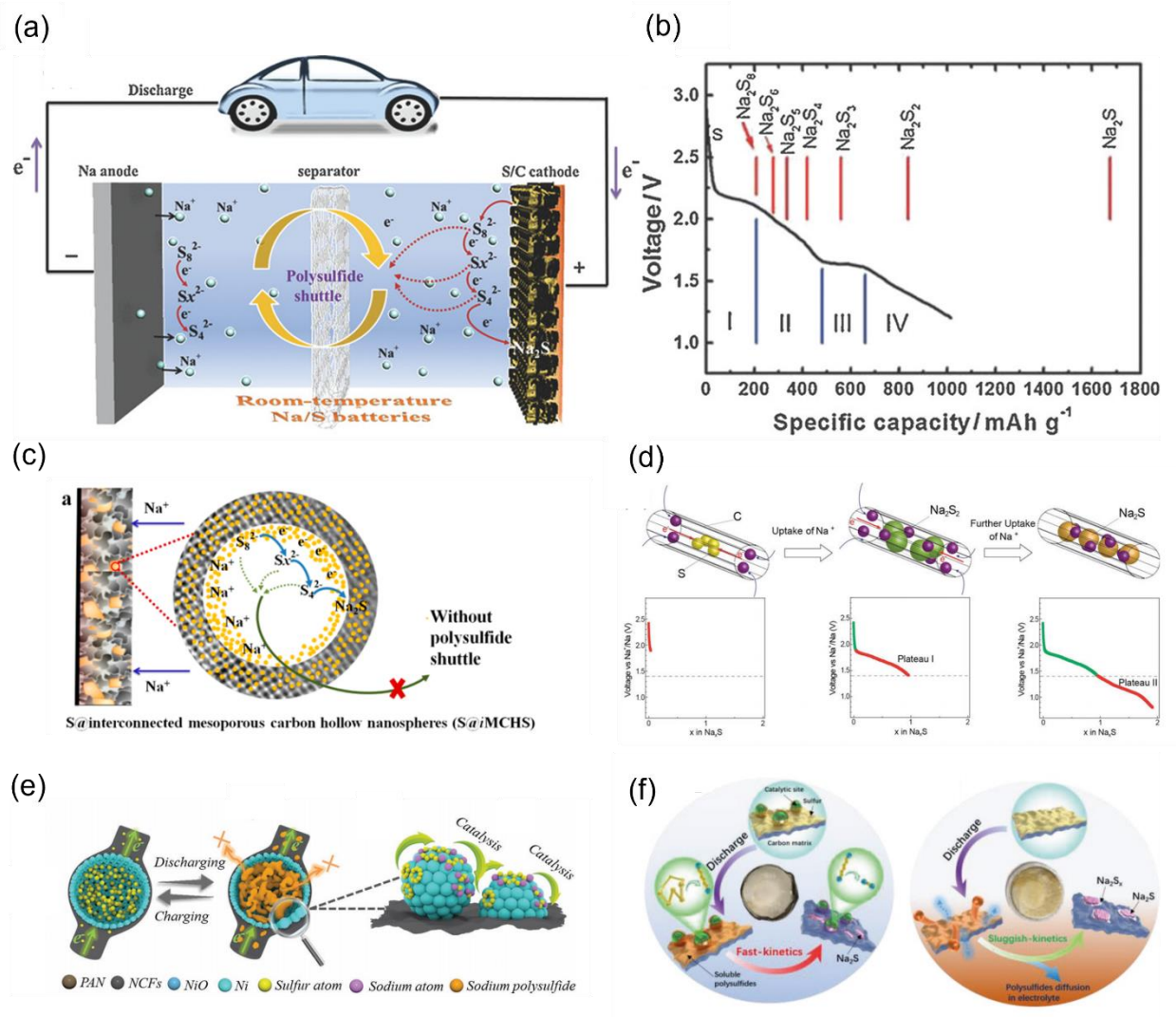

Figure 8 (a) The schematic of room temperature sodium-sulfur batteries. Reproduced with permission: Copyright 2017, Wiley-VCH.[129] (b) The discharge potential curve and the comparison between the theoretical (red) and practical discharge capacities (black). Reproduced with permission: Copyright 2014, Wiley-VCH. [132] (c) Sulfur encapsulated in the interconnected mesoporous carbon hollow nanospheres. Reproduced with permission: Copyright 2016, American Chemical Society.[135] (d) Small sulfur molecules (S_{2-4}) confined in microporous carbon and the corresponding discharge curves. Reproduced with permission: Copyright 2014, Wiley-VCH.[138] (e) The schematic illustration of the hollow nickel unit to accommodate volumetric expansion of sulfur and the catalytic effect of nickel atoms. Reproduced with permission: Copyright 2020, Wiley-VCH. [143] (f) sulfur reaction mechanisms in FeS_2@ hierarchical carbon and pure hierarchical carbon. Reproduced with permission: Copyright 2020, Wiley-VCH.[144]

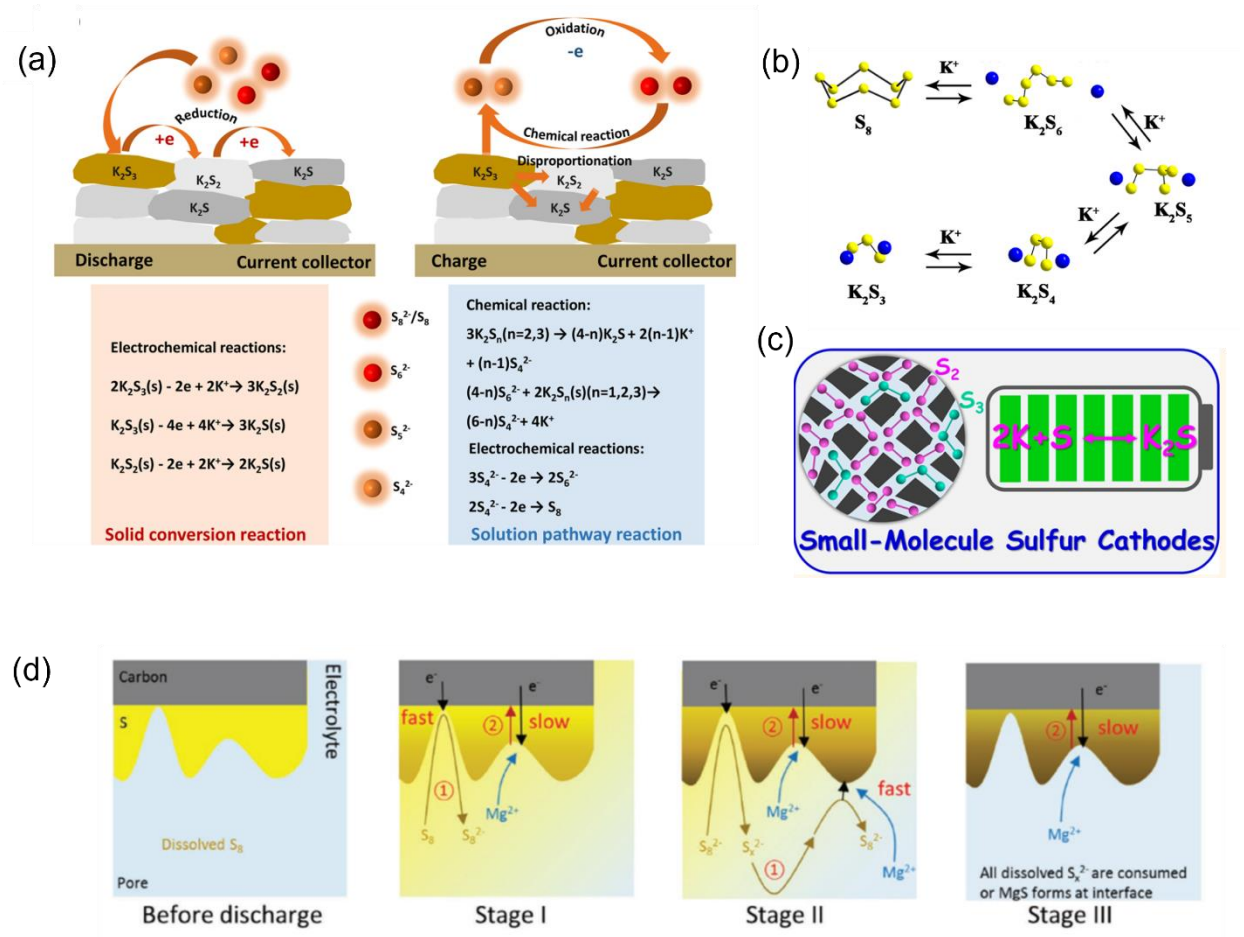

Figure 9 (a)The electrochemical reactions and chemical reactions in K-S batteries. Reproduced with permission: Copyright 2018, American Chemical Society.[145] (b) The schematic of potassium-sulfur batteries reaction process with discharging product K_2S_3. Reproduced with permission: Copyright 2020, American Chemical Society.[154] (c) The schematic of potassium-sulfur batteries reaction process in microporous carbon with the discharging product K_2S. Reproduced with permission: Copyright 2019, American Chemical Society.[151] (d) The schematic of the sulfur discharge reaction mechanism. Reproduced with permission: Copyright 2017, Wiley-VCH.[159]

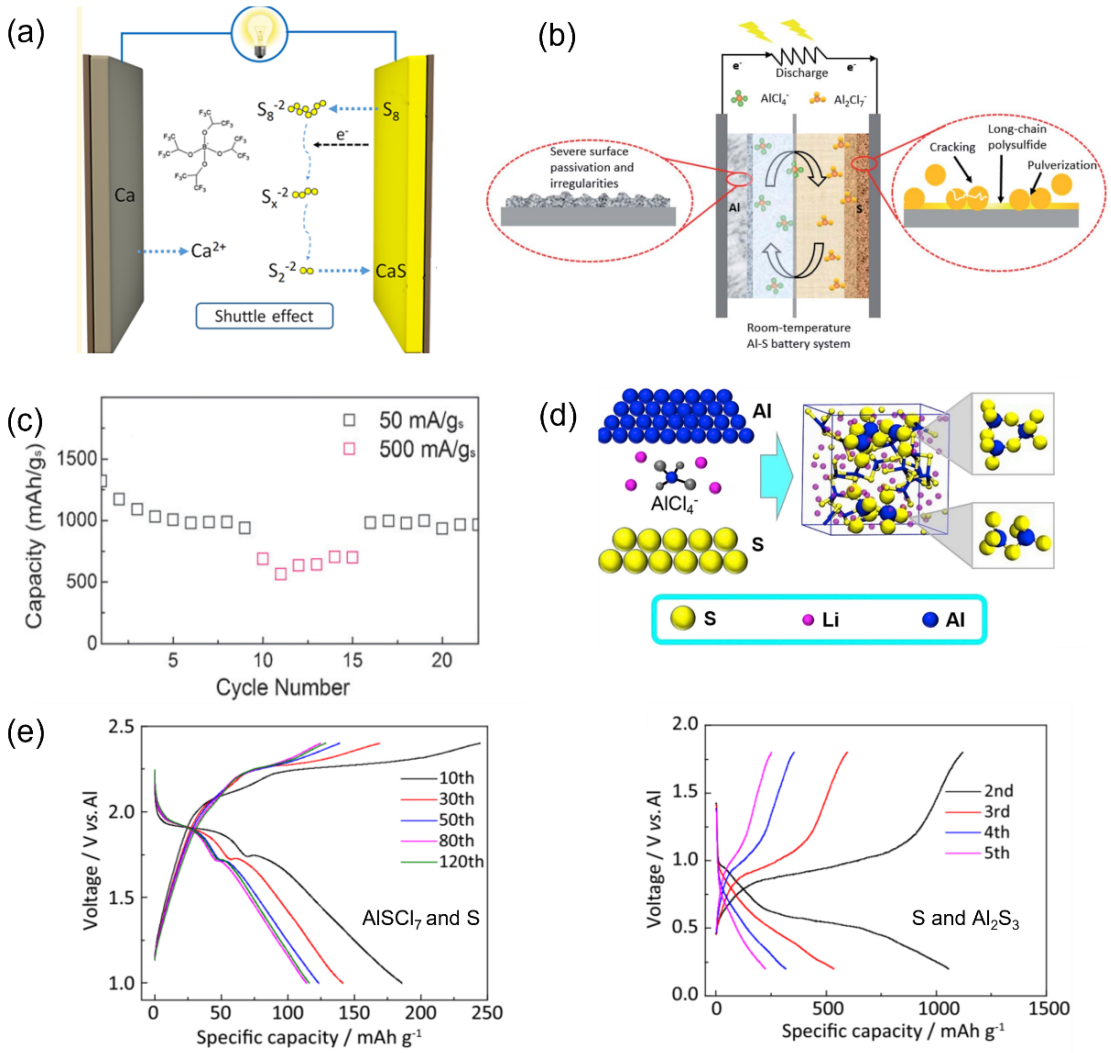

Figure 10 (a) Schematic diagram of Ca-S batteries reaction process. Reproduced with permission: Copyright 2020, American Chemical Society.[172] (b) Schematic diagram of the reaction process and problems for aluminum-sulfur batteries in ionic liquid electrolyte. Reproduced with permission: Copyright 2021, Royal Society of Chemistry.[186] (c) The cycling performance of Al-S batteries using microporous activated carbon/sulfur cathode. Reproduced with permission: Copyright 2016, Wiley-VCH.[178] (d) Introducing Li^+-ion mediation into the [EMIM]$AlCl_4$ ionic liquid in Al-S batteries system. Reproduced with permission: Copyright 2017, Elsevier.[188] (e) The charge and discharge curve of sulfur oxidation (S and $AlSCl_7$) and sulfur reduction(S and Al_2S_3) of Al-S batteries. Reproduced with permission: Copyright 2021, Nature Research.[179]

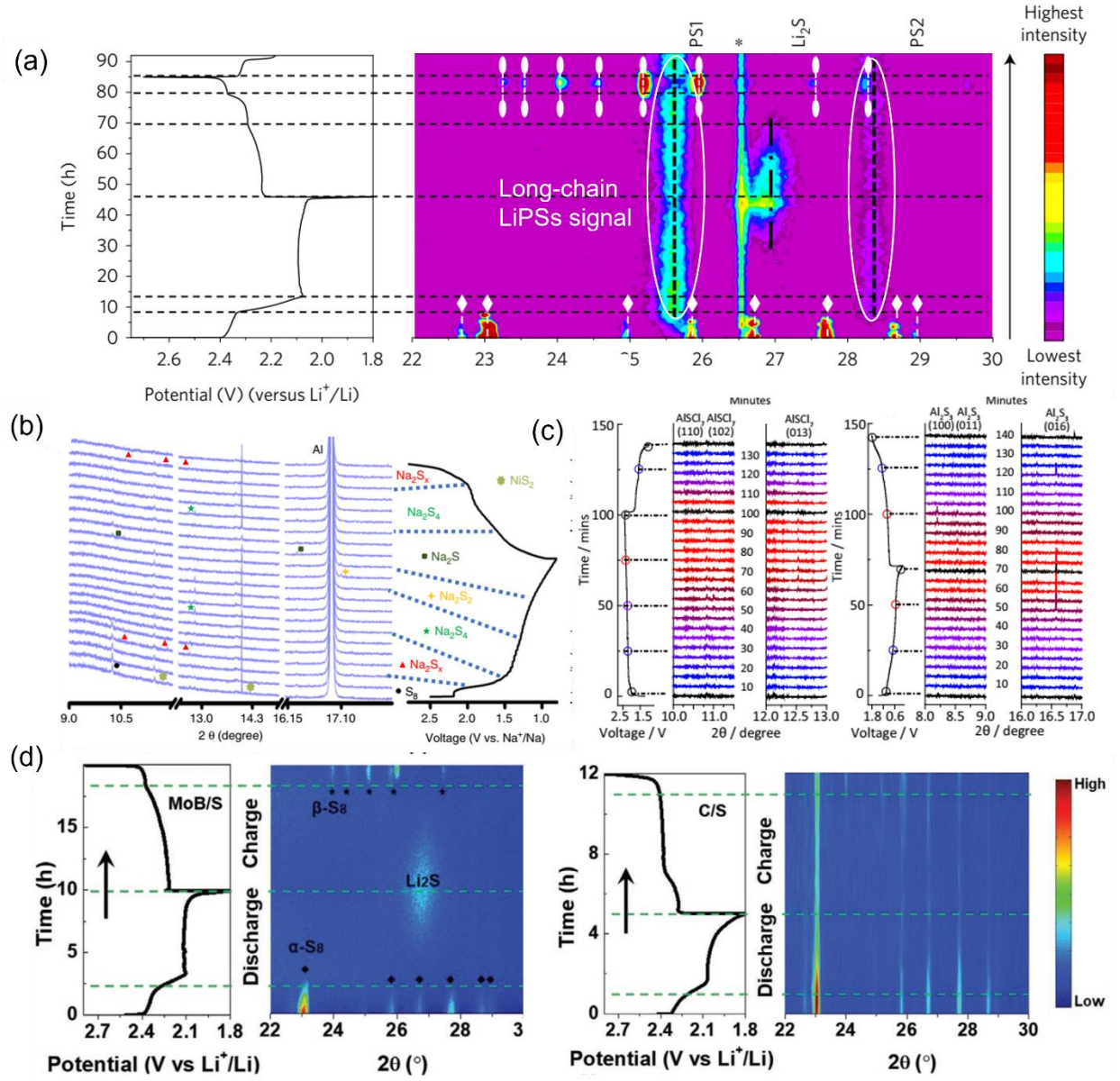

Figure 11 (a) In situ XRD for Li-S batteries during discharge and charge process. Reproduced with permission: Copyright 2017, Springer Nature.[9] (b) In situ XRD for Na-S batteries and no sulfur signal at the end of charge state. Reproduced with permission: Copyright 2019, Nature Research. (c) In situ XRD for sulfur oxidation and reduction process in Al-S batteries. Reproduced with permission: Copyright 2020, Nature Research.[179] (d) In situ XRD contour images of MoB/S and C/S cathode of Li-S batteries, and the corresponding charging-discharging curve. Reproduced with permission: Copyright 2020, Wiley-VCH.[208]

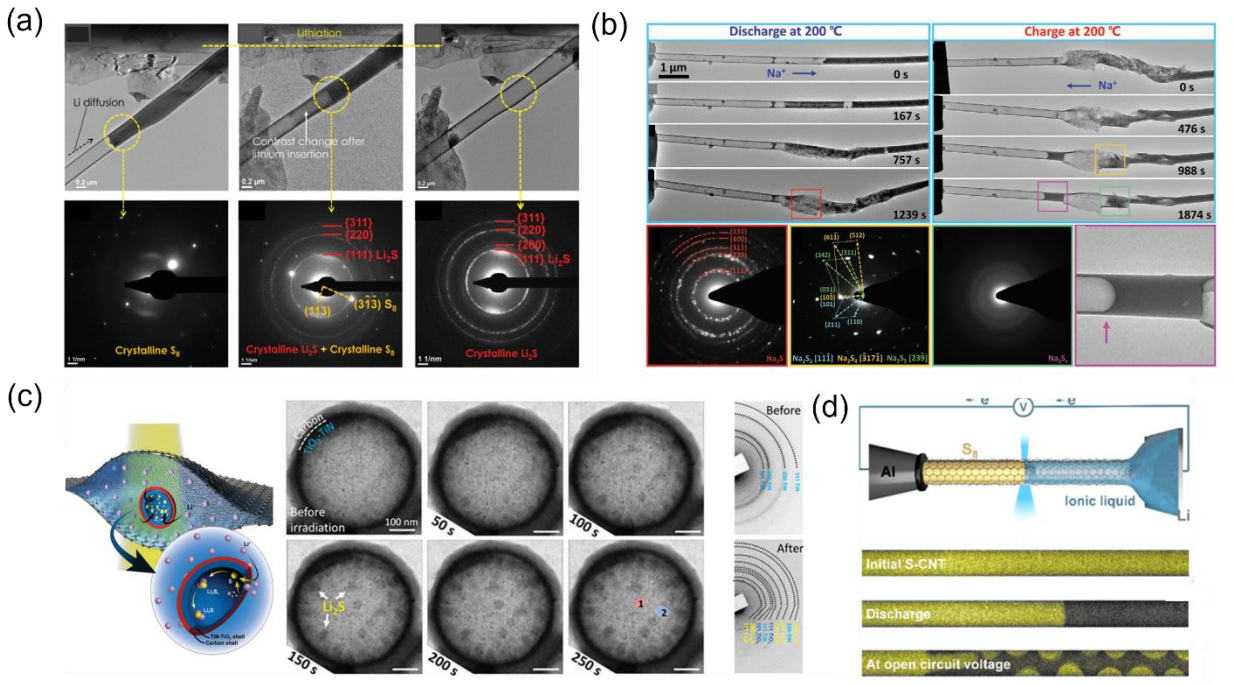

Figure 12 (a) In situ TEM shwoing sulfur reduced to Li_2S directly in Li-CNT/S solid-state batteries. Reproduced with permission: Copyright 2015, Wiley-VCH.[14] (b) In situ TEM showing the evolution of sulfur going through Na_2S_x ($x \geq 6$), Na_2S_5, Na_2S_4, Na_2S_2, Na_2S in in Na-CNT/S solid-state batteries. Reproduced with permission: Copyright 2021, Wiley-VCH.[192] (c) Schematic illustration of graphene liquid battery and in-situ TEM images of the Li_2S nucleation and growth in TiO_2-TiN hollow sphere. Reproduced with permission: Copyright 2019, Royal Society of Chemistry.[93] (d) Schematic of the in-situ devices and sulfur distribution at initial, discharge, open circuit voltage stages. Reproduced with permission: Copyright 2020, American Chemical Society. [212]

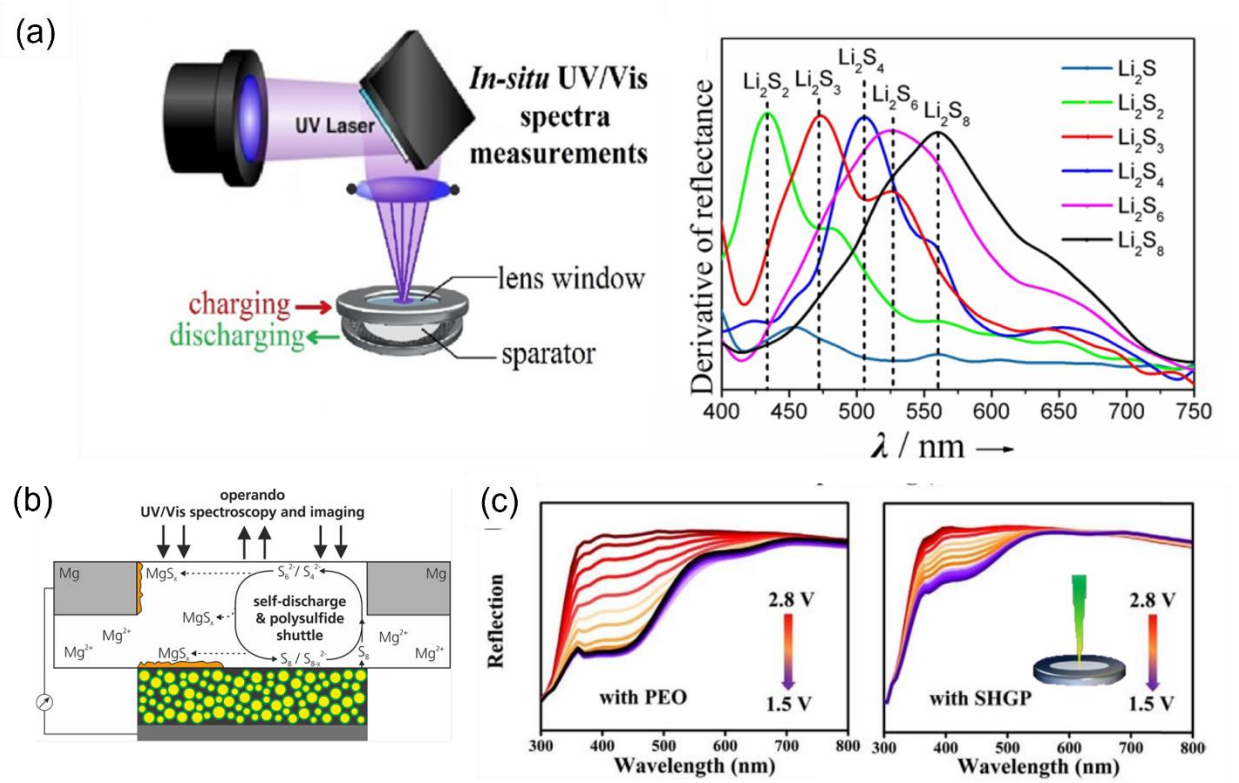

Figure 13 (a) Schematic of the in situ UV-vis devices and related peaks of different sulfur species. Reproduced with permission: Copyright 2016, American Chemical Society.[194] (b) Schematic illustration of the proposed reaction process of the Mg-S battery based on the operational UV-VIS spectroscopy and imaging results. Reproduced with permission: Copyright 2021, American Chemical Society.[215] (c) In situ UV-vis spectrum of using poly (ethylene oxide) electrolyte and using ultra-high ion-conducting gel polymer electrolyte. Reproduced with permission: Copyright 2019, Elsevier.[195]

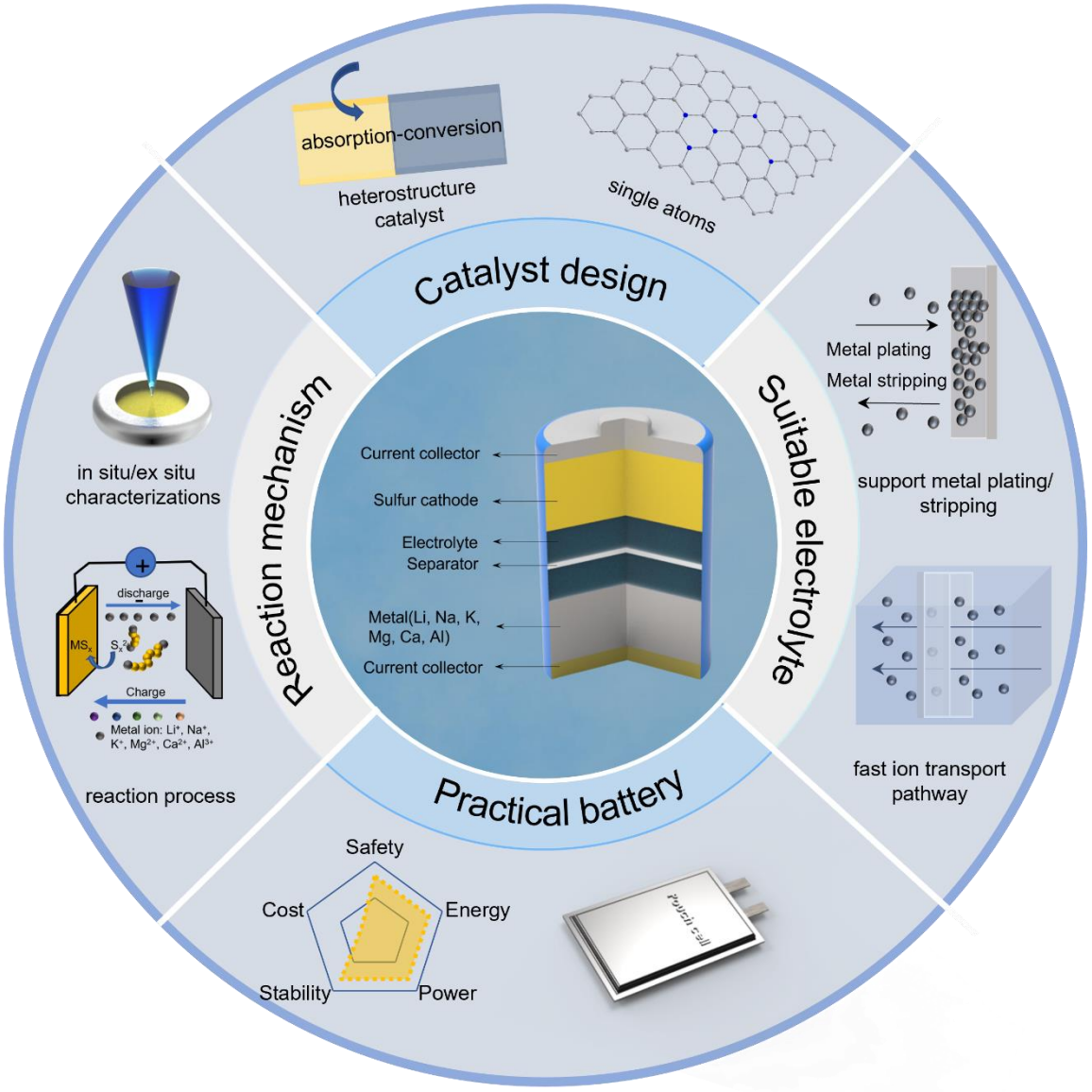

Figure 14 The schematic illustrates the prospects of metal-sulfur batteries.

Table 1 The comparison of metal-sulfur batteries.

Metal-sulfur batteries	Discharge products	Theoretical voltage (E^0/V)[8]	Volume expansion (ΔV, %)	Gravimetric energy density (Wh kg^{-1})[8]	Volumetric energy density (Wh L^{-1})[8]	Metal abundance (ppm)[7]
Li-S	Li_2S	2.24	80%	2612	2955	20
Na-S	Na_2S	1.85	180%	1270	1545	23600
K-S	K_2S/K_2S_3	1.88	309%	916	952	20900
Mg-S	MgS	1.77	24%	1685	3221	950
Ca-S	CaS	2.47	80%	1838	3202	41500
Al-S	Al_2S_3	1.23	40%	1319	2981	82300

Table 2 Summary the performance of the state-of-the-art lithium-free metal sulfur batteries.

Materials	Electrolyte	Sulfur content (wt%)/or sulfur loading (mg cm^{-2})	Initial discharge capacity (mAh g^{-1})	Discharge (mAh g^{-1}) @~n cycles	Specific current [mA g_s^{-1}]
Na-S					
S/ multiporous carbon fibers[127]	NaTFSI(2M)/PC:FEC(1:1)+InI_3(10 mM)	1.57 mg cm^{-2}	1170	1007@50	167 mA
S/Fe-HC[130]	$NaClO_4$(1M)/EC: DMC (1:1) +5 wt% FEC	40%	1023	394@1000	100
S/MOF-C[136]	$NaClO_4$(1M)/P+5 wt% FEC	37%	650	467@100	100
			360	270@1000	1000
SPAN[139]	$Na(PF)_6$/EC:DMC(1:1)	37.4%	1502	1405@100	2700
S/ZnS and CoS_2[141]	$NaClO_4$(1M)/EC: DMC (1:1) +5 wt% FEC	45.6%	~1410	570@1000	200
			~900	250@2000	1000
S/Ni- nitrogen-doped carbon fibers[143]	$NaClO_4$(1M)/TEGDME	45%	431	233@270	1673
S/carbon nanocage/FeS_2[144]	$NaClO_4$(1M)/EC: DMC (1:1) +3 wt% FEC	45.85%	1471	524@300	100
			500	395@850	1000
S/Ni-MOF[202]	$NaClO_4$(1M)/EC: DMC (1:1) +5 wt% FEC	38.88%	~470	347@1000	~1673
			~380	241@1000	~3346
S/NiS_2@N-doped CNT[203]	$NaClO_4$(1M)/EC: DMC (1:1) +3 wt% FEC	22.4%	960	401@750	1000
S/Mo_2N–W_2N@spherical carbon[209]	NaTFSI(2M)/PC: FEC(1:1)	34.16%	~1050	517@400	1000
K-S					
S/CNT[145]	KFSI (0.6 M)/ DME	70 %	720	184@5	50
S/CNF[147]	KCF_3SO_3 (1 M)/ TEGDME	50 %	1160	~600@50	~167
SPAN with PAA binder[149]	KPF_6(0.5 M)/ EC:DMC(1:1)	45.5 %	1050	997.5@100	837.5
Microporous carbon/ S[151]	KPF_6(0.8 M)/ EC: DEC	20 %	~1220(2nd)	870@150	20
S/CMK-S[152]	KTFSI (5 M)/ DEGDME	60.8%	606	~300@10	10
S/ Vulcan carbon/[153]	$Cu(TFS)_2$(0.3 M)/ KTFS(0.1 M)/ Me-Im	56%	~650	~540@200	800
N-doped Co nanocluster inlaid porous N-doped carbon/S[154]	KPF_6(0.8M)/EC: DEC(1:1)	63.4%	657.1	355.3@150	200
Iodine-doped/Span[220]	KPF_6(0.8 M)/EC: DEC(1:1)	17.7 %	994	768@500	~837.5
Mg-S					
S/ Ketjenblack[161]	LAGP/Mg $(TFSI)_2$ or $Li(TFSI)_2$/DMSO(cathode) Phenylmagnesium chloride solution/THF/$AlCl_3$/LiCl	76%	~1500	700@300	~668
S@CMK-3[163]	$Mg(B(hfip)_4)_2$ (0.8 M)/DEG:TEG(1:1)	41.25%	800	200@100	167

S/CNT[166]	0.5 M $[Mg_4Cl_6(DME)_6][B(HFP)_4]_2$	64%	1247	1019@100	500
S/Co,N-doped MOF[170]	$Mg(HMDS)_2$(0.5 M)/ $AlCl_3$(1 M)/ LiTFSI(1M)/ DGE	29.2	600	~400@200	1673
S@microporous carbon[169]	$(PhMgCl)_2$–$AlCl_3$(0.4 M)/ LiCl(1M)/ THF	64.7 %	878	368.0@200	167
S/ activated carbon cloth(cathode)with CNF-coated separator[171]	0.4 $Mg[B(hfip)_4]_2$/DME	~10%	930	200@100	~167
S/MOF derivative carbon[170]	$(HMDS)_2Mg$–$2AlCl_3$/ LiTFSI	32.97%	600	400@200	1673
S@mesoporous carbon[221]	THFPB (0.5M)/ MgF2(0.05M) /DME	85 %	1081	~900@30	50
S@rGO with N,S doped carbon cloth current collector with CNF coated separator[222]	$(HMDS)_2Mg/2AlCl_3$/ $MgCl_2$/ TEGDME	49%	~1000	388@40	20
Ca-S					
S/ activated carbon cloth[172]	$Ca[B(hfip)_4]_2$(0.5M)/ DME	10%	~900	200@15	~167
S/ Ketjenblack[175]	$Ca[B(hfip)_4]_2$(0.25M)/ DME	53%	~920	120@15	n/a
S/CNF paper[174]	$LiCF_3SO_3$(0.5)/ Ca $(CF_3SO_3)_2$(0.2)/TEGDME	2 mg cm^{-2}	~800	300@20	~167
Al-S					
S/CNT[179]	urea-AlCl3 (1:1.3)	18%	225	~120@200	200
S/activated CNF(cathode) with SWCNT coating on glass fiber separator [180]	EMICl-AlCl3 (1:1.3)	33%	1220	~600@10	~84
S/SPAN[181]	EMICl-AlCl3 (1:1.5)	10%	320(605 4th)	~201@21	25
BN/S/C[182]	EMICl-AlCl3 (1:1.5)	10%	~700	532@300	100
S/CNT[183]	EMICl-AlCl3 (1:1.5)	58.8%	2129	375@10	50
	urea-AlCl3 (1:1.5)	58.8%	2359	125@10	50
S/Co-base MoF[184]	EMICl-AlCl3 (1:1.3)	42%	693	~160@160	300
S/carbonized-MOF[187]	EMICl-AlCl3 (1:1.3)	n/a	1200	~460@500	1000
S/ activated CNF[188]	$LiCF_3SO_3$(0.5 M)/EMICl-AlCl3 (1:1.25)	33%	1000	~600@50	~170
S/CMK-3[189]	EMIBr-$AlCl_3$	40%	1500	~180@20	251

	(1:1.3)				
	NBMPBr-$AlCl_3$ (1:1.3)	40%	1390	~450@20	251

Table 3 Capabilities, limitations and application examples of *in-situ* characterization techniques of metal-sulfur batteries.

In situ techniques	Capabilities	Limitations	Application in metal-sulfur battery study
XRD	Monitoring phase transitions of sulfur species during cycling.	Direct observation of soluble polysulfides by XRD remains challenging	1. Probing sulfur and sulfur species evolution during cycling.[9,20,179,223] 2. Provide evidence of the profitable catalytic effect. [204-207] 3. Probe the phase evolution of electrocatalysts. [21,210,211]
XANES	Probe S element reduction and oxidation state changes no matter crystal or amorphous, solid or liquid; Monitor the contributions of different sulfur compounds in the cathode during cycling.	X-ray absorption fine structure is affected by the sulfate groups in the salt or the solvent	1.Study the capacity degradation mechanism.[199,224] 2.Explore the reaction process and intermediates during the redox process. [61,179,199,200] 3. Provide evidence of the profitable catalytic effect. [225,226]
XPS	Study chemical composition, charge transfer, chemical bond in the surface.	The cell design is complex	1. Analysis interfaces of electrode and electrolyte.[227-229] 2. Provide evidence of the profitable catalytic effect. (semi-in situ XPS)[230]
NMR	Monitor changes in the chemical structure which involves detection radio-frequency; Quantitative tracking of the species concentration.	The experiment setup is expensive. The resolution hard below 100 μm; The alternating currents in the EC and NMR existing interferences.	Explore the reaction process.[143,150,172,231]
Raman	Monitor the compositional and structural changes of sulfur species /related species in the electrolyte or the surface of the electrode.	Hard detect the signal of low-concentration soluble polysulfides.	1. explore the reaction process.[143,150,172,231] 2. Provide evidence to the profitable catalytic.[231,232] 3. Identify reaction intermediates in the electrolyte.[179,189,233] 4. Provide evidence to suppress the shuttle effect.[234-236]
UV-vis	Monitor the evolution of soluble polysulfides qualitatively and quantitatively	Limited detection of solid metal sulfides and cannot be applied in solid-state batteries as well as carbonate-based electrolytes.	1. Exploration of the conversion process between sulfur and sulfur species. [32,193,194] 2. Monitor the shuttle effect.[15-18]
FTIR	Detect the chemical information of surface species	The reflective is quite low for the conductive carbon additives	1. detect polysulfides and electrolyte interactions.[237] 2. quantify the order and concentration of soluble LiPSs in the electrolyte during cycling.[238]
AFM	Observe surface morphology and structure	The large volume change may make trackable features in the topography unrecognizable	Observe the interfacial evolution of electrode/electrolyte.[239-241]
TEM	1. Morphologies change of solid sulfur and metal sulfides. 2. Phase change and chemical composition transformations.	1. Open-cell setups cannot be applied in liquid electrolyte systems. 2. The lithiated process of graphene liquid cell is ignited by electron beam, cannot achieve the cycling process.	1. Monitor the chemical composition transformation and volume expansion of the lithiation/delithiation process. [13,93,190,191] 2. Observe the nucleation and growth of metal sulfides.[191] [93]